TECHNISCHE UNIVERSITÄT MÜNCHEN

Lehrstuhl für Biochemie
und
III Medizinische Klinik und Poliklinik
am Klinikum rechts der Isar der Technischen Universität München

The role of NIPA in DNA damage response

Michal Andrzej Kulinski

Vollständiger Abdruck der von der Fakultät für Chemie
der Technischen Universität München
zur Erlangung des akademischen Grades eines

Doktors der Naturwissenschaften

genehmigten Dissertation.

Vorsitzender:	Univ.-Prof. Dr. A. Itzen
Prüfer der Dissertation:	1. Univ.-Prof. Dr. M. Groll
	2. Univ.-Prof. Dr. J.G. Duyster, Universität Freiburg

Die Dissertation wurde am 15.07.2013 bei der Technischen Universität München eingereicht und durch die Fakultät für Chemie am 21.11.2013 angenommen.

Abbreviations

α	Alpha
β	Beta
γH2A.X	Phosphorylated Histone 2A.X
μg	10^{-6} g (mass unit)
μL	10^{-6} L (volume unit)
53BP1	p53 binding protein 1
ALK	Anaplastic lymphoma kinase
APC/C	Anaphase promoting complex/cyclosome
APS	Ammonium persulfate
ATM	Ataxia telangiectasia mutated
ATP	Adenosine-5'-triphosphate
ATR	ATM-Rad3-related
BER	Base excision repair
BIR	Baculovirus IAP repeat domain
bp	base pair
BrdU	Bromodeoxyuridine
BRCA1	Breast cancer type 1 susceptibility protein
BSA	Bovine serum albumin
C	Celsius (temperature measurement unit)
CDK	Cyclin-dependent kinase
CHK1	Checkpoint kinase 1
CHK2	Checkpoint kinase 2
CHX	Cycloheximide
CPT	Campthothecin
CRS	Cytoplasmic retention signal
Da	Dalton (unified atomic mass unit)
DAPI	4',6-diamidino-2-phenylindole
DDR	DNA damage repair
DMEM	Dulbecco's modified eagle medium
DMSO	Dimethyl sulfoxide
DNA	Deoxyribonucleic acid
dsDNA	double stranded DNA
ssDNA	single stranded DNA
dNTP	2'-desoxynucleoside-5'-triphosphate
DTT	Dithiothreitol
E.coli	*Escherichia coli*
EDTA	Ethylenediaminetetraacetic acid
ERK2	Extracellular signal-regulated kinase 2
ETO	Etoposide
FITC	Fluorescein isothiocyanate
FLIP	Fluorescence loss in photobleaching
FRAP	Fluorescence recovery after photobleaching
G_1	„Gap"-phase 1

G_2	„Gap“-phase 2
G_2/M	Transition from „Gap“-phase 2 in mitosis
GFP	Green fluorescent protein
Gy	Grey (radiation unit)
h	hour, hours (time unit)
HA	Hemagglutinin
HJ	Holliday junction
HR or HRR	Homologous recombination or homologous recombination repair
IAP	Inhibitor of apoptosis protein
Ig	Immunoglobulin
IP	Immunoprecipitation
IR	Ionizing radiation
IRIF	Ionizing radiation-induced foci
J	Joule (energy unit)
kb	kilo base
LB	Luria-Bertani
m	mili (10^{-3})
M	mol per Liter, molar (unit of concentration, molarity)
mA	mili Ampere (electric current unit)
MDC1	Mediator of DNA damage checkpoint protein 1
MDM2	Mouse double minute 2 homolog
MEFs	Mouse embryonic fibroblasts
MG132	N-carbobenzoxyl-Leu-Leu-leucinal
min	minute, minutes (time unit)
MPF	Maturation promoting factor
MRN	MRE11, RAD50, NBS1 complex
mRNA	messenger RNA
NHEJ	Nonhomologous-end-joining
NIPA	Nuclear interaction partner of ALK
NLS	Nuclear localization signal
nm	nano meter
NPC	Nuclear pore complex
NUPs	Nucleoporins
O.D.	Optical density
OTM	Olive tail moment
PBS	Phosphate-buffered-saline
PBST	PBS with Tween20
PCR	Polymerase chain reaction
PI	Propidium iodide
PLK1	Polo-like kinase 1
PMSF	Phenylmethanesulfonyl fluoride
PVDF	Polyvinylidene fluoride
Rb	Retinoblastoma
RFP	Red fluorescent protein
RING	Really interesting new gene
RNA	Ribonucleic acid
ROI	Region of interest
RPM	Round per minute
RT	Room temperature
s	second, seconds (time unit)

SAC	Spindle assembly checkpoint
SCF	SKP1/CUL1/F-box protein
SDS	Sodium dodecyl sulfate
SDS-PAGE	Sodium dodecyl sulfate polyacrylamide gel electrophoresis
siRNA	small interfering RNA
SKP1	S-phase kinase associated protein 1
SSB	Single strand break
TAE	Tris base – acetic acid – EDTA buffer
TEMED	Tetramethylethylenediamine
TPR	Translocated promoter region
TRIS	Tris(hydroxymethyl)aminomethane
TUNEL	(TdT)-mediated biotin-16-dUTP nick-end labeling
Ub	Ubiquitin
UV	Ultraviolet
WT	Wild type
ZC3HC1	Gene coding for NIPA
ZnF	Zinc-finger motif

Amino acids

A	Ala	Alanine
C	Cys	Cysteine
D	Asp	Aspartic acid
E	Glu	Glutamic acid
F	Phe	Phenylalanine
G	Gly	Glycine
H	His	Histidine
I	Ile	Isoleucine
K	Lys	Lysine
L	Leu	Leucine
M	Met	Methionine
N	Asn	Asparagine
P	Pro	Proline
Q	Gln	Glutamine
R	Arg	Arginine
S	Ser	Serine
T	Thr	Threonine
V	Val	Valine
W	Trp	Tryptophan
Y	Tyr	Tyrosine

Table of contents

1. Introduction

1.1 The cell cycle

The fate of an individual cell throughout the body is to pass the undamaged genetic information in timely manner to the next generation. This fundamental feature of life is mainly determined by the control and regulation of protein expression, an essential mechanism of recurring cyclic phases defined as the cell cycle.

The division cycle of most eukaryotic cells consists of four discrete phases: G_1, S, G_2 and M. The G_1 phase (gap 1) is covering the interval between mitosis and initiation of DNA replication, where the cell is metabolically active and grows continuously. During this gap phase, information is integrated in order to determine the readiness of a cell to enter S phase – a precise point where the decision has to be made called restriction point (R point). If appropriate growth factors that signal cell proliferation are not available in G_1, cell can enter a quiescent stage of the cell cycle called G_0 and stop further progression. G_1 is followed by the S phase (synthesis), where the DNA replication takes place. After the completion of DNA synthesis, cell enters the G_2 phase (gap 2) during which it continuous to grow and proteins are synthesized in preparation to enter the next stage. Mitosis (M phase) is a next step in the cell division and the most conspicuous stage of the cell cycle characterized by the separation of daughter chromosomes and usually ending with cytokinesis[1,2].

Mitosis is additionally divided in five distinct phases: prophase, prometaphase, metaphase, anaphase and telophase. These phases can be distinguished due to their morphological differences in chromosomes structure and the presence of mitotic spindle[3] (Fig.1.1). At the onset of prophase loosely bundled chromatin fibers are condensing into chromosomes, mitotic spindle begins to form in the cytoplasm, nucleolus disappears and centrioles migrates to the opposite pole of the cell and are duplicated. Following step where the nuclear envelope disintegrates, microtubules invade the nuclear interior and attach to the centromeres via kinetochores, is referred to as prometaphase. The highlight of metaphase is formation of the metaphase plate and is characterized by the equatorial alignment of chromosomes. In anaphase, sister chromatids are being pulled to the opposite ends of the cell through attractions of the kinetochore fibers. Mitosis ends with telophase, where the nuclear envelopes are

reconstituted, nucleoli reappears and chromosomes begin the relaxation to chromatin. Cell division is completed after the contractile ring divides the cytoplasm between two daughter cells in cytokinesis.

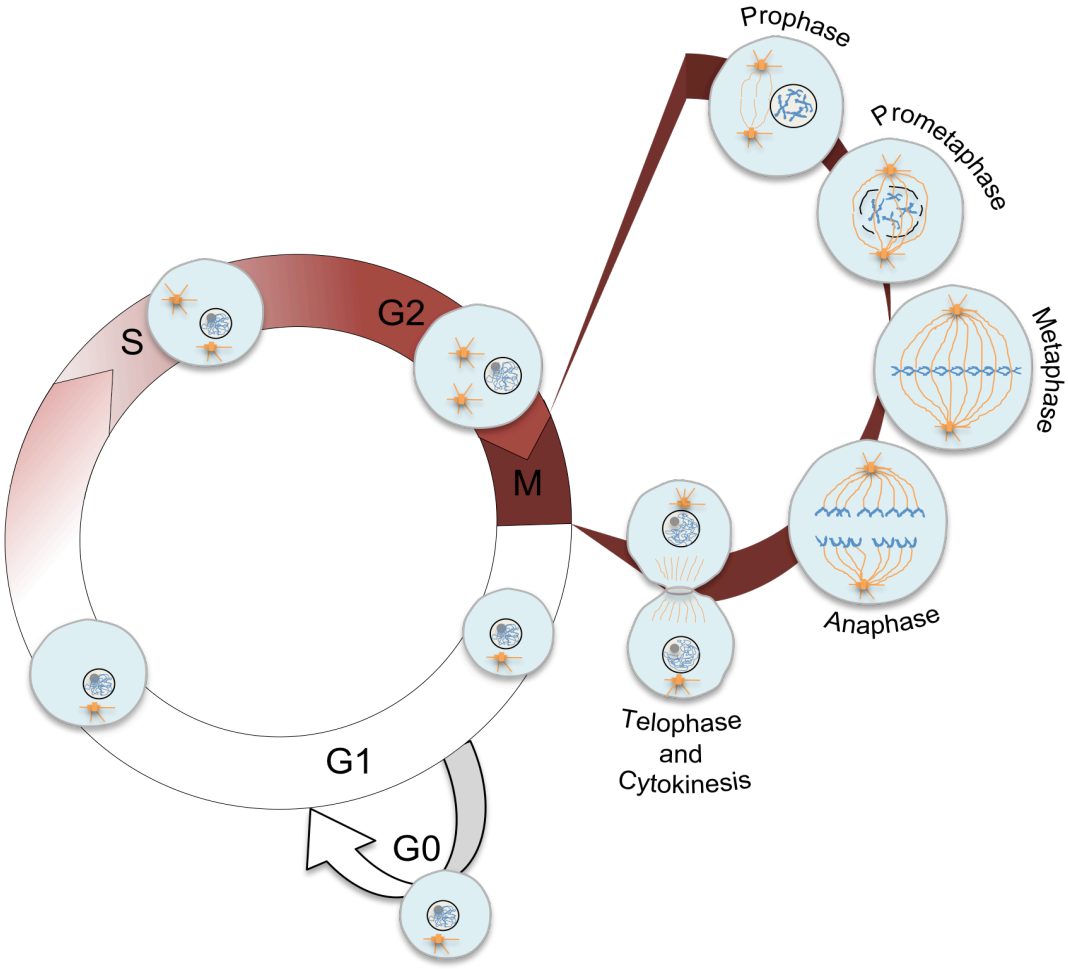

Fig.1.1: Schematic overview of the mammalian cell cycle clock. G_0: Quiescent state; G_1: Phase between mitosis and synthesis; G_2: Phase between synthesis and mitosis; S: Phase of synthesis; M: Mitosis

1.2 Control of the cell cycle

The most important cell cycle regulation is based on the activation or inactivation of a member of the conserved family of heterodimeric serine/threonine protein kinases known as the cyclin-dependent kinases (CDKs)[4]. The catalytic activity of CDKs requires binding of activating partners that are synthesized and degraded during each cell cycle and thus has been designated as cyclins[5] (Fig.1.2). CDK4 and CDK6 form active complexes with the D-type cyclins (D1, D2 and D3) and are thought to be involved in early G_1. CDK2 is required to complete G_1 and initiate S phase and is sequentially activated by the cyclin E1 and E2 during G_1/S transition, and cyclin A1 and A2 during S-phase[6]. Later in S-phase, A-type cyclins associate with CDK1. As cell moves into G_2

phase, A-type cyclins are replaced by the B-type cyclins (B1 and B2) to form the kinase complex that is active during the late G_2 and M-phase.

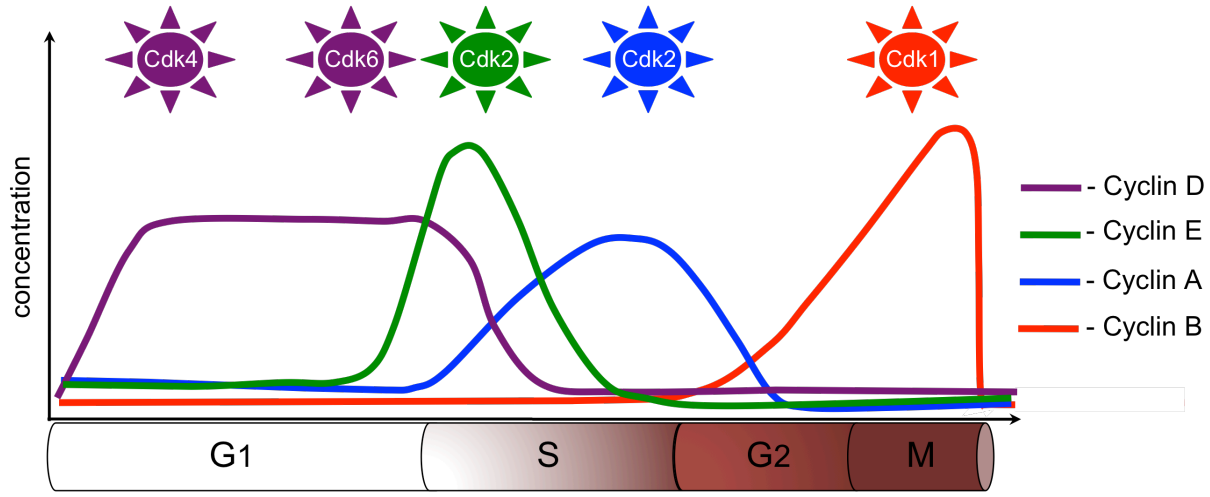

Fig.1.2: Distribution of cyclin levels during the cell cycle. Cyclin fluctuation shown as colored lines with their corresponding CDK partners active in each cell cycle phase depicted as a cartoon. G_1: Gap between mitosis and synthesis; S: Synthesis phase; G_2: Gap between synthesis and mitosis; M: Mitosis (Adapted from Weinberg, 2007)[7]

CDKs are regulated *i.a.* by cyclin-dependent kinase inhibitors (CKIs), which are the members of two inhibitor families CIP/KIP and INK4. $p21^{Cip1/Waf1}$, $p27^{Kip1}$ and $p57^{Kip2}$ belong to CIP/KIP family and are binding to variety of cyclin-cdk complexes through a conserved amino-terminal domain[8-10]. INK4 family instead comprises $p16^{INK4a}$, $p15^{INK4b}$, $p18^{INK4c}$, $p19^{INK4d}$ and interacts specifically only with CDK4 and CDK6[11].

Since the role of cyclin-cdk complexes was found to be highly important for the proper cell division, it has become clear that cells must have developed evolutionary mechanisms to regulate their activation and inactivation in a timely dependent manner[12]. The most important guardians are therefore constituted by the cell cycle checkpoints and ubiquitin-mediated proteolysis.

1.2.1 Cell cycle checkpoints

Transition from one cell cycle phase to another is exclusively allowed if all features of the previous phase were properly accomplished. These transitions are coordinated by the highly conserved checkpoint pathways and occur at a precise time and in a defined order[13].

1.2.1.1 G_1/S and Intra-S checkpoints

Decision to start proliferation is taken in the G_1 phase therefore G_1/S checkpoint is the first important surveillance mechanism of the cell division cycle. Loss of this checkpoint can lead to genomic instability, inappropriate survival of genetically damaged cells, and to the evolution of cells to malignancy[14]. The G_1/S arrest operates on the tripartite axis: through CDC25A phosphorylation, pRb/E2F pathway and p53 dependent.

The cascade operating via phosphorylation of CDC25A ensures an early response in the cell cycle, temporarily slowing down progression to provide more time for DNA repair[15]. CDC25A is able to diminish inhibitory phosphorylation of CDK2 on Thr14/Tyr15, and thus activating CDK2-Cyclin E and CDK2-Cyclin A for progression into S-phase[16]. Upon DNA damage or faulty DNA replication, CDC25A is rapidly phosphorylated by CHK1 and CHK2 resulting in damage-induced ubiquitination and accelerated turnover of the CDC25A protein by the proteasome[17-19]. As a result persistent inhibitory phosphorylation of CDK2 drives cells into cell cycle arrest at the G_1/S boundary[20].

The importance of the pRb pathway for normal cell growth and development is emphasized by the frequent inactivation of retinoblastoma protein in human tumors, deregulated in almost one third of all cancer cases[21]. In G_0 pRb is essentially unphosphorylated. Upon entrance into G_1, D-type cyclins together with their CDK4/6 kinase partners are initiating pRb phosphorylation, leading to its hypophosphorylation. Such an activated form of pRb binds and inactivates the E2F family of transcription factors, which play a pivotal role in regulating the expression of genes (such as cyclin E, cyclin A, CDK1, CDC25A, E2F1) involved in the G1/S transition and DNA synthesis, leading to the cell cycle arrest[22-24]. During a normal cell cycle, cyclin E associates with CDK2 and, at the R-point, drives pRb hyperphosphorylation leaving it in the functionally inactive state. Now expression of E2F driven genes allows for cycle progression to the next phase[25].

p53 is a transcription factor and its induction by the stress results in cell cycle arrest, senescence, apoptosis or autophagy and as a tumor suppressor is very frequently mutated in human cancer[26]. It induces the expression of genes involved in cell cycle regulation like $p21^{Waf1/Cip1}$, Bax, cyclin G, GADD45 and MDM2[27-29]. MDM2 is a member of the RING E3 ubiquitin ligase family, which together with MDMX function as a

heterodimeric pair to augment proteasome-dependent p53 degradation[30]. Upon genotoxic stress at the G_1/S transition, the ataxia-telangiectasia mutated (ATM) and ataxia-telangiectasia and Rad3 related (ATR) kinases phosphorylate multiple serine residues in RING domains of MDM2 and MDMX, which leads to their destabilization and possible dissociation of MDM oligomers and in turn stabilizes p53[31,32]. Additional stabilization is obtained through DNA-dependent protein kinase (DNA-PK) and ABL by phosphorylation of Ser17 of MDM2 and Tyr99 of MDMX, respectively[33]. In the following step ATR and ATM activates p53 by phosphorylation at Ser15[34]. Inactivation of negative regulators results in accumulation of active p53 in the nucleus and leads to expression of CDK inhibitor $p21^{Waf1/Cip1}$. G_1/S arrest is sustained through inhibition of CDK2/cyclin E and CDK4,6/cyclin D complexes by p21[35,36].

The Intra-S checkpoint operates similarly to the G_1/S checkpoint based on the CDK2 inhibition through the degradation of CDC25A, however without involvement of the p53 signaling pathway. Significantly, a feature shared by all these pathways is their convergence on the control of CDK2, whose activity together with cyclin E and cyclin A is a rate-limiting and essential factor for DNA replication[37].

1.2.1.2 G_2/M checkpoint

The G_2/M checkpoint prevents cells from entering mitosis if the DNA is damaged, providing essential time for repair and for stopping proliferation. Mitotic events are initiated by the formation of active CDK1-cyclin B complex, so called maturation promoting factor (MPF)[38]. Before cell enters mitosis, CDK1 is harboring inhibitory phosphorylation at Tyr15 due to activity of Wee1 kinase and at Thr14 and Tyr15 due to Myt1 kinase[39-41]. Phosphatase CDC25C is responsible for the activation of CDK1 during G_2/M transition through dephosphorylation of these residues[42].

Function of G_2/M checkpoint relies on preservation of this inhibitory phosphorylation. CHK1 and CHK2 phosphorylate CDC25C on Ser216 which in turn creates the binding site for small acidic protein, 14-3-3[43-45]. Binding of 14-3-3 protein inactivates CDC25C through its sequestration to the cytoplasm[46]. Sustained phosphorylation of CDK1 results in cell cycle arrest at the G_2/M boundary.

p53 though mostly implicated to have an impact exclusively on the G_1/S arrest, recently has also been proposed to play a role in the G_2/M checkpoint[47,48]. Several transcriptional targets of p53 could inhibit CDK1, including p21, by direct inhibition, 14-3-3 σ by

anchoring CDK1 in the cytoplasm where induction of mitosis is avoided or by GADD45, which destabilizes CDK1/Cyclin B complex leading to dissociation of CDK1 from cyclin B[49-51].

1.2.1.3 Spindle assembly checkpoint (SAC)

Entering anaphase is the most crucial decision for the cell to be made during mitosis in order to properly accomplish division cycle. Any mistake in the accurate alignment of the chromosomes would result in dramatic consequences for the new cell generations. Mitotic spindle assembly checkpoint (SAC) is a regulatory mechanism required for proper segregation of chromosomes during cell division[52]. SAC acts by inhibiting anaphase in response to defects in the assembly of the mitotic spindle or errors in the chromosome alignment. Detection of unattached kinetochores contributes to the creation of the mitotic checkpoint complex (MCC) composed of three SAC proteins: MAD2 (mitotic arrest deficient 2), BUBR1/MAD3 and BUB2 as well as CDC20, a co-factor of the ubiquitin ligase anaphase-promoting complex/cyclosome (APC/C)[53,54]. APC/C is responsible for polyubiquitylation and 26S proteasomal degradation of the two key substrates, cyclin B and securin[55]. Proteolysis of cyclin B is required for inactivation of MPF complex and subsequent exit from mitosis. Destruction of securin, stoichiometric inhibitor of separase, leads to cleavage of the cohesin complex, which holds sister chromatids together by separase, and is followed by the start of anaphase[56]. SAC inhibits the ability of CDC20 to activate APC/C through a direct binding of MAD2, preventing that whole chain of events until all chromosomes have become bi-orientated between the separated spindle poles on the metaphase plate[57-59].

1.2.2 Ubiquitin-mediated proteolysis

Selective and programmed degradation of the cell cycle regulatory proteins is an essential event in the cell cycle progression and is mediated by the ubiquitin-dependent proteolysis[60]. Ubiquitination was shown to play important role not only in protein degradation, but also in transcription, DNA replication, endocytosis as well as in the regulation of immune and inflammatory responses and DNA repair[61,62].

1.2.2.1 Mechanism

Ubiquitin (Ub), a small, highly conserved protein, assembles an ubiquitin chain on the lysine residue of a given substrate, which target it for degradation by the 26S

proteasome[63]. Polyubiquitin chain formation is carried out in three steps. First Ub is activated on the C-terminal Gly residue in an ATP-requiring step by the E1 activating enzyme with thioester linkage between Ub and cysteine residue of E1 and subsequent release of AMP. Such activated ubiquitin is next transferred to the active cysteine side chain of the ubiquitin-carrier protein, E2 enzyme (also called Ubiquitin-conjugating enzyme or UBC). In the third step catalyzed by E3 enzyme, called ubiquitin ligase, ubiquitin is linked through an amide isopeptide linkage of its C-terminus to an ε-amino group of lysine residue in the substrate protein[64,65] (Fig.1.3). Ubiquitin can be covalently linked to several lysine residues, what in turn results in different response. For example K48-linked chains are the targeting signal for degradation, whereas K63-linked chains act as molecular scaffolds, tethering subunits of oligomeric kinase or DNA repair complexes together[66,67]. Thus ubiquitination can serve as a code which cells use to control the key signaling pathways.

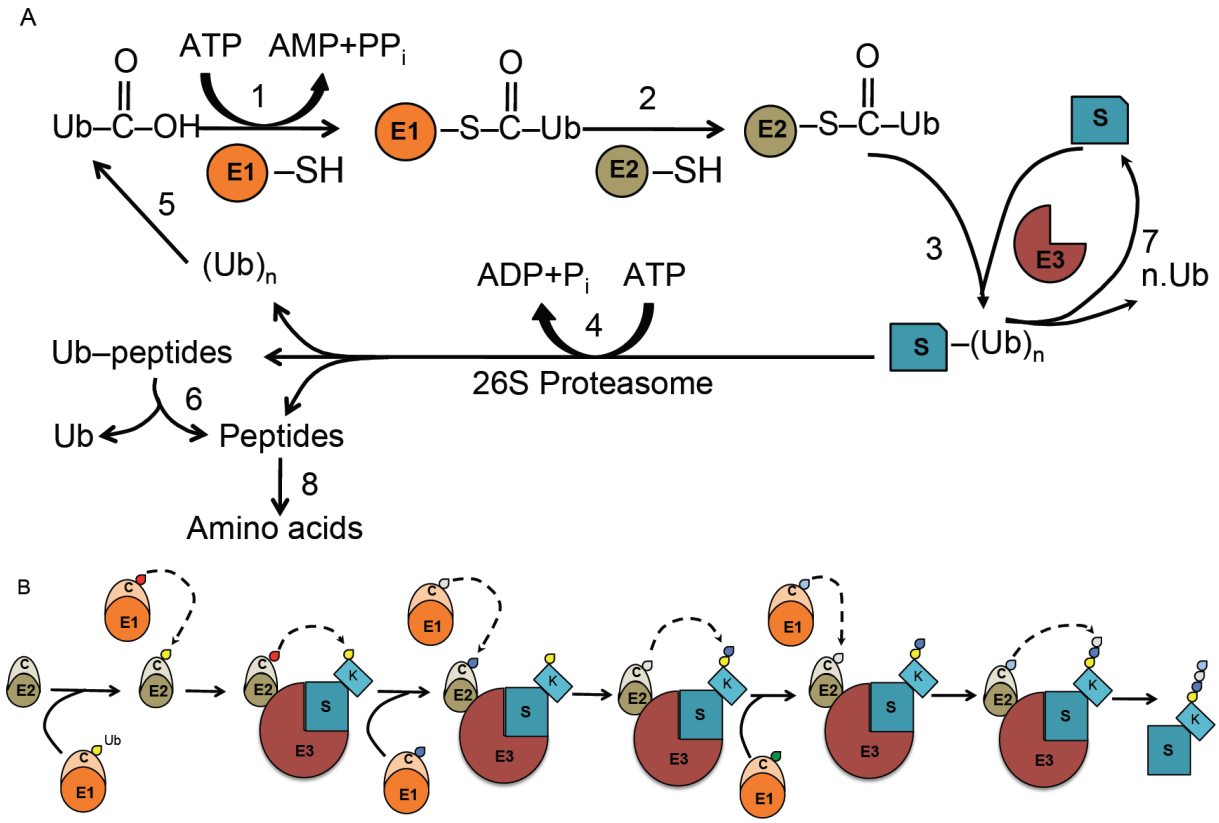

Fig.1.3: Schematic overview of the polyubiquitin-chain synthesis. (A) Sequence of enzymatic reactions in the proteolytic pathway of the ubiquitin system (Adapted from Hershko and Ciechanover, 1998)[61]. (B) Standard, sequential addition model for ubiquitin chain formation, in which Ub molecules are added one at a time, first to lysine on the substrate protein and then to specific lysine in the ubiquitin at the distal end of the ubiquitin chain (Adapted from Hochstrasser, 2005)[68]. C: Cysteine residue; K: Lysine residue; S: substrate protein; Ub – ubiquitin; E1: ubiquitin-activating enzyme; E2: ubiquitin-conjugating enzyme; E3: ubiquitin ligase.

1.2.2.2 RING-domain type E3 ligase – SCF complex

RING-domain type E3 ligases transfer ubiquitin directly onto substrates. Two crucial members of the RING-finger-containing E3 Ub ligase family are involved in the cell cycle control: the already mentioned APC/C complex and the SCF (Skp-Cullin-F-box) complex. APC functions primarily during mitosis and G1 phase, whereas SCF complexes are active throughout the whole cell cycle[69]. The SCF complex, one of the best-characterized RING ligase, consists of three primary and invariable components – SKP1 (S-phase-kinase-associated protein-1), CUL1 (Cullin), and RBX1/ROC1 – as well as variable component,

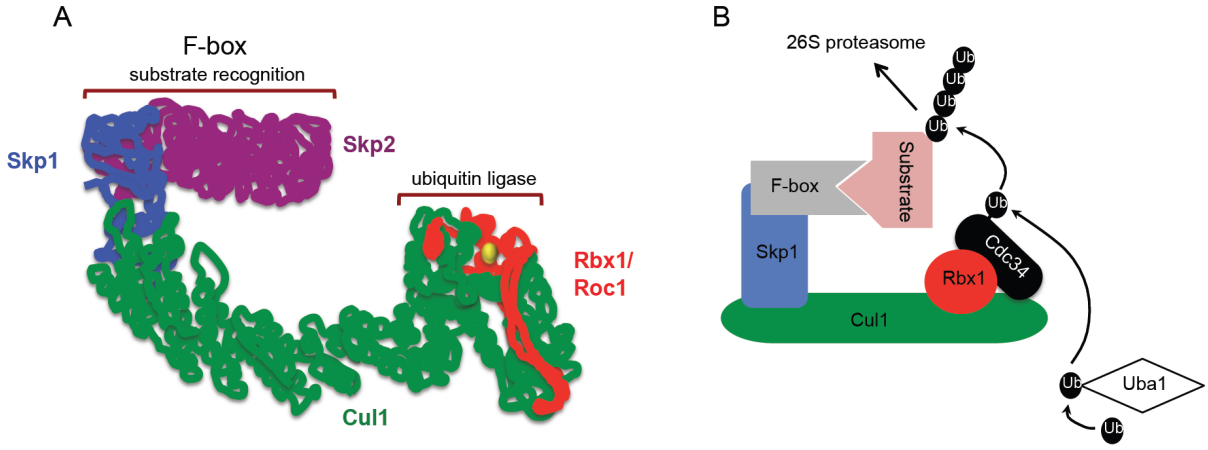

Fig.1.4: SCF complex structure and mode of action (A) Structure of the RING-finger family member SCF^{Skp2} as an example of SCF complex. (B) The generic architecture of SCF complex and its mode of action (Adapted from Weinberg, 2007 and Willems, 2004)[7,70]

known as an F-box[71] (Fig.1.4). CUL1 is a scaffold protein that interacts with ROC1 at its carboxyl-terminus and forms the E3 Ub-ligase core to recruit Ub-conjugated E2, such as UBC3, UBC4 or UBC5. The amino terminus of CUL1 interacts with the crucial adaptor protein SKP1, which binds to the F-box motif of an F-box protein[72]. The F-box motif, named after presence of this motif in the mammalian cyclin F protein, has approximately 50 residues and functions as a site of protein-protein interaction[73]. According to motif sequence at the carboxyl-terminus, F-box proteins are classified into three families: FBXL bearing F-box and Leucine Reach Repeats (LRR), FBXW with F-box and WD repeats and the third family FBXO with an F-box and either another or no other motif[74]. F-box proteins directly recruit ubiquitination substrates and bridge the interaction between UBC and the substrate thus being responsible for substrate specificity[75,76]. Many different SCF E3 ligases are involved in control of the cell cycle transitions and among them, a member of the FBXO family – NIPA – is involved in the timing of mitotic entry.

1.2.2.3 F-box protein NIPA

Nuclear **I**nteraction **P**artner of **A**lk (NIPA) was identified as a novel downstream target of NPM-ALK in a yeast two-hybrid screen where the ALK fusion protein was used as bait. NIPA has been shown to bind ALK, only in cells expressing kinase-active ALK fusion proteins and that it is phosphorylated in these cells[77].

The localization of NIPA in human genome was aligned to chromosome 7q23.2 and is coding for the protein of 10 exons with 502 amino acids and a molecular mass of about 60kDa. NIPA is exquisitely localized in the nucleus due to classical NLS sequence at the C-terminal end, characterized by the presence of positively charged residues arginine and lysine[77] (Fig.1.5).

Fig. 1.5: Schematic overview of the human NIPA protein. N: N-terminus; ZnFbm: Zinc finger binding motif; F-box: F-box domain; S354: Serine residue 354; NLS: nuclear localization signal; N: N-terminus (Adapted from Christine von Klitzing, PhD thesis [78]).

NIPA owes its second name ZC3HC1 (zinc finger C3HC-type protein 1) to the zinc-finger motif located at the N-terminus. Zinc-finger domains are small protein motifs, which contain multiple finger-like protrusions with conserved cysteine and histidine ligands that make tandem contacts with their target molecule. They are usually coordinated by one or more Zn^{2+}-ions to stabilize the structure. Function ranges from DNA or RNA binding to protein-protein interactions and membrane association[79]. However NIPA ZnF binding motif was reported to constitute a prototypic BIR (baculovirus inhibitor of apoptosis repeat; IAP) domain by the algorithm of protein structure prediction[80]. This domain was found in the number of proteins involved in the regulation of cell cycle, proliferation, cytokinesis, mitotic spindle formation and apoptosis thus generally acting as regulators of cell division[81,82].

At the same N-terminal end NIPA possesses beside the ZnF also an F-box motif what altogether allows to classify it in the FBXO family of F-box proteins. NIPA defines a nuclear SCF-type ubiquitin E3 ligase (SKP1-ROC1-CUL1-^{NIPA}), which targets nuclear cyclin B1 for ubiquitination and proteasomal degradation in interphase[83]. The activity of MPF must be exquisitely controlled, particularly during interphase, since the untimely activation can trigger premature mitotic entry, thereby compromising the fidelity of

genome replication. Next to the cytoplasmic sequestration, NIPA provides an additional mechanism to inhibit premature nuclear accumulation of cyclin B1 during the mammalian cell cycle.

To enter mitosis cells require accumulation of cyclin B and active MPF formation. Thus cyclin B rise begins after the G_2 phase entrance with the highest peak in mitosis (Fig.1.2). NIPA is phosphorylated at the G_2/M transition what in turn leads to the dissociation from SKP1 and subsequent inactivation of the SCF^{NIPA} E3 ligase. This allows for cyclin B1 accumulation and the cell is able to progress toward mitosis. Therefore NIPA plays a direct role in timing of mitotic entry.

The first cell cycle-dependent phosphorylation of NIPA in late G_2 phase was found to occur at Ser-354[83]. The expression of the phosphorylation-deficient mutant $NIPA^{S354A}$, which forms a constitutively active $SCF^{NIPA\text{-}S354A}$ complex, was reported to block cyclin B1 accumulation and to delay mitotic entry. Later on, a 50-amino-acid region spanning from amino acids 352-402 was identified in the C-terminus of NIPA as the relevant binding region to its substrate cyclin B1[84]. In the same study phosphorylation of two additional serine residues, Ser-359 and Ser-395, was identified as necessary for efficient dissociation of NIPA from the SCF core. Cyclin B1/CDK1 was shown to be involved in the G_2/M-specific phosphorylation of NIPA both *in vitro* and *in vivo*, and Ser-395 was pointed as a relevant phosphorylation site[84]. This exemplifies a positive feedback-loop where cyclin B1/CDK1 augments own activity through the phosphorylation and inactivation of its regulator. Recently, Illert et al. specified Ser-354 and Ser-359 to undergo ERK2 dependent phosphorylation as a crucial initial step for SCF^{NIPA} inactivation at the G_2/M transition[85]. Thus existing model suggest that the initial phosphorylation at Ser-354 and Ser-359 leads to dissociation of the SCF^{NIPA} complex initiating its inactivation, and cyclin B1/CDK1 accumulation enhances phosphorylation of Ser-395 thereafter, to ensure its own activity. Interestingly, NLS in NIPA is located at the same amino acid region as the binding site of cyclin B1. The presence of this motif in the substrate-binding region suggests an evolutionary mechanism, which ensures only nuclear interaction between cyclin B1 and SCF^{NIPA}, since the proteasomal degradation of cyclin B1 occurs exclusively in the nucleus[84,85]. NIPA siRNA treated mitotic HeLa cells, were found arrested in prometaphase. This phenotype however cannot be explained with the elevated nuclear cyclin B1 levels like it was by the premature mitotic entry. The observed prometaphase arrest may indicate an involvement of another important substrates, which could be ubiquitylated by NIPA[78,83].

The phosphorylated form of NIPA disappears in the late mitosis while simultaneously nonphosphorylated protein starts to accumulate. APC/C^{CDH1} is responsible for this late mitotic degradation by targeting phosphorylated NIPA for the ubiquitylation and proteasomal degradation. However, not phosphorylation itself triggers this turnover but the following dissociation of NIPA from the SCF complex. Binding to the SKP1 subunit of SCF seems to protect NIPA from the APC/C-mediated depletion, restricting degradation exclusively to the phosphorylated form[86]. Hence one cell cycle guardian is hunted by another demonstrating the complexity of the cell cycle control.

NIPA-deficient mice are viable, develop normally and no obvious malformations were found with the exception of the gonads. In comparison to control mice, $NIPA^{-/-}$ animals characterize compromised size with complete infertility of males, showing progressive atrophy of the gonads, and reduced fertility of females. $NIPA^{-/-}$ zygotene and early pachytene spermatocytes fail to complete meiotic prophase by aberrant SC formation and asynapsis, therefore arrest at the epithelial stage IV checkpoint and undergo apoptosis[87]. Brain and liver tissues as well as GCs from NIPA deficient mice showed high levels of cyclin B1 in the nucleus, consistent with already described function of SCF^{NIPA}. Also cytological markers for meiotic double strand brake repair (DSB) proteins like DMC1 were persistently exhibited in $NIPA^{-/-}$ meiocytes arguing for an involvement of NIPA in the repair of DSBs. Additionally, NIPA-deficient spermatocytes exhibit abnormalities in SYCP3 staining indicating possible chromosome axis defects together with abnormalities in STAG3 staining often associated with compromised chromosome axis integrity, leading to overt chromosome fragmentation[87].
Ba/F3 cells were protected from IL-3 withdrawal-induced apoptosis by over-expression of NIPA wild-type protein and the nuclear localization was shown essential for its anti-apoptotic function. That's why it has been suggested, that NIPA could regulate the transcription of anti-apoptotic proteins[77]. Also preliminary data show that NIPA is phosphorylated after exposition to DNA damaging agents in a time-and-dose-dependent manner[78]. Therefore it is intriguing to consider NIPA as a player in the DNA damage response pathway.

1.3 The DNA damage response (DDR)

Each human cell has to face a rate of about 50 endogenous double strand breaks (DSBs) per mammalian cell cycle in most cases due to the reactive oxygen intermediates or inaccurately replicated DNA[88]. Additionally, cells will suffer from exogenous environmental risk factors like UV light, chemicals or radiation, which could lead to the harmful chromosomal re-arrangements and result in genomic instability or even cell death[89]. Since a single unrepaired DNA damage can cause dangerous mutations or death it has been clear that the cell developed a very efficient and sophisticated mechanism evolved to detect and repair any DNA break.

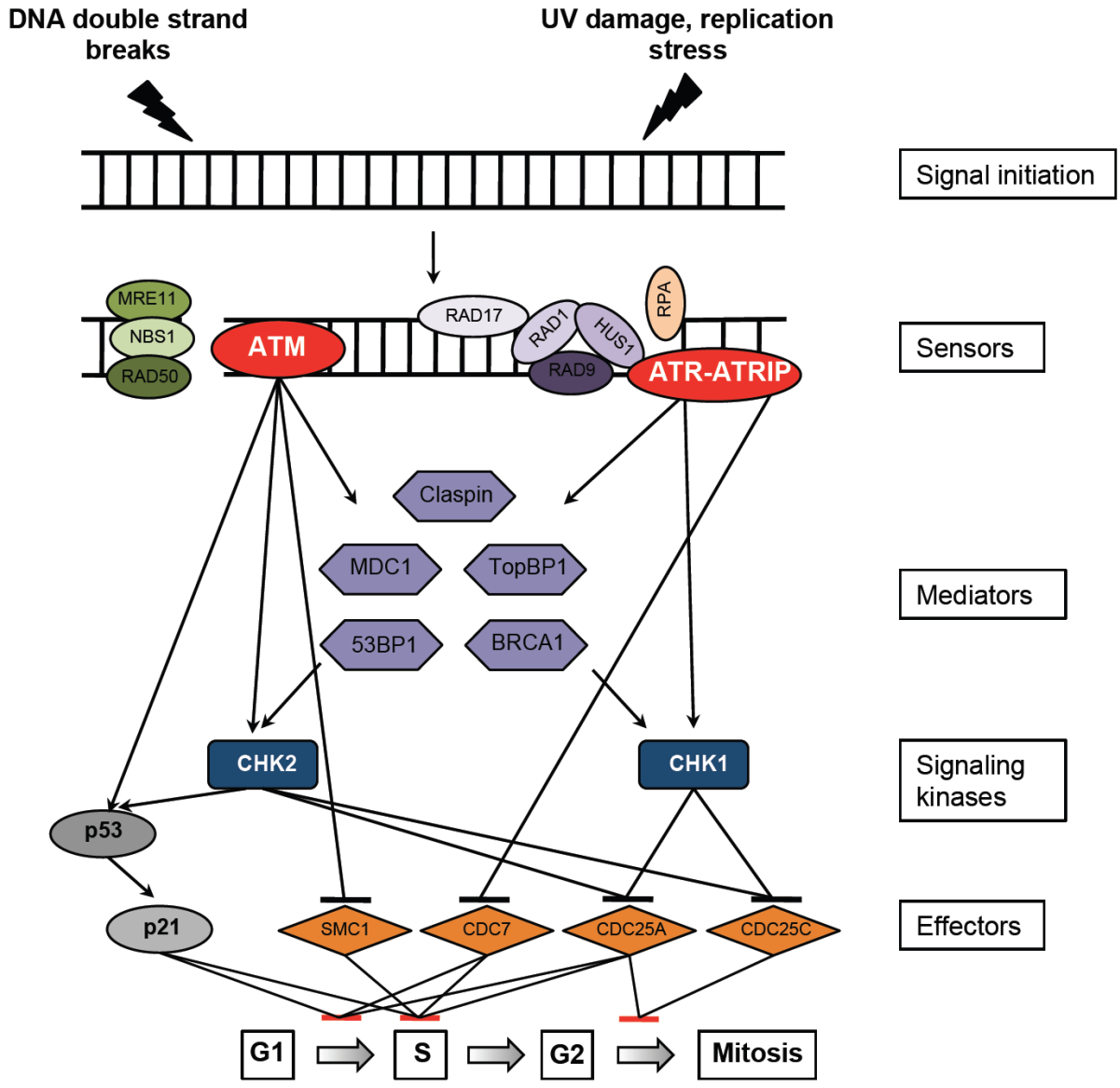

Fig. 1.6: Model of DNA damage checkpoints. Cell cycle phases: G_1, S, G_2, Mitosis. Bars indicate inhibition, arrows indicate activation (Adapted from Li and Zou, 2005)[90].

Major categories of DNA lesions include dimmers, mismatches, base modifications, bulky adducts, intrastrand and interstrand cross-links, single strand breaks (SSB) and DSBs. Base excision repair (BER), nucleotide excision repair (NER), nonhomologous-end-joining (NHEJ) or homologous recombination repair (HRR or HR) are specialized repair pathways, which detect each type of a lesion by the damage recognition proteins[91-94].

1.3.1 DNA damage signaling pathways

ATM and ATR protein kinases, known as "sensors" of DNA damage, are the earliest signaling molecules that are known to initiate the transduction cascade at a site of damage. After the initial activation by the sensors, different "mediators" carry over to recruit or stimulate other kinases involved in further processing of repair function. Concomitant to the repair of the breaks, a rapid signaling cascade must be coordinated at the lesion site that leads to the activation of cell cycle checkpoints and/or apoptosis[90] (Fig.1.6).

1.3.1.1 ATM signaling pathway

In the standard paradigm of DNA damage signaling ATM kinase pathway is activated in response to DNA double strand breaks[95]. ATM is autophosphorylated after exposure to ionizing radiation on multiple residues what is crucial for maintaining ATM activation by the dissociation of inactive homodimmers[96]. Upon activation ATM monomer is recruited to the site of damage and induces phosphorylation on Ser139 of histone 2A.X (H2A.X)[97]. This in turn attracts MDC1 protein, which functions as a molecular bridge between the phosphorylated H2A.X (γH2A.X) and the NBS1 component of the MRN complex (MRE11, RAD50 and NBS1)[98]. Mediator of DNA damage checkpoint 1 (MDC1) builds a platform to promote transient multiple interactions of checkpoint and repair proteins near the DNA damage sites. MRN complex was shown to sustain autophosphorylation of ATM and possibly targets activated ATM to the sites of DNA damage[99]. MDC1 and γH2AX allow for recruitment of many additional factors, among them 53BP1 and BRCA1, leading to the generation of IR-induced foci (IRIF)[100]. Phosphorylation of MDC1 recruits RNF8, an E3 ubiquitin ligase, which ubiquitinates γH2A.X and possibly other substrates for the subsequent recruitment of 53BP1 and BRCA1[101]. Histone ubiquitination has been suggested in the remodeling of chromatin in order to facilitate accumulation of the DNA repair proteins[102]. Activation of p53 and

CHK2 by ATM is mediated by 53BP1, however it is not clear if its precise function is downstream or upstream of ATM[103]. In the pathway leading to the assembly of repair/signaling foci in response to damage, 53BP1 is able to control BRCA1 to form foci. BRCA1 instead is a downstream target of ATM and contributes to the cell cycle arrest and DNA repair mechanism[104]. After signaling transduction and successful IRIF formation, ATM in concert with mediators induces cell cycle arrest to promote DNA damage repair mechanisms.

1.3.1.2 ATR signaling pathway

In contrast to ATM, ATR seems to recognize molecular species of single-stranded DNA (ssDNA) flanked by the double-stranded DNA. The first ssDNA sensing protein is replication protein A (RPA), which detects and binds any abnormal stretch of ssDNA, such as arrested replication fork. RPA recruits ATR protein to the ssDNA through its regulatory subunit ATR-interacting protein (ATRIP)[105]. It has been shown that activation of ATR through ATRIP requires direct interaction with TopBP1 through a PIKK regulatory domain[106]. TopBP1 functions in both, initiation of DNA replication and checkpoint signaling[107]. Once the active ATR kinase is localized to the ssDNA region, it can phosphorylate further critical substrates, such as the clamp-loading, RAD17-containing complex, which participates in the loading of the RAD9-RAD1-HUS1 (9-1-1) sliding clamp onto chromatin[108]. The next crucial step is the independent recruitment of claspin to the damage site and its phosphorylation by ATR. Phosphorylated claspin may recruit BRCA1 and CHK1 to ATR for the phosphorylation and activation of the appropriate cell-cycle checkpoints[109,110].

1.3.1.3 Cross talk between ATM and ATR

Our current understanding places ATM and ATR in two separate and alternate pathways of checkpoint activation, whereas ATM is primarily activated by DSBs in contrast to the activation of ATR driven by the ssDNA. Although ATM and ATR respond to the different stimuli they share a common downstream substrates like p53 or BRCA1[110]. Also recent studies have shown that ATM and ATR function in the same signaling pathway leading to the phosphorylation of CHK1[111]. Regulatory involvement of ATM and NBS1 in the formation of RPA-coated ssDNA, essential for ATR recruitment, could be a possible explanation[112]. Importantly, MRE11-nuclase activity is also required[113]. Additionally Jazayeri et al. showed that the activation of ATR induced by DSBs is regulated during the

cell cycle, where ATM triggers the efficient generation of RPA-coated ssDNA, ATR recruitment and CHK1 phosphorylation only in S and G_2 phases. Therefore this model could be restricted only to cells with high CDK activity[112]. Other group suggested ATR loading onto chromatin in response to IR as the ATM-dependent event, demonstrating an active cross talk between ATM and ATR in the DNA damage response[114].

After functional signal transduction from the damage site, cell has to switch on a repair mechanism to ensure genome integrity. Two major pathways efficiently repair DSBs: nonhomologous-end-joining and homologous recombination

1.3.2 Nonhomologous-end-joining (NHEJ)

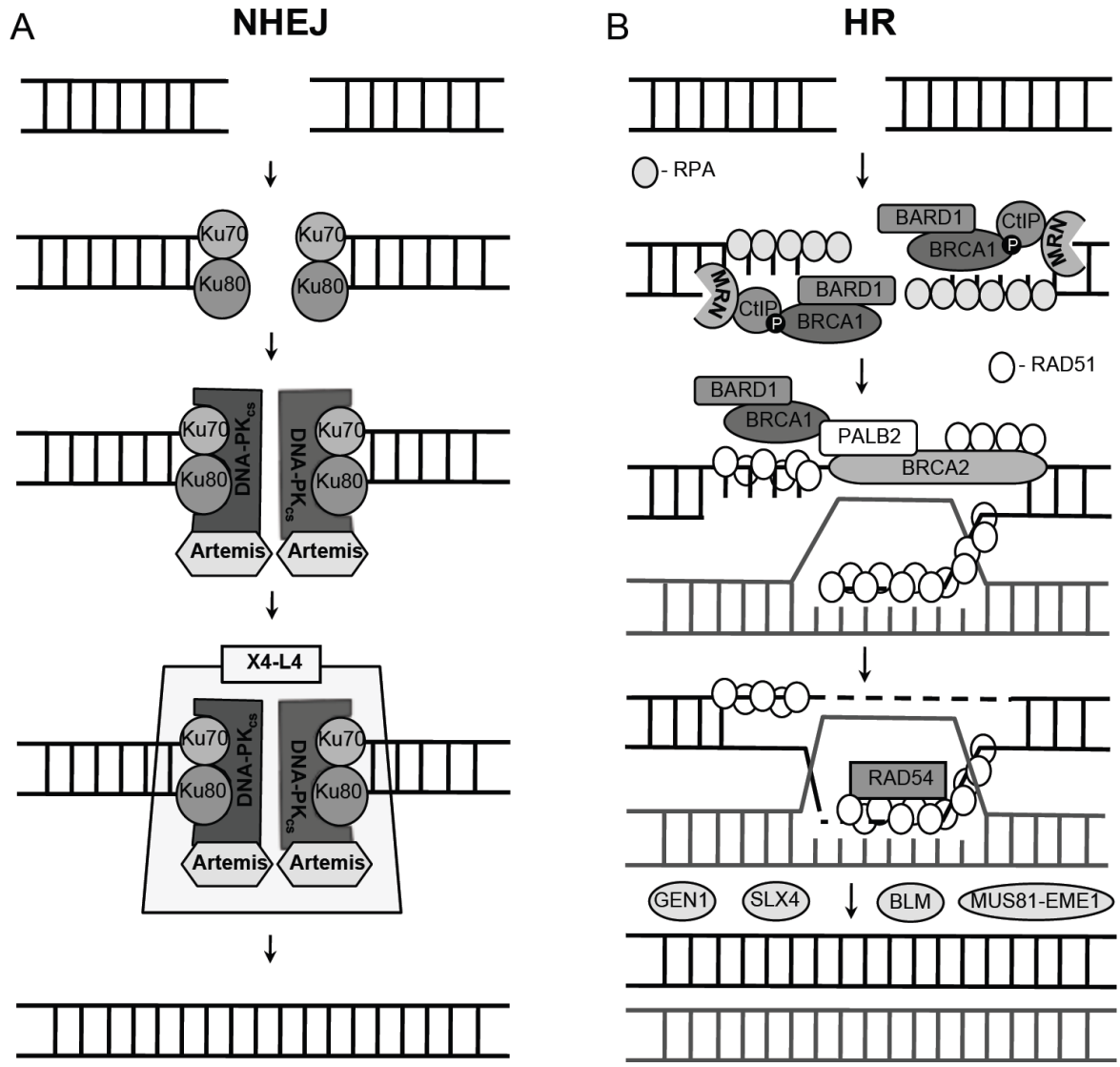

Fig. 1.7: Schematic, simplified mechanisms of double strand break repair. (A) Nonhomologous-end-joining (NHEJ) repair pathway. (B) Homologous recombination repair (HR) pathway.

Nonhomologous-end-joining is an error prone mechanism of DNA damage repair, which modifies the broken DNA ends and ligates them together with little or no homology, generating deletions or insertions. It is active throughout the cell cycle, with a major DSB repair capability in G_1 phase. NHEJ is also indispensable in the V(D)J recombination, an intrinsic DSB production and repair in vertebrate immune system as a mechanism of diversification of the B- and T-lymphocyte repertoire.

The overall course of action in NHEJ can be summarized in three steps: (i) end- binding and bridging, (ii) terminal processing, and (iii) ligation (Fig. 1.7 A). In the initial step Ku70/Ku80 heterodimer protein binds in a structure-specific manner and with high affinity to DNA ends, promoting alignment of the two DNA termini[115]. Ku recruits DNA-PK_{cs} (DNA-dependent protein kinase catalytic subunit), a 460 kDa member of the PIKKs (phophoinositide 3-kinase-like family of protein kinases), and activates its kinase function. Inward translocation of Ku allows for two DNA-PK_{cs} to contact DNA, and form synapse between the two DNA ends[116]. In order to further process the repair function, termini must be transformed to 5'-phosphorylated ligatable ends. This step is mediated by the 5'-to-3' exo- and endonuclease activity of a member of the matallo-β-lactamase superfamily protein – Artemis – which is a key end-processing enzyme recruited to the DSBs through an interaction with DNA-PK_{cs}[117]. NHEJ is completed by the ligation of the DNA ends carried out by the X4-L4 complex (XRCC4, DNA ligase IV and XLF). XRCC4 acts as a scaffold on Ku and DNA, stimulating together with XLF the activity of DNA ligase IV, which is able to ligate compatible overhangs as well as blunt ends[118-120].

1.3.3 Homologous recombination (HR)

Homologous recombination is a very precise repair mechanism, in which homologous chromatid serves as a template to guide the repair of broken strand with a high fidelity. It has been reported to be active only during S and G_2 phases of the cell cycle, when the sister chromatids are available.

HR requires processing of the DSB to yield ssDNA containing a 3'-hydroxyl overhang (Fig.1.7 B). In the initial steps the site of DNA damage is recognized by the MRN complex holding the broken DNA ends and is followed by the recruitment of BRCA1-CtIP (CtBP-interacting protein) through a direct binding to phosphorylated CtIP. BRCA1-CtIP together with MRN complex, mediates DSB end resection that generates ssDNA overhangs[121,122]. The ssDNA is than rapidly bound by RPA, which dissolves the DNA's secondary structure. RPA binds very efficiently to ssDNA however DNA strand invasion

and homology search steps of HR require the formation of RAD51 recombinase nucleoprotein filaments bound to ssDNA[123]. A critical mediator complex, including BRCA1/BARD1 (BRCA1-associated RING domain) and BRCA2 (breast cancer type 2 susceptibility protein) bridged by the PALB2 (partner and localizer of BRCA2), is involved in the loading of RAD51 onto ssDNA and in the displacement of RPA[124,125]. BRCA1 ubiquitin function has been also implicated in HR[126]. Direct RAD51-loading function is provided by BRCA2, which interacts directly with RAD51[127]. The role of RAD51 is critical in homology-mediated repair and its deficiency leads to early embryonic lethality[128]. In the next step RAD51 captures duplex DNA and searches for homology. Strand invasion into a homologous sequence forms a D-loop intermediate and the 3'-end of the invading strand is extended by a polymerase. Holliday junctions (HJs) are formed if the D-loop captures the second end of the break. After the formation of HJ, ATP-dependent branch migration occurs along the DNA in both directions, generating heteroduplex DNA promoted by the RAD54 protein[129]. Resolution of HJ can lead to the crossover or non-crossover products, however crossing over is rare in somatic cells[120]. Different enzyme complexes can execute HJ resolution: BLM (Bloom's syndrome gene) together with topoisomerase IIIα can lead to non-crossover products, MUS81-EME1 complex may cleave HJs to produce crossovers, GEN1 can promote junctions resolution by symmetrical cleavage to produce both non- and crossovers, and recently reported SLX4 has been also reported able for Holliday junction resolution in eukaryotes[130-133].

1.4 Nuclear pore complex (NPC)

The nuclear pore complex (NPC), a supramolecular assembly embedded in the double nuclear membrane of the nuclear envelope (NE), is mainly responsible for the trafficking between the nucleus and the cytoplasm. Its core structure of eightfold-radial symmetry consists of central globular subunits, which encases the main nuclear transport channel flanked by a ring-like structure at both the cytoplasmic and the nucleoplasmic side. The nuclear ring is assembled from eight long fibrils that join to form a distal ring – a structure called nuclear basket. Asymmetrical filamentous structures are building peripheral cytoplasmic NPC extensions, connecting it to its molecular milieu outside the nucleus[134]. NPC is assembled of multiple copies of about 30 different proteins called nucleoporins (NUPs). These proteins are assigned to particular substructures in the NPC and can be classified into six groups: (1) integral transmembrane proteins of the

nuclear envelope pore membrane domain (POMs), (2) core scaffold (inner ring and outer ring), (3) adaptor nucleoporins, (4) channel nucleoporins, (5) nuclear basket nucleoporins and (6) cytoplasmic filament nucleoporins[135] (Fig. 1.8).

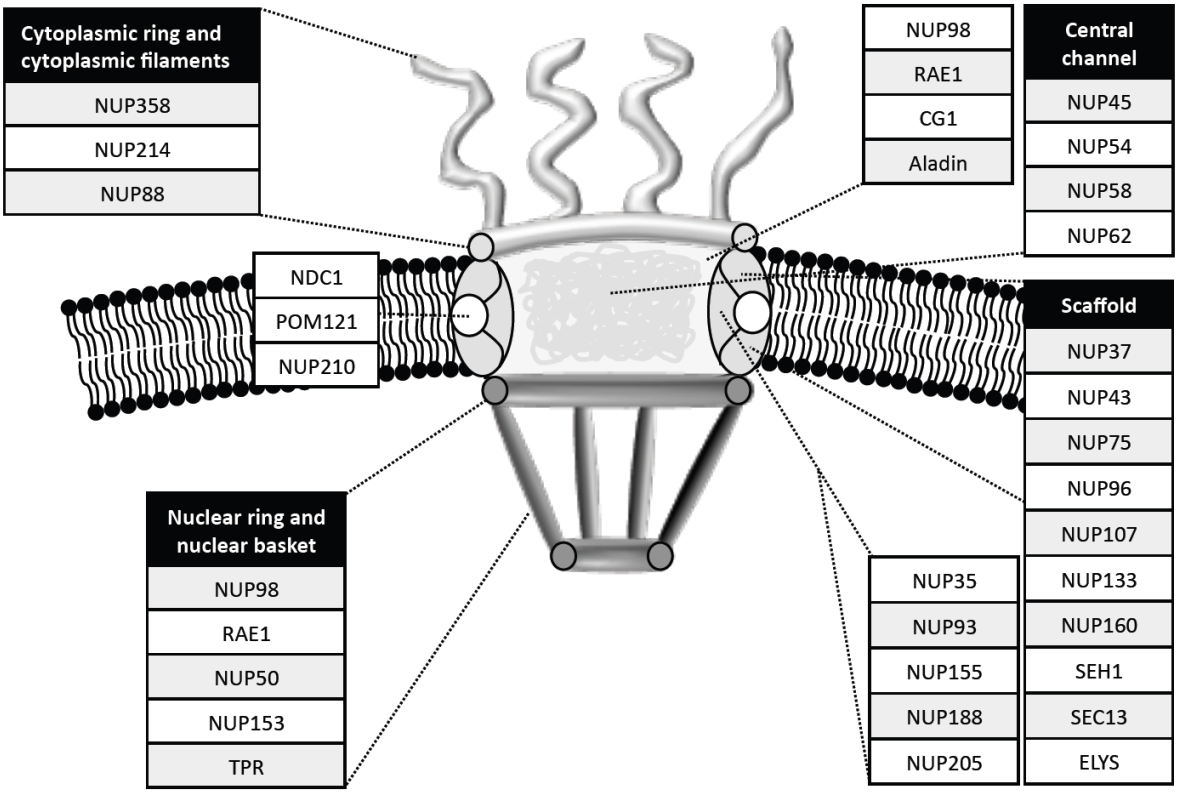

Fig. 1.8: Schematic illustration of the nuclear pore complex (NPC). Depicted the cross-section perpendicular to the plane of the nuclear envelope. Nucleoporins are presented in boxes. CG1: candidate gene 1; NDC1: nuclear division cycle protein; POM121: pore membrane protein of 121 kDa; RAE1: RNA export 1; SEH1: SEC13 homologue protein 1 (Adapted from Raices et al., 2012)[136]

Nucleoporins possess limited set of domains, including transmembrane domains (found in only 4 mamalian NUPs), α-helices, β-propellers, WD domains and most common Phe-Gly (FG) repeats. NUPs carrying FG repeats fill the central channel of the NPC and through a meshwork formation control the nucleocytoplasmic transport.

Cytoplasmic filaments are composed of NUP88, NUP214/CAN and NUP358/RANBP2 (RAN binding protein 2). Nucleoporin NUP358 is a SUMO E3 ligase, which provides binding sites for RAN and RanGAP1 transport factors[135]. Proteins which forms NPC scaffold, such as NUP107-160 complex, are stably embedded in the NE in contrast to themore peripheral, highly dynamic components like NUP50 or NUP153[137]. The nuclear basket consists mainly of NUP153, localized at the terminal ring, and the nucleoplasmic fibrils, as well as NUP98 and NUP93[138,139]. NUP153 tethers a 267 kDa coiled coil protein

– TPR (translocated promoter region) to the basket through a direct interaction, suggesting that these nucleoporins may be involved in holding NPC in place[138,140].

NPC assembly takes place at the end of mitosis, when the nuclear envelope reforms around the segregated chromosomes. It is rebuilt from the cytoplasmic subcomplexes dispersed after the NE breakdown in a highly organized stepwise manner. In the first steps, the scaffold complex NUP107-160 essential for NPC assembly is recruited onto chromatin, followed by recruitment of NUP153 and NUP50 proteins. These early recruited nucleoporins together with others not yet analyzed NUPs may form a chromatin-bound intermediate that creates a binding platform for the recruitment of transmembrane and more peripheral NUPs for the final assembly of the functional NPC[139]. Disassembly of the NPC takes place at the beginning of mitosis when the NE breaks down. It is also an organized process however it doesn't occur in exact reverse order. First, the basket nucleoporins NUP98, NUP153 and TPR are released followed by the release of NUP214 from the cytoplasmic ring. NUP107-160 complex is released before the later recruited central channel protein NUP58. Subsequent release of peripheral NUPs leads to the loss of nuclear permeability[139,141].

Nucleocytoplasmic transport is a main function of the NPC. Ions and small proteins (<40 kDa) can diffuse through the pore, however bigger proteins have to be actively transported. During nuclear import, cargo binds to the transport receptor importin in cytoplasm, which interacts with FG reach repeats of NUPs at the NPC and pass through the central transport channel. Upon entrance to the nucleus transport receptor binds to RAN-GTP and through a conformational change allows for the release of cargo, with subsequent translocation of RAN-GTP and importin back to the cytoplasm. During nuclear export instead, cargo binds to exportins and RAN-GTP in the nucleus and moves through the NPC to the cytoplasm. The dissociation of export complexes is triggered at the cytoplasmic filaments of the NPC by an interaction of RAN GTPase-activating protein (RANGAP) and RANBP1 or RANBP2. RAN-GTP levels are restored by the action of RAN exchange factor (RCC1) after the NTF2 mediated translocation of RAN-GDP complexes back to the nucleus[142].

In the past decade, it has become clear that NPC plays an important role in additional not transport-related processes. It is implied to play a role in gene expression and transcription, regulation of genome architecture, cell cycle control, differentiation and development, modulation and activity of sumoylation and desumoylation enzymes as well as in DNA damage repair[136,139,143]. Thus future studies may allow us to uncover

many new cellular roles for these structures and to gain new insights into already discovered functions.

1.5 Aims of the thesis

Proper regulation of cellular processes including cell cycle and checkpoint activation in response to genotoxic threats is crucial to maintain genomic stability. NIPA was characterized as a cell cycle regulatory protein, controlling the proper timing of mitosis by ubiquitylation and degradation of cyclin B1 in interphase. NIPA itself was shown regulated by phosphorylation in the cell cycle dependent manner. Posttranslational modification was also proposed for NIPA after induction of DNA damage with UV irradiation. Given that NIPA was implicated in the antiapoptotic function, it role in the DNA damage response has become more apparent.

The main goal of this thesis was to study involvement of NIPA in the regulation of distinct DNA repair mechanisms. It was aimed to gain more insights into how NIPA could regulate the cellular homeostasis after DNA damage. Finally, it was sought to understand the detailed mechanistic role of NIPA in the DNA damage repair signaling pathways. Thus, the interplay between cell cycle regulation and the DNA damage response is a potential target for anticancer therapies and better understanding of these processes could provide us with powerful tools in fight against human malignancies.

2 Materials and methods

2.1 Materials

2.1.1 Antibodies

Anti-β-Actin (AC-15) Mouse mAb IgG_1	Sigma-Aldrich, Deisenhofen
Anti-β-Tubulin (AA2) Mouse mAb IgG_1	Sigma-Aldrich, Deisenhofen
Anti-FLAG (M2), Maus mAb IgG1	Sigma-Aldrich, Deisenhofen
Anti-FLAG (M2), Agarose coupled	Sigma-Aldrich, Deisenhofen
Anti-Goat IgG, Alexa Fluor® 594, Goat IgG	Invitrogen, Karlsruhe
Anti-Goat IgG, HRP-conjugated, Donkey IgG	Santa Cruz Biotech., Heidelberg
Anti-HA (Y-11), Rabbit pAb IgG	Santa Cruz Biotech., Heidelberg
Anti-HA, Agarose coupled pink	Sigma-Aldrich, Deisenhofen
Anti-p-Histone H2A.X (Ser^{139}) Mouse mAb IgG_1	Millipore, Darmstadt
Anti-p-Histone H2A.X (Ser^{139}) Rabbit mAb IgG	Cell Signaling, Beverly (USA)
Anti-MDC1 (ab11169) Rabbit pAb IgG	Abcam, Cambridge (UK)
Anti-Mouse IgG, Alexa Fluor® 488, Goat IgG	Invitrogen GmbH, Karlsruhe
Anti-Mouse IgG, Alexa Fluor® 594, Goat IgG	Invitrogen GmbH, Karlsruhe
Anti-Mouse IgG, HRP-conjugated, Donkey IgG	Amersham, Braunschweig
Anti-NIPA (B-10) Mouse mAb IgG_1	Santa Cruz Biotech., Heidelberg
Anti-p-NIPA (Ser^{354} ab63557) Rabbit pAb IgG	Abcam, Cambridge (UK)
Anti-NUP153 (QE5) Mouse mAb IgG_1	Abcam, Cambridge (UK)
Anti-Rabbit IgG, Alexa Fluor® 488, Goat IgG	Invitrogen, Karlsruhe
Anti-Rabbit IgG, Alexa Fluor® 594, Goat IgG	Invitrogen, Karlsruhe
Anti-Rabbit IgG, HRP-conjugated, Donkey IgG	Amersham, Braunschweig
Anti-RAD51 (H-92) Rabbit pAb IgG	Santa Cruz Biotech., Heidelberg
Anti-TPR (C-20) Goat pAb IgG	Santa Cruz Biotech., Heidelberg
Anti-ZC3HC1 Rabbit pAb IgG	Sigma-Aldrich, Deisenhofen
Anti-53BP1 (ab36823) Rabbit pAb IgG	Abcam, Cambridge (UK)

2.1.2 Bacterial strains

Escherichia Coli DH5α™ F-Φ80d*lac*ZΔM15, Δ(*lac*ZYA-*arg*F)U169, *deo*R, *rec*A1, *end*A1, *hsd*R17(r_K^-, m_K^+), *pho*A, *sup*E44, λ-*thi*-1, *gyr*A96, *rel*A1	Invitrogen GmbH, Karlsruhe
Epicurian Coli™ XL-1 Blue Supercompetent Cells *rec*A1, *end*A1, *gyr*A96, *thi*-1, *hsd*R17, *sup*E44, *rel*A1, *lac* [F'*pro*AB, *lacI*^{q}ZΔM15 Tn10 (Tet^r)]	Stratagene, Heidelberg
OneShot® BL21 Star™ (DE3) Chemically Competent E.coli F- *omp*T, *hsd*SB(rB-,mB-), *gal*, *dcm*, *rne*131 (DE3)	Invitrogen GmbH, Karlsruhe

2.1.3 Chemicals and reagents

Acetic acid, glacial	Roth, Karlsruhe
Acetone	Fluka, Deisenhofen
Acrylamide/Bis-acrylamide	Roth, Karlsruhe
Agarose	Roth, Karlsruhe
Agarose, comet assay	Amresco, Solon (USA)
Agarose, low melting comet assay	Serva, Heidelberg
Ammonium acetate	Sigma-Aldrich, Deisenhofen
Ammonium chloride	Fluka, Deisenhofen
Ammonium persulfate (APS)	Sigma-Aldrich, Deisenhofen
Ampicillin	Sigma-Aldrich, Deisenhofn
Bacto Agar	Difco, Detroit (USA)
Bacto Tryptone	Difco, Detroit (USA)
Bacto Yeast Extract	Difco, Detroit (USA)
BES Buffered Saline	Sigma-Aldrich, Deisenhofen
Bleomedac® bleomycin sulfate	Medac, Hamburg
Bromophenol blue	Sigma-Aldrich, Deisenhofen
Bovine serum albumin, BSA Fraction V	Roth, Karlsruhe
Calcium chloride	Roth, Karlsruhe
Chloroquine diphosphate salt	Sigma-Aldrich, Deisenhofen

Crystal violet	Sigma-Aldrich, Deisenhofen
Complete™ Protease Inhibitor Cocktail	Boehringer, Mannheim
Cycloheximide (CHX)	Sigma-Aldrich, Deisenhofen
D-desthiobiotin solution (10x Buffer E)	IBA, Göttingen
Dimethylsulfoxide (DMSO)	Sigma-Aldrich, Deisenhofen
Disodium hydrogen phosphate (Na_2HPO_4)	Merck, Darmstadt
Dithiothreitol (DTT)	Promega, Heidelberg
dNTP-Mix, 10mM	Invitrogen GmbH, Karlsruhe
Ethanol	Merck, Darmstadt
Ethidium bromide	Roth, Karlsruhe
Ethylenediaminetetraacetic acid (EDTA)	Fluka, Deisenhofen
Etoposide	Sigma-Aldrich, Deisenhofen
FLAG-peptide 3x	Sigma-Aldrich, Deisenhofen
Formaldehyde solution	Sigma-Aldrich, Deisenhofen
GeneRuler 1kb DNA Ladder	Fermentas, St. Leon-Rot
Glucose	Roth, Karlsruhe
Glycerol	Fluka, Deisenhofen
Glycerin	Fluka, Deisenhofen
Glycerol-2-phosphate	Sigma-Aldrich, Deisenhofen
Glycine	Merck, Darmstadt
Hexadimethrine bromide (Polybrene)	Sigma-Aldrich, Deisenhofen
Hydrochloric acid	Merck, Darmstadt
Isopropanol	Merck, Darmstadt
Magnesium chloride	Roth, Karlsruhe
Methanol	Merck, Darmstadt
MG132, proteasome inhibitor	Sigma-Aldrich, Deisenhofen
Milk powder	Fluka, Deisenhofen
Monosodium phosphate (NaH_2PO_4)	Merck, Darmstadt
Nonidet® P 40 Substitute	Fluka, Deisenhofen
Ocadaic acid	Sigma-Aldrich, Deisenhofen
Penicillin/Streptomycin solution	PAA, Pasching
Percoll®	Sigma-Aldrich, Deisenhofen
Phosphate buffered saline (PBS), 10X solid	Biochrom AG, Berlin
Potassium bicarbonate	Sigma-Aldrich, Deisenhofen

Potassium chloride	Merck, Darmstadt
Propidium iodide	Sigma-Aldrich, Deisenhofen
Protein A Sepharose	GE Healthcare, Freiburg
Protein G Sepharose	GE Healthcare, Freiburg
PVDF membrane (Immobilon P)	Millipore, Schwalbach/Ts
Ribonuclease A	Sigma-Aldrich, Deisenhofen
Silver nitrate	Merck, Darmstadt
Sodium azide	Sigma-Aldrich, Deisenhofen
Sodium carbonate	Sigma-Aldrich, Deisenhofen
Sodium chloride	Roth, Karlsruhe
Sodium dodecyl sulfate (SDS)	Roth, Karlsruhe
Sodium fluoride	Fluka, Deisenhofen
Sodium hydroxide, pellets	AppliChem, Darmstadt
Sodium orthovanadate	Sigma-Aldrich, Deisenhofen
Sodium thiosulfate	Sigma-Aldrich, Deisenhofen
Strep-Tactin® Superflow® beads	IBA, Göttingen
SuperSignal® Chemiluminescent Substrate	Thermo Fisher, Karlsruhe
Tetramethylethylenediamine (TEMED)	Fluka, Deisenhofen
Thymidine	Sigma-Aldrich, Deisenhofen
Trichloroacetic acid	Fluka, Deisenhofen
Tris-(hydrohymethyl)-aminomethan (TRIS)	Roth, Karlsruhe
Trisodium citrate	Fluka, Deisenhofen
Triton X-100	Sigma-Aldrich, Deisenhofen
Trypan blue	Invitrogen GmbH, Karlsruhe
Tween 20	Fluka, Deisenhofen

2.1.4 Enzymes

2.1.4.1 Restriction enzymes

BamHI (100 U/µl)	Fermentas, St. Leon-Rot
BglI (10 U/µl)	Fermentas, St. Leon-Rot
DpnI (10 U/µl)	Fermentas, St. Leon-Rot
EcoRI (100 U/µl)	Fermentas, St. Leon-Rot
KpnI (10 U/µl)	Fermentas, St. Leon-Rot

MfeI (10 U/µl)	Fermentas, St. Leon-Rot
NheI (10 U/µl)	Fermentas, St. Leon-Rot
NotI (10 U/µl)	Fermentas, St. Leon-Rot
SalI (10 U/µl)	Fermentas, St. Leon-Rot
XbaI (10 U/µl)	Fermentas, St. Leon-Rot
XhoI (100 U/µl)	Fermentas, St. Leon-Rot

2.1.4.2 DNA polymerases

Phusion Hot Start-DNA Polymerase	Fermentas, St. Leon-Rot
Pfu-DNA Polymerase	Fermentas, St. Leon-Rot
Taq-DNA Polymerase	Fermentas, St. Leon-Rot

2.1.4.3 Other enzymes

CIAP 20-30 U/µl (Alkaline Phosphatase)	Invitrogen, Karlsruhe
T4-DNA Ligase	Fermentas, St. Leon-Rot

2.1.5 Mammalian cell lines

HEK-293T (human embryonic kidney)	DSMZ, Braunschweig
HeLa (human cervical cancer)	DSMZ, Braunschweig
K562 (human chronic myeloid leukemia)	DSMZ, Braunschweig
NIH/3T3 (mouse embryonic fibroblast)	DSMZ, Braunschweig
MEF NIPA $^{-/-}$ (mouse embryonic fibroblast)	A.L.Illert, MRI, München
MEF NIPA $^{+/+}$	
ΦNX-ECO (PhoenixE)	G.P.Nolan, Stanford (USA)
U2OS (human osteosarcoma)	ATCC, Wesel
U2OS DR-GFP	S.Y.Lin, Houston (USA)

2.1.6 Materials and kits for molecular biology

APO-DIRECT™ Kit	BD Biosciences, Heidelberg
Bio-Rad Protein Assay	Bio-Rad, München
GeneRuler™ 1kb DNA Ladder	Thermo Fisher, Waltham (USA)
QIAGEN® Plasmid Maxi Kit	Qiagen, Hilden

QIAGEN® Spin Miniprep Kit	Qiagen, Hilden
QIAquick® Gel Extraction Kit	Qiagen, Hilden
QIAquick® Spin Purification Kit	Qiagen, Hilden
PageRuler™ Prestained Protein Ladder	Thermo Fisher , Waltham (USA)
Rapid DNA Ligation Kit	Roche Diagnostics, Penzberg

2.1.7 Materials for microscopy techniques

4',6-diamidino-2-phenylindole (DAPI)	Sigma-Aldrich, Deisenhofen
High precision microscope cover glasses	Roth, Karlsruhe
Histofluid	Marienfeld, Lauda-Königshofen
Microscopy chamber 1 μ-Slide 8 well ibiTreat	Ibidi, Martinsried
SuperFrost® PLUS microscope slides	Thermo Fisher, Karlsruhe
Comet assay microscope slides ESW-370	Erie Scientific, Portsmouth (USA)
VECTASHIELD® mounting medium	Vector Lab., Burlingame (USA)
SYBR®Green	Molecular Probes, Eugene (USA)

2.1.8 Media and supplements for cell culture

Diptheria Toxin (DT)	Calbiochem, Darmstadt
DMEM, cell culture medium	PAA, Pasching (Austria)
FCS Gold	PAA, Pasching (Austria)
G418 (Neomycin)	Calbiochem, Darmstadt
HANK`s BSS	PAA, Pasching (Austria)
Hygromycin	Calbiochem, Darmstadt
L-Glutamine 100x	Gibco/Invitrogen, Karlsruhe
Lipofectamin® 2000, Transfection reagent	Invitrogen, Karlsruhe
McCoy's 5A modified cell culture medium	Biochrom AG, Berlin
Opti-Mem®	Gibco/Invitrogen, Karlsruhe
PBS, 10X, sterile	PAA, Pasching (Austria)
Pencillin and streptomycin 100x	PAA, Pasching (Austria)
Puromycin	Merck, Darmstadt
RPMI 1640, cell culture medium	PAA, Pasching (Austria)
Trypsin-EDTA- 10X	PAA, Pasching (Austria)

TurboFect®, Transfection reagent	Thermo Fisher, Karlsruhe

2.1.9 Oligonucleotides

All oligonucleotides listed below (except siRNAs) were purchased from Eurofins MWG Operon, Ebersberg.

2.1.9.1 Primers for cloning

FLAG-NIPA BamHI forward
5'-ATAGGATCCGCCACCATGGATTACAAGGATGACGACGATAAGATGGCGGCGCCCTGTGAGGG-3'

miR30 XhoI common forward
5'-CAGAAGGCTCGAGAAGGTATATTGCTGTTGACAGTGAGCG-3'

mir30 EcoRI common reverse
5'-CTAAAGTAGCCCCTTGAATTCCGAGGCAGTAGGCA-3'

NIPA wt XbaI forward
5'-ATGTCTAGAATGGCGGCGCCCTGTGAGGG-3'

NIPA wt BamHI reverse
5'-AATGGATCCTCAGCATGAGCACAGAGATTC-3'

NIPA wt XhoI reverse
5'-AATCTCGAGTCAGCATGAGCACAGAGATTC-3'

NIPA wt XhoI forward
5'-ATGCTCGAGATGGCGGCGCCCTGTGAGGG-3'

Cyclin B1 XhoI forward
5'-AATCTCGAGTTATGGCGCTCCGAGTCACCAG-3'

Cyclin B1 MfeI reverse
5'-AATCAATTGTTACACCTTTGCCACAGC-3'

FLAG-TPR KpnI forward

5’- ATAGGTACCGCCACCATGGATTACAAGGATGACGACGATAAGATGGCGGCGGTGTTGCAG-3’

TPR KpnI forward

5’-ATAGGTACCATGGCGGCGGTGTTGCAGC-3’

TPR NotI reverse

5’-ATAGCGGCCGCATTAATTAATATTTCCTCTG-3’

2.1.9.2 Primers for site directed mutagenesis

Cyclin B1 Ser-200-Glu

5’-GAAGAAAAACTTGAACCTGAGCCTATTTTGG-3’ forward

5’-CCAAAATAGGCTCAGGTTCAAGTTTTTCTTC-3’ reverse

Cyclin B1 Ser-210/212 – Glu

5’-GGTTGATACTGCCGAACCAGAGCCAATGGAAACATC-3’ forward

5’-GATGTTTCCATTGGCTCTGGTTCGGCAGTATCAACC-3’ reverse

Cyclin B1 Ser-217-Glu

5’-CCAATGGAAACAGAAGGATGTGCCCCTG-3’

5’-CAGGGGCACATCCTTCTGTTTCCATTGG-3’

Cyclin B1 Ser-231-Glu

5’-GTGTCAGGCTTTCGAAGATGTAATTCTTG-3’

5’-CAAGAATTACATCTTCGAAAGCCTGACAC-3’

2.1.9.3 Sequencing primers

T3	5’-AATTAACCCTCACTAAAGGG-3’
T7	5’-TAATACGACTCACTATAGGG-3’
MSCV-MCS-5’	5’-CGTTCGACCCCGCCTCGATCC-3’
pBabe-5’	5’-CTTTATCCAGCCCTCAC-3’

2.1.9.4 Small interfering RNA (siRNA) oligonucleotides

Luciferase	5'-CGUACGCGGAAUACUUCGA-3'	Eurofins, Ebersberg
NIPA	5'-CAGAUUGAAUCGUCCAUGATT-3'	Eurofins, Ebersberg
TPR	5'-GUAAUGAGCAAGCCAGTT-3'	Eurofins, Ebersberg

2.1.9.5 MicroRNA (miR) oligonucleotides

NIPA miR Eurofins, Ebersberg

5'-TGCTGTTGACAGTGAGCGACTGGGTCACAGTGGAATGTGATAGTGAAGCCACAG-3'

2.1.10 Software

FlowJo Flow Cytometry Analysis Software, Version 4.6.2	Tree Star, Ashland (USA)
Metafer4	MetaSystems, Altlussheim

2.1.11 Standard instruments

Agarose gel electrophoresis chamber	Biometra, Göttingen
Centrifuge GS-6K	Beckman, Fullerton (USA)
CO_2-Incubator SW J 500 TV BB	Nunc, Wiesbaden
Cold centrifuge J2-HS, Rotor JA-14	Beckman, Fullerton (USA)
Cold centrifuge 5417R, 5810R	Eppendorf, Hamburg
Developer Hyperprocessor	Amersham, Braunschweig
Digital scale LC1200 S	Satorius, Göttingen
Electrophoresis chamber HE 100 Supersub	Amersham, Braunschweig
ELISA Reader SUNRISE	Tecan, Crailsheim
Epifluorescence microscope Axioplan2	Zeiss, Jena
FACS (EPICS® XL)	Beckman-Coulter, Krefeld
Fluorescence microscope	Olympus Optical Co., Hamburg
Incubator HERAcell	Thermo Scientific, Karlsruhe
Incubator-Shaker Innova 4000	New Brunswick Scientific, Edison (USA)
Light microscope Axiovert 25	Zeiss, Jena
LKB Ultraspec III, Spectrophotometer	Pharmacia, Uppsala (Sweden)
Magnetic stirrer IKAMG RH	Janke & Kunkel, Staufen
Microfuge	Tomy Seiko, Tokyo (Japan)

Microscope V 200	Hund, Wetzlar
Mini-Gel Electrophoresis chamber	Biometra, Göttingen
Mini-Gel Long Electrophoresis chamber	Biometra, Göttingen
Neubauer Haemocytometer	Reichert, New York (USA)
PCR-Thermocycler	MWG-Biotech, Ebersberg
pH-Meter Φ32	Beckman, Fullerton (USA)
Power supplier Powerpack P25	Biometra, Göttingen
Sterile work bench HERAsafe	Thermo Scientific, Karlsruhe
Shaker WT 12	Biometra, Göttingen
Stratalinker 2400	Stratagene, Heidelberg
Table centrifuge 5417R	Eppendorf, Hamburg
Thermo heater 5436	Eppendorf, Hamburg
Transphor Electrophoresis Unit	Hoefer, San Francisco (USA)
Trio-Thermoblock	Biometra, Göttingen
Vortex Genie2	Scientific Ind., New York (USA)
Water bath 1083	GFL, Burgwedel

2.1.12 Standard media and buffers

Amidoblack stain:	0.2% Naphtol Blau Schwarz 25% Isopropanol 10% Acetic acid
Amidoblack destain:	25% Isopropanol 10% Acetic acid
Blocking solution for Western blot:	5% BSA or Milk powder 0.1% Tween 20 in PBS
Coomassie stain	0.25% Coomassie-blue 45% Methanol 10% glacial acetic acid
Coomassie destain:	45% Methanol

	10% glacial acetic acid
Cell lysis buffer:	10 mM Tris/HCl (pH 7.5) 130 mM NaCl 5 mM EDTA 0.5% Triton X-100 20 mM Na_2HPO_4/NaH_2PO_4 (pH 7.5)
Denaturing buffer (2x)	2 mM DTT 100 mM Tris/HCl (pH7.5) 1 mM EDTA 2% SDS
DNA loading buffer:	60% Glycerol 0.2% Bromophenol blue 0.2 M EDTA in A.d.
LB medium:	1% Bacto-Tryptone 0.5% Bacto-Yeast extract 1% NaCl
LB-Agar:	1% Bacto-Tryptone 0.5% Bacto-Yeast extract 1.5% Bacto-Agar 1% NaCl
RBC (Red Blood Cell)-Lysis buffer:	150 mM NH_4Cl 1 mM $KHCO_3$ 0.1 mM Na_2EDTA, pH 7.3 in A.d.
Resolving gel buffer for SDS-PAGE (4x):	1.5 M Tris (pH 8.8) 0.4% SDS in A.d.

SDS-PAGE running buffer:	25 mM Tris 192 mM Glycine 0.1% SDS in A.d.
SDS-PAGE loading buffer (2x):	1 M Tris/HCl (pH 6.8) 200 mM DTT 4% SDS 0.2% Bromophenol blue 20% Glycine in A.d.
Stacking gel buffer for SDS-PAGE (4x):	0.5 M Tris (pH 6.8 < 9) 0.4% SDS in A.d.
TAE buffer (10x):	0.4 M Tris 1.1% Acetic acid 10 mM EDTA (pH 8.0) in A.d.
Western transfer buffer:	25 mM Tris 192 mM Glycine 20% Methanol 0.1% SDS in A.d.

2.1.13 Vectors and DNA constructs

2.1.13.1 Vectors

MSCV MigR1	J.Miller/W.Pear, Philadelphia (USA)
N-SF-TAP-pcDNA3	C.J.Gloeckner/M.Ueffing, München
pAcGFP1-C3	Clontech, Mountain View (USA)
pBabe Puro	J.P. Morgenstern, London (UK)
pBabe Zeo	F.Bassermann, München
pcDNA3.1 Zeo (+)	Invitrogen, Karlsruhe
pLMP	Thermo Scientific, Karlsruhe

2.1.13.2 DNA constructs

Cyclin B1 5D in mRFP	This work
Ecotropic receptor in pBabe Zeo	F.Bassermann, MRI
Fbx09 in pcDNA3.1/Zeo	F.Bassermann, MRI
Fbw2 in pcDNA3.1/Zeo	F.Bassermann, MRI
Fbw11 in pcDNA3.1/Zeo	F.Bassermann, MRI
FLAG-NIPA wt in pcDNA 3.1/Zeo	T.Ouyang, MRI
FLAG-NIPA wt in MSCV MigR1	C.von Klitzing, MRI
FLAG-NIPA F-Box mutant in pcDNA 3.1/Zeo	F.Bassermann, MRI
FLAG-NIPA ZnF (Zinc finger mutant) in pcDNA3.1/Zeo	C.von Klitzing, MRI
FLAG-NIPA RKK (NLS-mutant) in pcDNA3.1/Zeo	T.Ouyang, MRI
FLAG-NIPA wt in pBabe puro	This work
FLAG-TPR in pcDNA3.1/Zeo	This work
HA-Ubiquitin in pCMV	W.Krek, Zürich (Switzerland)
NIPA miR in pBabe puro	This work
NIPA wt in pcDNA3.1/Zeo (tag free)	C. von Klitzing, MRI
NIPA wt in N-SF-TAP-pcDNA3	This work
NIPA wt in pAcGFP1-C3	This work
NIPA ZnF in pAcGFP1-C3	This work
SceI endonuclease in pCBA	A.Pierce, Lexington (USA)
TPR in pEGFP-C2 (+)	Addgene, Cambridge (USA)

2.2 Methods

2.2.1 Methods based on nucleic acids

2.2.1.1 Agarose gel electrophoresis

Plasmid-DNA as well as DNA-fragments are analyzed and isolated by native agarose gel electrophoresis. Agarose is an algal polysaccharide, which forms a matrix after boiling and subsequent cooling in a buffer. Charged molecules will migrate through the gel in response to an electric field, thus negatively charged nucleic acids are migrating toward anode. Separation of DNA molecules is dependent on the size of the particles. High percentage agarose gels (1.5-2%) are used to separate small DNA fragments (<500 bp) and low percentage gels (0.5-1%) to separate high molecular DNA (>1000 bp). An intercalating, fluorescent tag like ethidium bromide can be used for visualization.

To prepare agarose gel, agarose was carefully boiled in the TAE buffer. After cooling to 50°C ethidium bromide was added (0.5 μg/ml), and warm solution was poured into a gel caster and left to solidify. DNA samples were mixed with 6x DNA gel loading buffer before loading onto the gel. Separation of DNA bands takes place in the DNA-electrophoresis chamber (at constant voltage 20-210 V) filled with TAE buffer until bands were resolved. DNA fragments were visualized using a UV transilluminator and documented with photography. For preparative isolation bands were cut with clean scalpel and extracted using gel extraction protocol.

2.2.1.2 Generation of DNA constructs

Human WT NIPA was subcloned from pcDNA 3.1/Zeo (C.von Klitzing). WT NIPA was cloned into N-SF-TAP-pcDNA3 by using XhoI and XbaI enzymes to digest PCR product and NheI and XhoI for vector digestion. The S200E, S210/212 E, S217E and S231E mutations in cytoplasmic retention signal (CRS) of Cyclin B1 were introduced by site-directed mutagenesis and primers were described in the material section. FLAG-TPR was subcloned from TPR-pEGFPC2 vector (Addgene) into pcDNA 3.1/Zeo using KpnI and NotI enzymes. WT NIPA and NIPA ZnF mutant were cloned into pAcGFP1-C3 vector by using XhoI and BamHI enzymes. FLAG-NIPA WT was subcloned from pcDNA3.1/Zeo (T.Ouyang) into pBabe puro using BamHI and XhoI along with BamHI and SalI for vector digestion.

2.2.1.3 Isolation, purification and measurement of DNA

QIAGEN plasmid purification protocols are based on the principle of alkaline lysis, followed by binding of plasmid DNA to anion-exchange resin under low-salt and low pH conditions. Medium-salt washing steps allows for exclusion of contaminants. Plasmid DNA was eluted in a high-salt buffer, concentrated and then desalted by isopropanol precipitation. For gel extraction, gel slices are dissolved in a buffer with optimal pH for DNA binding followed by placing DNA-buffered solution into the QIAquick® spin column. Nucleic acid adsorb to the silica membrane in the high-salt buffer. Contaminants are washed away and DNA is eluted with a low-salt buffer.

DNA was isolated and purified using "QIAprep® Spin Miniprep Kit" for minipreps (5 ml of bacterial culture) and with "QIAGEN® Plasmid Maxi Kit" for maxipreps (200 ml of bacterial culture). DNA was extracted and purified from agarose gels using "QIAquick® Gel Extraction Kit". NanoDrop was used to measure yield and purity of the isolated DNA. Absorbance of 1.0 at 260 nm equates DNA concentration of 50 mg/ml for double stranded DNA and 40 mg/ml for single stranded DNA and RNA. DNA or RNA with ratio of absorbances at 260 nm and 280 nm around 1.8-2.0 can be considered as relative pure.

2.2.1.4 PCR (polymerase chain reaction)

Amplification of DNA *in vitro* can be very efficiently performed with the help of specific enzymatic approach: polymerase chain reaction (PCR)[144]. In this process, number of synthesized DNA is doubled after one full cycle. First, double-stranded DNA matrix provided in the reaction mixture is denatured at 95°C, yielding single-stranded DNA molecules. Cooling to 50-65°C allows for annealing of the complementary primers to the single-stranded DNA template. In the next step usually at 72°C (depending on the polymerase used) DNA polymerase synthesizes a new DNA strand complementary to the DNA template strand by adding dNTPs that are complementary to the template in 5' to 3' direction followed by final elongation step to ensure full extension of any remaining single-stranded DNA. Reapplied denaturation is starting a new cycle. Reaction is performed in an automatic Thermocycler with adjustable programming interface.

2.2.1.5 PCR based mutagenesis

Point mutations were introduced intro target DNA using "QuickChange™ Site-Directed Mutagenesis Kit". This PCR-based mutagenesis technique involves two complementary

Primers designed to bare desired mutation flanked by 10-20 base pairs on each site. Thereby a complete double-stranded circular plasmid can be amplified.

PCR compilation:

5 µl	10x reaction buffer
50 ng	dsDNA template
125 ng	3'-Primer
125 ng	5'-Primer
2.5 mM	dNTP mix
2.5 U	*Pfu* DNA polymerase

PCR reaction conditions:

1x		95°C,	30s
16-18x	⎧	95°C,	30s
	⎪	55-62°C,	1 min
	⎩	72°C,	2 min/kb template DNA
1x		72°C,	10 min

The resulting PCR product contains both the template DNA as well as the mutated product. *Dpn*I restriction digestion was performed to deplete unmutated template from the PCR product. Since only a methylated substrate DNA is digested by the *Dpn*I, PCR product stays intact. The nicks left in the product DNA are sealed upon transformation into appropriate bacteria strain. Bacterial colonies were then picked for the minipreps and the DNA product was sequenced for the further analysis.

2.2.1.6 Restriction digestion, ligation and cloning of DNA

For cloning of DNA inserts into the vector, restriction endonucleases were used. These enzymes recognize short palindromic sequences in double-stranded DNA and digest sugar-phosphate backbone leaving (depending on enzyme) complementary sticky ends or blunt ends.

DNA compatible for cloning was prepared by digesting the vector and the insert with an appropriate restriction enzyme for 2 hours at 37°C. To avoid re-ligation of a vector, treatment with calf intestine alkaline phosphatase was performed for 1 hour at 37°C.

This enzyme removes phosphate groups from the 5' end making a vector DNA strand incompatible for re-ligation. Digested DNA was then separated on the agarose gel, bands were cut out and DNA extracted using gel extraction kit.

DNA ligation kit was used to clone insert into a vector. For ligation, 50-100 ng of linear vector was mixed with triple molar excess of insert DNA and after addition of 5x ligation buffer along with T4 DNA ligase mixture was left at RT for 1h before transforming into DH5α *E.coli* bacteria.

2.2.1.7 Transformation of *E.Coli* and inoculation of culture for DNA isolation

Cultivation of bacteria transformed with DNA should be maintained in the presence of antibiotics to ensure the growth of bacteria that acquired resistance after incorporation of the appropriate plasmid DNA. LB medium and Petri dishes were supplied with 50 μg/ml of ampicillin or 30 μg/ml kanamycin. Medium with bacteria was agitated at 250 rpm at 37°C.

DNA was transformed into the competent DH5α strain of *E.Coli.* Competent cells (50 μl) were thawed on ice before mixing with 5 μl of ligated DNA or 0.1-1 μg of plasmid DNA. The mixture of cells and DNA was then incubated on ice for 30 min. followed by a heat shock at 37°C for 45 seconds. Cells were put again on ice for 2 min and plated on to LB plates, which were then incubated overnight at 37°C. Single clones were picked on the following day and inoculated either in 5 ml of antibiotic containing LB medium for minipreps or in 200 ml culture for maxipreps. On the following day, cells were centrifuged and bacterial pellet was used for DNA isolation.

2.2.2 Methods based on protein biochemistry

2.2.2.1 Isolation of proteins

Cells were harvested and centrifuged for 3 min at 1500 rpm. Medium was completely aspirated before the second round of centrifugation for 1 minute. The rest of the medium was carefully removed and cells either frozen in liquid nitrogen or subjected to lysis for 20 min on ice using freshly prepared lysis buffer (Section 2.1.12). After subsequent centrifugation (14.000 rpm; 4°C) supernatant was transferred into fresh tubes. Protein concentration was determined using Bradford method[145]. SDS loading buffer was then added and protein samples heated at 95°C for 5 minutes. Samples were

centrifuged for 30 s before loading onto SDS-PAGE. Remaining protein samples were frozen at -20°C for future use.

2.2.2.2 Immunoprecipitations (IPs)

Antibodies against specific antigen can be used to perform precipitation of a protein from a cell lysate – so called immunoprecipitation. Antibody-protein conjugate is adsorbed on sepharose-coupled protein A or agarose-coupled protein G. Such complexes can be separated from the lysates by centrifugation.

Cell lysates were pre-cleared with protein A or protein G beads in a cold room at 4°C for 30 minutes. After centrifugation beads were discarded and supernatant transferred to the fresh reaction tube followed by addition of 2 μg of specific antibody and subsequent incubation for 2-4 h at 4°C while rotating. Then 30 μl of protein A/G suspension was added and submitted to further incubation (with rotation) for 30 min at 4°C. Protein complexes bound to protein A/G beads were then centrifuged and washed five times with 1 ml lysis buffer (without protease inhibitors). After washing remaining lysis buffer was aspirated using very thin injection needle, mixed with 30 μl 1x Laemmli buffer and heated at 95°C for 5 minutes. After brief centrifugation samples were loaded on the SDS-PAGE gel. Instead of antibody, agarose conjugated anti FLAG-beads were used if the protein of interest exhibited a FLAG-tag. Lysates were incubated with 30 μl of FLAG-beads at 4°C for 1 h while rotating. Beads where then centrifuged, washed and processed as already described above.

2.2.2.3 *In vivo* ubiquitination

To check if proteins are ubiquitously regulated under specific conditions or in the particular cell cycle phase, *in vivo* ubiquitination assay was performed. Therefore hemagglutinin epitope (HA) – tagged ubiquitin is transfected in the cells in high excess to form polyubiquitin chains instead of endogenous ubiquitin. Cells are then treated with proteasome inhibitors before harvesting to prevent the proteasomal degradation of ubiquitinated proteins. After preparation of cell lysates, denaturing buffer is added to the samples and boiled to ensure exclusion of unspecific ubiquitination. Afterwards immunoprecipitation is performed and ubiquitination detected by Western blot.

293T cells were transfected with 10 μg pCMV-HA-ubiquitin and additionally with 5 μg pcDNA3.1-FLAG-NIPA WT, pcDNA3.1-FLAG-NIPA ZnF mutant or NIPA siRNA. 48h after

transfection MG132 was added to the cells for 6h prior to harvesting. Cell lysates were mixed 1:1 with denaturing buffer and heated at 95°C for 10 minutes. After cooling, immunoprecipitation with HA conjugated agarose pink beads (Sigma) was performed for 2 h at 4°C while rotating. Ubiquitination was detected by Western blot with HA-antibody.

2.2.2.4 SDS – PAGE and staining of polyacrylamide gels

Sodium dodecyl sulfate polyacrylamide gel electrophoresis (SDS-PAGE) is a widely used technique to separate protein fractions. Tertiary and secondary protein structure is linearized in anionic detergent (SDS) and negative charge applied in proportion to its mass. After destruction of disulfide bridges between cysteine residues with DTT, only the molar mass can be considered as a separation criterion. Proteins are then separated according to their electrophoretic mobility. Passing through the stacking gel allows for focusing of protein mix and for the subsequent separation in separating gel at higher pH. Self-made resolving Tris-Glycine gels were prepared with desired polyacrylamide concentrations (5-15%) according to the molecular mass of the protein of interest. Gel solution supplemented with 10 µl of TEMED and 50 µl APS was poured between BIO-RAD plates with 1 mm spacer, and coated with ethanol. After polymerization ethanol was removed and stacking gel was poured onto resolving gel with 10 or 15 well sample comb. Comb was removed after polymerization of stacking gel and such prepared gel-plates were placed in the electrophoresis chamber. Separation of proteins was achieved by the application of a constant electric field (80-130 V) in running buffer. Following electrophoresis, gels were either subjected to Western Blot or stained with Coomassie Brilliant Blue. Therefore, gels were immersed in Coomassie staining solution for 1 h and destained with Coomassie destain at the room temperature until background staining was removed. For documentation, stained gels were equilibrated in H_2O and scanned.

2.2.2.5 Western blot

For immunodetection of proteins with antibodies, samples separated by SDS-PAGE where transferred from the gel to the Immobilion FL PVDF membrane (Milipore) by wet blotting. Therefore, the PVDF-membrane was first activated in ethanol prior to immersion in blotting buffer. Gel was transferred onto PVDF-membrane by avoiding air bubbles formation and both were placed between two layers of filter paper (Whatman).

Such prepared "sandwich" was placed in the Western transfer apparatus filled with transfer buffer, membrane towards anode while cathode behind the gel. Proteins were transferred by constant electric field intensity (0.3 A) with permanent cooling. Transfer duration depends on the molecular mass of transferred proteins (1 min per kDa).

After Western transfer, PVDF-membrane was incubated with 5% of milk for 1 h at RT to block non-specific binding of antibody to the membrane. BSA was used as a blocking solution for the detection of phosphorylated proteins. Primary antibody, which specifically reacts with an epitope of the analyzed protein, was added to the blocking solution in appropriate dilution and incubated with the membrane overnight at 4°C. Following day, PVDF-membrane was washed three times with PBS (with 0.1% Tween – PBST) solution for 10 min before incubating with secondary antibody (conjugated to HRP enzyme) at 1:10000 dilution for 30 minutes. The membrane was then washed thoroughly and a chemiluminiscence substrate was added to the membrane. Substrate is converted in the chemiluminescent reaction by peroxidase conjugated to the secondary antibody. Target protein bands were visualized by capturing the signal on a photographic film.

To test the blotting efficiency, membranes were incubated for 15 min in the amidoblack solution. Stained membranes were then incubated with amidoblack destain until protein bands were clearly visible.

Primary antibodies were removed from the membranes with 0.2 M NaOH solution followed by blocking in milk prior to use the membranes to analyze other proteins of interest.

2.2.3 Methods involving mammalian cell culture

2.2.3.1 Cell culture

All cultured cells were grown at 37°C in 5% CO_2 humidified atmosphere in incubators (HERAcell) obtained from Thermo Scientific. All laboratory work involving cell cultures was maintained in laminar flow safety cabinet HERAsafe (Thermo Scientific).

K562 NIPA microRNA (miR) and non silencing (ns) cells were cultured as suspension in the RPMI-1640 medium supplemented with 10% fetal calf serum (FCS), 2 mM L-glutamine, 1% penicillin/streptomycin solution (P/S) and 1 μg/ml puromycin.

U2OS and U2OS DR-GFP cells were cultured as a monolayer in McCoy's 5A medium supplemented with 10% FCS, 2 mM L-glutamine, 1% P/S and U2OS DR-GFP additionally with 200 μg/ml hygromycin.

All other cell lines used (2.1.5) were cultured in DMEM medium supplemented with 10% FCS and 1% P/S. Cells were grown up to 90% confluence followed by detachment with trypsine-EDTA and splited at appropriate ratio using fresh medium. Cell number was estimated by the Trypan blue staining and Neubauer haemocytometer.

Cryo-conserved cells were thawed rapidly in a water bath at 37°C and transferred to 10 ml supplemented medium. Cells were then centrifuged at 1500 g for 3 min, medium removed and the cells resuspended in 10 ml supplemented medium. Cells were then transferred either to a culture flask or to Petri dish and incubated under growth conditions. For cryo-conservation, cells were washed with PBS, detached with trypsine-EDTA and resuspended in 10 ml culture medium. After centrifugation at 1500 g for 3 min, medium was removed and the cell pellet resuspended with an appropriate supplemented medium followed by addition of freezing medium (2x; 80% FCS, 20% DMSO) in ratio 1:1. About 1-2 x 10^6 cells were transferred into cryo tubes (Nunc) and placed in a freezing container (Nalgene) field with isopropanol, allowing for progressive freezing of -1°C/min at -80°C. Cells were stored in the liquid nitrogen.

2.2.3.2 RNA interference

2.2.3.2.1 Small interfering RNA (siRNA)

Small interfering RNAs (siRNAs), generated by ribonuclease III cleavage from longer double stranded RNAs are mediators of seqence-specific mRNA degradation used for post-transcriptional gene silencing[146]. Therefore synthetic 21 nucleotide long RNAs were generated for a specific knock down of proteins of interest. siRNAs were introduced to cells by lipofection with TurboFect reagent according to the manufacturer's instructions. Cells were harvested 48 h after transfection or used for further experiments.

2.2.3.2.2 MicroRNA (miRNA, miR)

To overcome disadvantages of siRNA approach, which can be used only for short-term gene silencing, vector-based shRNA method was developed for the stable down regulation of protein expression[147]. A new generation of shRNAs, miR30-based shRNAs,

were designed, where endogenous miR30 (microRNA30) was replaced with target specific miR (miR^{TOI})[148]. A very strong RNA polymerase II promoter such as LTR (5' long terminal repeat) can regulate these shRNAs. The pLMP vector developed by Dickins et al. possess already flanking sequence of miR30 and target specific miR can be cloned into multiple cloning site (MCS) by *Eco*RI and *Xho*I enzymes[149].

NIPA specific miR was designed with computer-based algorithm "RNAi Central". *Eco*RI and *Xho*I cutting sites were introduced by the PCR reaction using miR common primers. PCR product and vector were digested with *Eco*RI and *Xho*I enzymes, ligated and transformed into *E.coli*. Obtained DNA construct was transfected into PhoenixE packaging cell line as described, and K562 along with U2OS were infected with PhoenixE-produced retrovirus. Non-silencing miR in pLMP vector was a kind gift from C. Albers and was used as a control. Cells were selected using puromycin.

2.2.3.3 Synchronization

2.2.3.3.1 In G_1/S phase

Thymidine at high concentration (2 mM) was used to synchronize cells in G1/S cell cycle stage. Addition of thymidine to exponentially growing cells leads to accumulation of thymidine triphosphate and in turn to an allosteric inhibition of the ribonucleotide reductase. Reduction of cytidine diphosphate is blocked resulting in the lack of deoxycytidine triphosphate at the replication forks what in turn impairs DNA synthesis. Cell cycle is blocked in S-phase by the checkpoint mechanism. Incubation of the cells for 24 h with thymidine is sufficient for the S-phase synchrony. Afterwards cells can be released from the block by washing out thymidine-containing medium and replacing it with a fresh medium for further experiments.

2.2.3.3.2 In mitosis

Nocodazole (methyl(5-[2-thienylcarbonyl]-1H-benzimidazol-2-yl) is a spindle poison, which blocks polymerization of microtubules causing the cell to arrest in prometaphase. It was used at 500 ng/ml to synchronize cells in mitosis. After 12 h of incubation time with nocodazole, rounded synchronized cells were collected by a "shake of" from the plate. Then the cells were centrifuged and resuspended in a fresh medium for further experiments.

2.2.3.4 Transfection methods

2.2.3.4.1 Lipofection of adherent cells

TurboFect reagent was used for the transient expression of human DNA constructs. DNA (10 μg) was mixed with 6 μl of TurboFect in 600 μl serum-free OPTI-MEM medium and incubated for 20 min in RT. Cells were seeded on the day before transfection in a 100 mm Petri dish and medium was replaced with 6 ml of a fresh medium prior to transfection. The mixture was added to the cell culture and incubated for 4h followed by medium exchange. Phoenix E cells were transfected with Lipofectamine 2000 reagent. 20 μl of Lipofectamine 2000 reagent was mixed with 0.5 ml of serum-free OPTI-MEM medium with a simultaneous mixing of 10 μg of DNA with 0.5 ml OPTI-MEM in a separate reaction tube and incubated for 5 min. DNA and lipofectamine mixtures were then combined and incubated for further 45 minutes and than added to Phoenix E culture on a 60 mm plate. Transfection medium was replaced by a fresh medium after 24 h of transfection.

2.2.3.4.2 Retroviral infection and establishment of stable cell lines

Stable cell lines were generated using retroviral vector system to infect mammalian cells. Virus was produced in PhoenixE packaging cell line with appropriate DNA construct. PhoenixE is a 293T-based cell line designed to produce gag-pol and env proteins for replication-incompetent ecotropic retrovirus production. Gag-pol (along with the hygromycin resistance marker) is expressed under CMV promoter while env (along with the diptheria resistance marker) is expressed from RSV promoter thus avoiding recombination between the constructs. Cells growing in suspension were targeted by spin infection whereas adherent cells were incubated with the virus in a Petri dish.

Retroviral vector (pLMP or pBabe) along with a target DNA (non silencing miR or NIPA miR) was transfected into the PhoenixE cells. Transfection mixture was prepared with Lipofectamine 2000 as already described (2.2.1.2.1) and added to PhoenixE cells. 24 h post transfection, transfection medium was exchanged with fresh medium and retroviral stocks were collected twice at 12-hour intervals. Medium containing retrovirus was purified using 0.45 μM syringe filter and stored at 4°C.

Because PhoenixE produce ecotropic virus, human cell lines has to express ecotropic receptor on their surface to be able for retroviral infection using this system. K562 and

U2OS cells were transiently transfected with ecotropic receptor and zeocin selected prior to retroviral infection.

For retroviral infection of K562, 50000 cells were placed in a 12-well plate and 2 ml of collected retrovirus were added. To increase the efficacy of infection, polybrene (4 μg/ml) was supplemented to the medium. 12-well plates were then subjected to centrifugation at 2400 rpm for 90 minutes at 32°C – spin infected. The entire procedure of spin infection was repeated at 12 h after first infection. Cells were then selected with puromycin.

For retroviral infection of U2OS, 5 x 10^5 cells were seeded in 100 mm Petri dish and 6 ml of a retrovirus along with polybrene where added and incubated for 24 h. Infection was then repeated with a new retrovirus stock and cells were selected with puromycin.

2.2.3.5 Treatment of the cells with proteasome inhibitors

MG132 (N-carbobenzoxyl-leu-leu-leucinal) was used for inhibition of the proteolytical activity of proteasome to prevent the proteasomal degradation of ubiquitinated proteins. MG132 was applied at 10 μM concentration.

2.2.3.6 Treatment of the cells with cycloheximide

Protein synthesis was blocked with the end-concentration of 50 μg/ml of cycloheximide in a culture medium.

2.2.3.7 Treatment of the cells with UV and IR irradiation

Adherent cells were treated with UV irradiation after removal of culture medium. Plates were then irradiated in UV Stratalinker 2400 (Stratagene) with an appropriate intensity (254 nm). After irradiation, fresh prewarmed medium was supplemented to the plate and the cells were further incubated for an indicated time.

For IR irradiation cells were placed in a Petri dish or 6-well plate on the table of the irradiation machine (RS 225A X-Ray Box + Research System, Gulmay Medical LTD; Camberley (Surrey) England) without medium removal. Cells were irradiated with an appropriate intensity (1 Gy ≅ 1min 7 seconds) and further incubated for an indicated time.

2.2.4 Methods involving DNA damage and repair

2.2.4.1 Colony formation assay

Colony formation assay or clonogenic assay is an *in vitro* cell survival assay based on the ability of cells, which retained the capacity of producing a large number of progeny after treatment causing cell reproductive death due to the chromosome damage, apoptosis etc. This assay can be used to determine differences in sensitivity to the radiation or to the chemotherapeutic agents.

U2OS cells expressing ecotropic receptor (U2OSE) were retrovirally transfected either with pLMP-ns miR or with pLMP-NIPA miR constructs to generate U2OS cells with stable non-silencing (ns miR) and NIPA (NIPA miR) knockdown, respectively. Exponentially growing cells were harvested using trypsinization. The accurate number of cells was determined by counting both cell lines in Neubauer haemocytometer (independently, three times each). Cells were plated in triplicates in a 6-well plates at appropriate dilutions: for sensitivity towards irradiation (IR) at 600 cells/well and for sensitivity towards ultraviolet light (UV) at 1000 cells/well. After attachment of the cells to the dishes (approx. 3 h), the cells were treated with an appropriate dose of damaging agent. In case of UV treated cells, medium was aspirated before treatment and immediately replaced thereafter. After treatment, dishes were placed in an incubator and left there for 10 days. Then medium was removed, cells washed with PBS and fixed in 4% formaldehyde for 15 min. Fixation solution was then washed with PBS and cells were stained with the crystal violet staining solution (4 mg/ml crystal violet in PBS, 10% EtOH). After several washing steps with PBS cells were dried and counted (colonies visible to naked eye were counted, approx. 50 cells per colony)[150].

Plating efficiency (PE) represents the ratio between the number of colonies and the number of cells seeded and was calculated from the formula:

$$PE = \frac{no.of\ colonies\ formed}{no.of\ cells\ seeded} \times 100\%$$

The number of colonies that arise after treatment, expressed in terms of PE, is called the surviving fraction (SF):

$$SF = \frac{no.of\ colonies\ formed\ after\ treatment}{no.of\ cells\ seeded \times PE}$$

Surviving fraction is then depicted on the diagram for each condition and cell type on the logarithmic scale including standard deviation from 3 independent experiments.

2.2.4.2 Comet assay

The COMET assay, also referred to as a single cell gel electrophoresis assay (SCGE), is a wide used, sensitive and cheap method to detect DNA damage at the single cell level. Different types of lesions can be detected like single and double-strand breaks or incomplete repair sites depending on the experimental conditions. This assay relies on the chromatin organization in the nucleus, where undamaged DNA is associated with matrix proteins. After the damage chromatin begins to relax. If subjected to an electrical field, small fragments are migrating in the gel toward anode, forming a structure similar to comet, where the head of the comet (circular shape) corresponds to the undamaged DNA and the tail (long, eroded shape) to the damaged DNA. The longer and brighter is the tail, than the higher the level of damage.

All experiments concerning comet assay were performed at the BSF (Bundesamt für Strahlensutz, Helmholtz-Zentrum München) in the group of Maria Gomolka according to the protocol[151].

2.2.4.2.1 Preparation of mouse lymphocytes and treatment

Blood was collected from NIPA $^{+/+}$ and NIPA$^{-/-}$ mouse at the mouse facility of Klinikum rechts der Isar. Isolation of mouse lymphocytes was performed by pipetting and gently mixing 20 μl of blood with 500 μl of 0.9% saline. Mixture was under layered with 100 μl of Percoll (Sigma-Aldrich) and centrifuged at 6400 rpm for 75 s (Microfuge, Tomy Seiko). The white layer of 75 μl lymphocytes was transferred to 500 μl of 0.9% saline, gently mixed and centrifuged again. After removing 545 μl of supernatant, lymphocytes were re-suspended in the remaining 30 μl. Each sample was divided into three 10-μl aliquots, two of which were subjected either to 6 Gy of ionizing radiation (^{137}Cs, 1.3 min ≅1 Gy) or to the bleomycin (30 μg/ml) while resting on ice. The total time required for the procedure was about 30 min. To mimic DNA damage repair conditions, one of the two treated aliquots was placed at 37°C for 60 min[152].

2.2.4.2.2 Comet assay procedure

Special microscopic slides (ESW-370) were pre-coated with 200 µl of 0.1% low-melting agarose (Serva) and dried at 20°C. Mouse lymphocytes were embedded in 100 µl of 0.5% agarose (50°C, Amresco) and then immediately transferred onto pre-warmed slides with a dry crystalline agarose layer. In order to ensure an even distribution of the cells over the surface of the slide, a Triton-X coated covered slip was placed gently over the agarose prior to chilling the slide for 5 min at 0°C on a cooling plate. After elapsed time the cover slips were removed and the microscopic slides immersed in a freshly prepared cold lysis buffer I (2.5 M NaCl, 100mM Na_4EDTA, pH 10, 10 mM Tris-HCl, pH10, 1% SDS, and 1% Triton X-100). Lysis was performed overnight. Afterwards, most nuclear proteins were removed by incubation in the lysis buffer II (2.5 M NaCl, 100 mM Na_4EDTA, pH 10, 10 mM Tris-HCl, pH 10) for 1 h at 37°C. Slides were transferred to a specially adapted tray to prevent their movement during electrophoresis. Microscope slides were incubated for 20 min in the electrophoresis buffer (300 mM NaOH, 2% DMSO, and 10 mM Na_4EDTA, pH 10; pH>13, pre-cooled to 4°C) to facilitate the unwinding of the nuclear DNA. Electrophoresis was performed in a specially adapted electrophoresis chamber (Amersham Pharmacia HE100 Supersub) for 30 min at 0.8V/cm (300 mA). The temperature during electrophoresis was kept constant at 4°C by a temperature control unit and additional stirring. Following electrophoresis, the DNA was precipitated and fixed by incubation in 1% ammonium acetate in ethanol (5 ml of 10 M ammonium acetate and 45 ml of 100% ethanol) for 30 min at room temperature. After dehydratation in 100% ethanol overnight, slides were rehydrated with 70% ethanol for 5 min (to avoid cracking of agarose during drying), air-dried and stored at room temperature prior to staining. Slides were incubated for 2 x 10 min in double-distilled water and than stained with 50 µl of a solution containing 745 µl water, 50 µl DMSO, 200 µl Vectashield, and 5 µl SYBR®Green stock solution (diluted 3:50 in DMSO)(Molecular Probes). Slides were evaluated after staining.

2.2.4.2.3 Image acquisition and software

Two hundred cells per slide were examined under an epifluorescence microscope (Axioplan2, 20x/0.5 Plan-Neofluar objective, filterset 10 (FITC) Zeiss) Slides were kept in the slide feeder in a humidified chamber to prevent drying during waiting time. An automated scanning system was implemented to analyze specific comet parameters, *e.g.*

olive tail moment (OTM), %DNA in tail (metafer4/CometScan). Comet images were taken with a high resolution CCD camera (resolution: 1280 x 1024) prior to analysis. Quality control was assured with visual checks of the comet images.

2.2.4.3 Flow cytometry

Flow cytometry is a biophysical technology employed in quantitative determination of both surface molecules and intracellular proteins. It uses the principles of light scattering, light excitation, and emission of fluorochrome molecules to generate specific multi-parameter data from particles and cells in the size range of 0.5 μm to 40 μm diameter. Laser is used as a light source. When the cell intercepts the light source it scatters light and fluorochromes are excited to a higher energy state with a release of a photon of light that possesses specific spectral properties unique for the fluorochrome used. Scattered and emitted light are converted to electrical pulse, amplified and processed, which in turn allows for events to be plotted on a graphical scale.

The data obtained from flow cytometry were analyzed using FlowJo Flow Cytometry Analysis Software.

2.2.4.4 Propidium iodide staining

Propidium iodide (PI) intercalates into double-stranded nucleic acids and is a fluorescent molecule what can be used to determine the cell cycle stage. PI bound to nucleic acids has the fluorescence excitation maximum at 535 nm and the emission maximum at 617 nm. Since it binds also to RNA, nuclease treatment is necessary to distinguish between RNA and DNA stain. PI is excluded from viable cells and thus can be used to differentiate necrotic, apoptotic and normal cells. Apoptotic cells possess smaller DNA content due to the nuclease activity during apoptosis thereby can be distinguished in PI stain as so called sub-G_1 population.

Cells were harvested, washed once with PBS and resuspended after centrifugation in 70% ethanol. Fixation was performed for 24 h at 4°C. Fixed cells were then incubated with 200 μg/ml RNaseA and 10 μg/ml propidium iodide at 37°C in the dark. Stained cells were subjected to flow cytometry.

2.2.4.5 HR repair analysis

Homologous recombination assay is based on the recombination reporter system using DR-GFP substrate designed by Pierce et al. to assay chromosomal gene conversion event in response to DSBs[153]. DR-GFP is composed of two differentially mutated GFP genes oriented as direct repeats, separated by a drug selection marker, the puromycin N-acetyltransferase gene and integrated into cellular genomic DNA. One of the GFP genes, *Sce*GFP, is mutated to contain the recognition site for the rare-cutting *I-SceI* endonuclease and, as a result, will undergo a DSB when the I-*Sce*I is expressed in vivo.

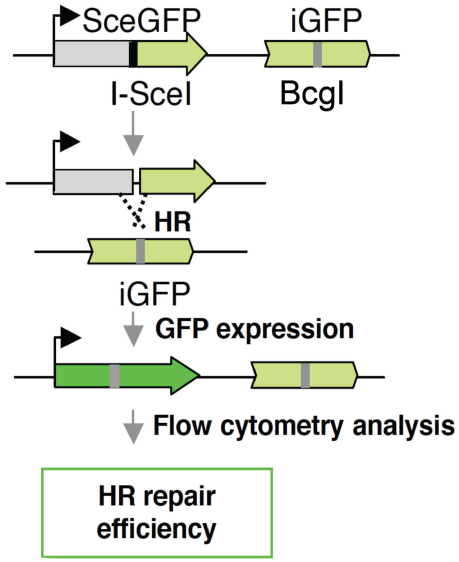

Fig. 2.1: Schematic illustration of HR assay. The DR-GFP reporter substrate is integrated into cellular genomic DNA. The I-SceI endonuclease site within the coding region abolishes GFP expression of the SceGFP. A truncated GFP, iGFP, contains homologous sequence for the SceGFP. Expression of I-SceI induces a single DSB in the genome and if repaired by HR can by analyzed by the flow cytometry. (Adapted from Peng et al. 2009)[154].

The *I-SceI* site is incorporated at the *Bcg*I restriction site by substituting 11 bp of wild-type GFP sequence with those of the *I-SceI* site. These substituted base pairs also supply two in-frame stop-codons, which terminate translation and inactivate the protein. Downstream of the *Sce*GFP gene is an 812-bp internal GFP fragment termed *i*GFP, a truncated GFP, which contains homologous sequence for the *Sce*GFP. Expression of *I-SceI* induces a single DSB in the genome. When this DSB is repaired by HR, the expression of GFP can be restored and analyzed by flow cytometry to indicate the efficiency of HR repair[153] (Fig.2.1).

Dr. Shiaw-Yih Lin kindly provided U2OS cells with a single copy of the HR repair reporter substrate DR-GFP in a random locus. These U2OS cells were transiently transfected with siRNAs against luciferase, NIPA or TPR to generate U2OS cells with

luciferase, NIPA and TPR knockdown. After 24 h these cells were transfected with mock or the pCBASce plasmid along with pEGFP-C3 as a control for transfection efficiency for 48h, and subjected to flow cytometry to analyze HR-repaired GFP-positive cells[154].

2.2.4.6 Immunofluorescence

Immunofluorescence is an antibody-based method, which allows for localization of the proteins in intact cells. Protein of interest is tagged with fluorescence-labeled specific antibody and can be detected by a fluorescence microscope. All immunofluorescence experiments were performed in cooperation with Katrin Schneider (Department of Biology II, Ludwig-Maximilians Universität (LMU Biozentrum), Martinsried) in the group of Prof. Heinrich Leonhardt.

2.2.4.6.1 Secondary (indirect) immunofluorescence

Cells were grown to 80% confluence on the cover glasses (cleaned in 80% ethanol) in 100 mm dish. Cells were briefly washed with PBS and cover slips were rapidly transferred to the fixation solution (3.7% formaldehyde) and incubated for 10 min at RT. Fixation solution was exchanged with PBST (PBS with 0.02% Tween) by removing only half of the fixation solution prior to complete exchange with PBST. At this stage cells were stored overnight at 4°C. On the next day cells were permeabilized for 5 min at 4°C in 0.2% Triton X-100 solution in PBS followed by the exchange with PBST and blocking in PBS with 5% BSA for 1 h at 37°C. Then the cells were incubated with a primary antibody for 1 h at 37°C at 1:200 dilutions in PBS with 5% BSA, and washed three times in PBST for 10 min. After washing cells were incubated with 1 μg/ml of secondary antibodies (typically 1:500-1:2000) in blocking solution for 1 h at 37°C and extensively washed prior to reduce background fluorescence of the sample and increase the signal-to-noise ratio. To maximally reduce background, cells were exposed to 10 min post-fixation with 3.7% formaldehyde/PBS at RT followed by the exchange of the solution by PBST. Next nuclei were counterstained with 1 μg/ml DAPI in PBST for 5 min and rinsed 4 times in PBST and once in H_2O to remove salts. Finally cover glasses were transferred onto VECTASHIELD® mounted microscope slides (SuperFrost® PLUS) and sealed with transparent histofluid. Imaging was carried out as described (2.2.4.6.7).

2.2.4.6.2 3D structured illumination microscopy (3D-SIM)

3D-SIM is a super-resolution microscopy technique working with traditional fluorescent proteins and dyes commonly used in the fluorescent imaging. It uses structured light patterns, which interacts with the fluorescent probes in the sample to generate interference patterns. By modulating the pattern, collecting and reconstructing the images, super-resolution image with double the lateral and axial resolution can be obtained (Applied Preicison, USA).

3D-SIM was performed on a DeltaVision OMX V3 (Applied Precision) system equipped with a 100x/1.40 NA PlanApo oil immersion objective (Olympus), Cascade II:512 EMCCD cameras (Photometrics) and 405, 488 and 593 nm diode lasers. Structured illumination (SI) image stacks were acquired with a z-distance of 125 nm and with 15 raw SI images per plane (5 phases, 3 angles). The SI raw data were then computationally reconstructed with channel specifically measured optical transfer functions using the softWoRX 4.0 software package (Applied Precision) to obtain a super-resolution image stack with a lateral (x, y) resolution of ~120 nm and an axial (z) resolution of ~300 nm. Images from the different color channels were registered with alignment parameter obtained from calibration measurements with 0.2 μm diameter TetraSpeck beads (Invitrogen)[155].

2.2.4.6.3 Live imaging

Direct immunofluorescence can be performed either using fluorescence-coupled primary antibody or by coupling a fluorescence tag e.g. GFP (Green Fluorescent Protein) to the protein of interest.

All fluorescence tagged constructs used in this work were cloned to pEGFP-C3 vector or to mRFP vector, transiently transfected into HeLa or U2OS cells and subjected to live imaging. Time-lapse microscopy was carried out as described (2.2.4.6.7).

2.2.4.6.4 Fluorescence recovery after photobleaching (FRAP)

Quantitative fluorescence microscopy can be applied to determine intracellular transport dynamics of proteins tagged with a suitable fluorophore. One of the technique, fluorescence recovery after photobleaching (FRAP), uses selective photo-destruction of fluorescence of the molecule of interest in one organelle and the movement of unbleached molecules from neighboring areas into the bleached area is recorded by the

time-lapse microscopy (Fig. 2.2). FRAP provides information about the mobility of the labeled molecules, altering only the fluorescence steady state in a cell without disrupting protein pathways[156]. HeLa and U2OS cells were transiently transfected with pEGFP-NIPA WT construct using Lipofectamine reagent, and after 48 h subjected to FRAP analysis. Time-lapse microscopy was carried out as described (2.2.4.6.7).

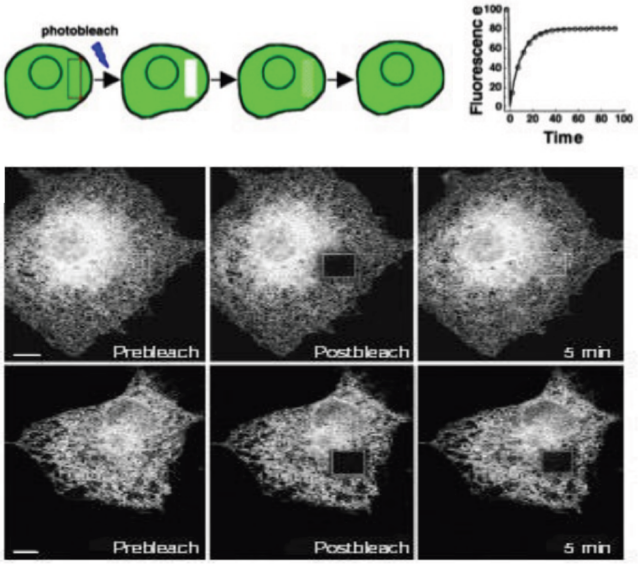

Fig. 2.2: Fluorescence recovery after photobleaching (FRAP). In this kinetic microscopy technique a region of the cell is selectively irradiated to photobleach fluorescent molecules. Mobile fraction and diffusion coefficients are determined by the quantitative measurement of recovery of fluorescent molecules back to that region. (Adapted from J. Lippincott-Schwartz, 2001; 2003)[156,157].

2.2.4.6.5 Fluorescence loss in photobleaching (FLIP)

Another fluorescence imaging technique, FLIP (fluorescence loss in photobleaching), provides information about a protein's kinetic properties (Fig. 2.3).

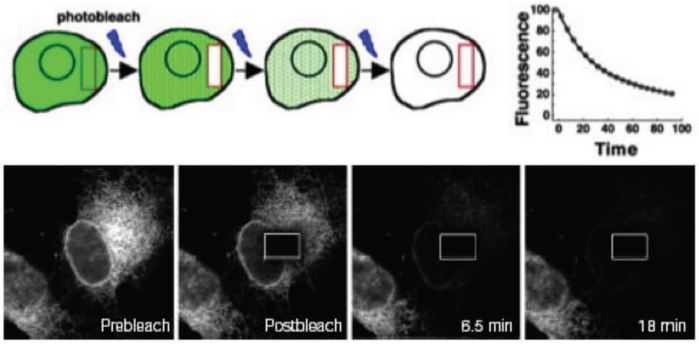

Fig. 2.3: Fluorescence loss in photobleaching. In FLIP the region of the cell is repeatedly photobleached. Loss of fluorescence is achieved due to the movement of fluorescent molecules from outside into the region being photobleached. It can be used to access the boundaries for a protein's diffusional movement within a cell (Adapted from J. Lippincott-Schwartz, 2001; 2003)[156,157].

In FLIP, one area of the cell is repeatedly photobleached by an intense laser pulse, while images are collected of the entire cell with reduced laser power between the bleaches. Using this technique the continuity of cellular environments can be determined, by monitoring the fluorescence in the nonphotobleached regions[156].

HeLa and U2OS cells were transiently transfected with pEGFP-NIPA WT and pEGFP-NIPA ZnF constructs using Lipofectamine reagent, and after 48 h fluorescence loss in photobleaching was analyzed. Time-lapse microscopy was carried out as described.

2.2.4.6.6 UVA laser microirradiation

Local nuclear irradiation of living cells can be used to gain insight into the localization of the protein of interest to the sites of DSBs in response do DNA damage. After appropriate sensitization of the cellular DNA, nuclear microirradiation with UVA can be used on a commercial laser-scanning microscope. This technique helps to answer the question if a protein could be a sensor of the DNA damage[158].

Cells were seeded on the 35 mm μ-slides (Ibidi) with 500-Grid and sensitized for microirradiation by incubation in a medium containing BrdU (10 μg/ml) for 24 h. Microirradiation was carried out with 405 nm diode laser coupled into a Leica TCS SP2/AOBS confocal laser scanning microscope. The 405 nm laser was set to maximum power at 100% transmission and was focused through a UV transmitting Leica HXC PL APO 63x/1.40-0.60 oil objective to locally irradiate preselected lines of ~1 μm in diameter within the nucleus for 1 s. After indicated time points, cells were fixed and stained with an appropriate antibodies. Imaging was carried out as described (2.2.4.6.7). Oliver Mortusewicz performed the experiment on HeLa cells.

2.2.4.6.7 Image acquisition and software

Live cell imaging and FRAP experiments were typically performed on an Ultra*VIEW*VoX spinning disc microscope with integrated FRAP PhotoKinesis accessory (PerkinElmer) assembled to an Axio Observer D1 inverted stand (Zeiss) and using a 63x/1.4 NA Plan-Apochromat oil immersion objective. The microscope was equipped with a heated environmental chamber set to 37°C. Fluorophores were excited with 488 nm or 561 nm solid-state diode laser lines. Confocal image series were typically recorded with 14-bit image depth, a frame size of 256 x 256 pixels, a pixel size of 110 nm and with time intervals of 154 ms. For photobleaching experiments, the bleach regions, typically with a

length of 8-10 μm, were chosen to cover the anterior half of the oval-shaped nucleus. Photobleaching was performed using two iterations with the acousto-optical tunable filter (AOTF) of the 488 nm and the 514 nm laser line set to 100% transmission.

2.2.4.7 TUNEL assay

Terminal deoxynucleotidyl transferase mediated dUTP nick end labeling (TUNEL) was applied for apoptosis measurement. This technique allows for detection of single and double strand breaks in genomic DNA caused by nuclease activity of endonucleases during apoptosis. Therefore terminal deoxynucleotidyl transferase is used to attach dUTP-FITC coupled nucleotides to the 3'-hydroxyl ends of cleaved DNA.

To determine the ratio of apoptosis, cells were harvested and centrifuged to remove culture medium. After washing with PBS, cells were fixed with 1% para-formaldehyde for 10 min at 4°C. PFA was replaced with 70% ethanol after washing once with PBS. Cells were incubated in ethanol at -20°C for 24 h prior to staining.

APO-DIRECT™ Kit was used for staining procedure according to the manufacturers instructions. Analysis was performed by flow cytometry.

2.2.5 Identification of NIPA interactors

Protein interaction partners can be identified by a precipitation-based method where an overexpressed and tagged protein is purified from the cell system (for example HEK 293T cells) and subjected to mass spectrometry in order to determine co-immunoprecipitated proteins by their molecular mass. NIPA-tandem-Strep-single-FLAG-tagged (NIPA-SF-TAP) construct was used to overexpress NIPA in HEK 293T cells and after purification NIPA interactors were identified by the proteomic approach.

2.2.5.1 Transfection of HEK293T cells with NIPA-SF-TAP

About $2x10^9$ HEK293T cells were transfected with an NIPA-tandem-Strep-single-FLAG-tagged (NIPA-SF-TAP) construct or SF-TAP empty vector using calcium chloride as a transfection reagent. On the day before transfection, HEK293T cells were plated at a high density on twenty 15 cm cell culture dishes (one set for each condition: untreated, UV irradiated and bleomycin treated). NIPA-SF-TAP construct (25 μg) was thoroughly mixed with 450 μl of water following by addition of 50 μl of a 2.5M $CaCl_2$. Transfection

efficiency was monitored by a simultaneous transfection of an empty pEGFP vector as a transfection marker. After mixing of DNA with $CaCl_2$, 500 µl of a 2x BES Buffer was slowly added by pipetting down to each reaction tube wall while rotating the tube. Such prepared transfection mix (one for each HEK 293T 15cm dish) was incubated for 20 min at room temperature (RT). During incubation time, 30 µl of 20 mM chloroquine stock solution was added to the medium of each 293T plate and mixed by swaying to enhance transfection efficiency. After elapsed time the entire transfection mix was put on cells, distributed by swaying and incubated for 4 h. Afterwards, transfection medium was replaced with a fresh cell culture medium and cells were left in incubator for 48 h. Prior to harvesting cells were irradiated with 100J/m^2, treated with bleomycin or left untreated for 2 hours. Harvested cells were collected in 50 ml Falcon tubes, washed three times with pre-warmed PBS and immediately frozen in the liquid nitrogen. Samples were sent for the proteomic analysis.

2.2.5.2 Purification of enriched NIPA protein

Each cell pellet was resuspended in 20 ml hypotonic buffer (10 mM HEPES; 1.5 mM $MgCl_2$; 10 mM KCl; 0.5 mM DTT; NP-40 0.1%; 1 mM glycerol-2-phosphate; 1 mM sodium orthovanadate; protease-inhibitor cocktail; 1 mM PMSF; 100 nM ocadaic acid), incubated 20 min on ice and in-between pressed 5 times through a 12-gauge needle and once through a 18-gouge needle followed by 30 min centrifugation at 4°C and 14000 rpm. Samples of supernatant representing cytosolic fractions were collected for coomassie and Western blot analysis (Fig. 2.4 A and B). The rest of the supernatant has been discarded and pellet resuspended in nuclear buffer (20 mM HEPES; 100 mM KCl; 100 mM NaCl; 1 mM PMSF; NP-40 10%; 0.5 mM DTT; 20% glycerol; 1 mM sodium orthovanadate; 1 mM glycerol-2-phosphate; protease-inhibitor cocktail; 100 nM ocadaic acid). In the next step solution was sonificated 5x 10 sec on ice at 57% amplitude and left for 20 min on ice. After 30 min centrifugation at 4°C and 14000 rpm, supernatant was placed in a fresh reaction tube and pre-cleared with Protein-G beads for 40 min at 4°C. Anti-FLAG beads as well as streptactin superflow beads were washed four times with nuclear buffer (without inhibitors and glycerol). After the pre-clear NIPA was precipitated with 2 ml streptactin superflow resin for 1.5 h at 4°C. The beads were than extensively washed and NIPA-interacting proteins were eluted twice using 10 ml desthiobiotin elution buffer at RT. The eluate was then subjected to a second

precipitation with anti-FLAG resin and then subjected to a further competition with 3xFLAG peptide in TBS at RT. Eluate samples were collected for coomassie and Western blot analysis (Fig. 2.4 A and B). Proteins were than precipitated with 10% TCA at 4°C overnight. Precipitate was washed twice with ice-cold acetone, centrifuged for 10 min at 13000 rpm and subjected to centrifugal evaporation for 20 min at 45°C (SpeedVac® Concentrator; Savant USA).

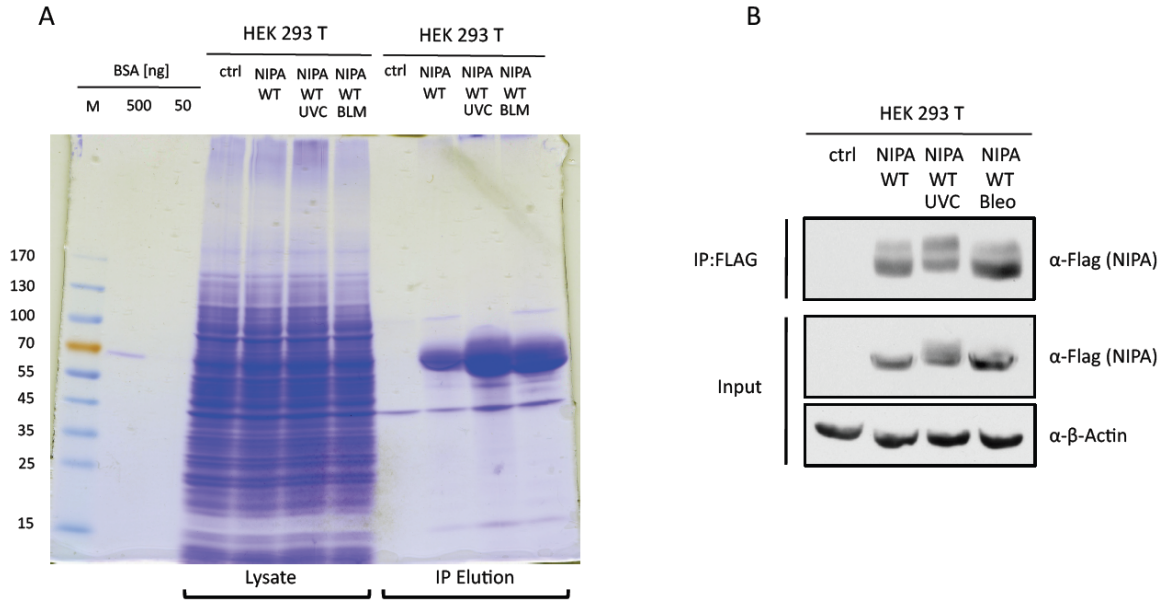

Fig. 2.4: The quality of purification has been analyzed by coomassie stain and Western blot. Lysates and eluates samples of purified NIPA protein (control – NIPA WT; UV treated – NIPA WT UVC and bleomycin treated – NIPA WT BLM) together with BSA standards were separated on the SDS-polyacrylamide gel followed by the analysis with coomassie and Western blot.

2.2.5.3 Silver staining

Silver staining is used to detect proteins after electrophoretic separation on polyacrylamide gels. Due to its high sensitivity (in the very low ng range) it is also compatible with downstream processing such as mass spectrometry and widely used as a confirmation of protein purification prior to proteomic analysis. In this assay proteins bind silver ions, which can be reduced under appropriate conditions to build up a visible image made of finely divided silver metal[159]. Untreated, UV irradiated or bleomycin treated FLAG-NIPA WT proteins were purified from 293T cells as described (2.2.5.2). Protein samples were subjected to electrophoresis on a gradient polyacrylamide gel. Gel was then briefly immersed in water and transferred to the fixation solution (50%

methanol; 12% acetic acid; 500 µl/l formaldehyde 37%). Fixation was performed twice for 30 min with an exchange of fixation solution. The gel was rinsed twice in 20% ethanol for 20 min with a subsequent washing step in water for 10 minutes. Next sensitization of the gel was performed in 0.8 mM sodium thiosulfate by soaking for 1 min followed by two washing steps for 1 min each.

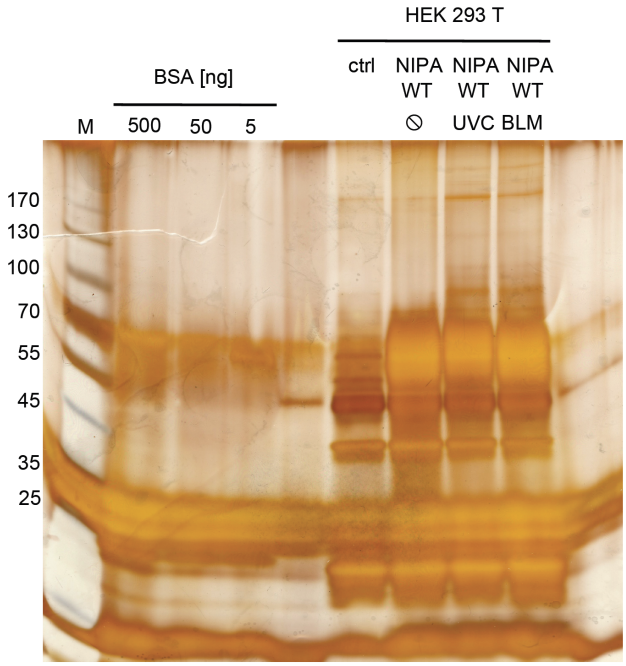

Fig. 2.5: Gradient SDS-polyacrylamide gel of purified NIPA proteins after silver staining. Eluates of purified NIPA protein (control – NIPA WT; UV trated – NIPA WT UVC and bleomycin treated – NIPA WT BLM) together with BSA standard were separated on the SDS-polyacrylamide gel and silver stained.

The gel was then impregnated in 12 mM silver nitrate for 20 min, rinsed with deionized water for 10 seconds and transferred to the developer solution (60 g/l sodium carbonate; 5 mg/l sodium thiosulfate; 500 µl/l formaldehyde 37%) until adequate degree of staining has been achieved (usually 3 to 20 min). Then the gel was immediately transferred to stop solution (50% methanol; 12% acetic acid) for at least 30 minutes. After washing the gel twice for 30 min preservation of the staining was performed for 20 min in preserver solution (20% ethanol; 2% glycerin). The gel was scanned for analysis (Fig. 2.5).

2.2.5.4 Proteomic analysis of NIPA interactors

All proteomic analyses were performed in cooperation with Simone Lemeer from the group of Prof. Bernhard Kuster at the Deparmtent of Proteomics and Bioanalytics (Technische Universität München). Peptides generated by in-gel trypsin digestion were

dried and dissolved in 0.1% formic acid. Liquid chromatography with tandem mass spectrometry was performed by coupling a nanoLC-Ultra (Eksigent) to a LTQ Orbitrap XL mass spectrometer (ThermoFisher Scientific), using a 60 min gradient from 0 to 40% solution B (0.1% formic acid in acetonitrile).

3 Results

3.1 Regulation of NIPA after DNA damage

After detection of DNA damage, the cell stops proliferation by arresting the cell cycle, which in turn provides sufficient time to start and conduct the repair process. Most of the checkpoints (Chapter 1.2-1.3) rely on the negative regulation of cyclin-CDK complexes where also NIPA was implied to play a distinct role. This work aims to gain more insight into NIPA's involvement in the signal transduction, maintenance and execution of repair pathways after DNA damage.

3.1.1 NIPA is phosphorylated after DNA damage

During a normal cell cycle activity of NIPA is restricted to interphase, where its ubiquitin ligase activity is responsible for a degradation of the substrate, cyclin B1, and protects the cell from premature mitotic entry. At the G_2/M transition NIPA is phosphorylated by ERK2 and inactivated, what allows for cyclin B1 accumulation and subsequent mitosis. However it was already reported that NIPA is also phoshorylated after irradiation with UVC[78] or treatment with DNA damaging agents[160]. Therefore it was important to confirm if NIPA phosphorylation is dependent on the source of DNA damage. Ultraviolet and ionizing radiations were chosen to induce NIPA phosphorylation due to their contrary mode of action. UV light is known to induce pyrimidine cross-linking, which leads to stalk replication forks. IR instead is well established to cause DNA double strand breaks. These two agents are supposed to induce DNA repair by different signaling pathways – ATR and ATM respectively.

For this reason NIH/3T3 mouse embryonic fibroblasts were stable transfected with FLAG-NIPA construct and subjected to different intensities of UV irradiation as well as different doses of IR (Fig.3.1).

In untreated controls NIPA remains in unphosphorylated form. The kinetics of phosphorylation is relatively fast where the half of the protein is phosphorylated already after 10 min (Fig. 3.1 A) with a complete phosphorylation of NIPA after 30 min in the UV treated cells. At the longer time points (6h, 8h) a gradual decrease in phosphorylation can be observed. Elevated phosphorylation of NIPA after UV is obviously dependent on the intensity of the treatment (Fig. 3.1 B), where radiation of 20 J/m^2 has shifted about 50% of the protein to the phosphorylated form and 50 J/m^2

triggers a complete phosphorylation, which is even more profound at the higher intensities and is consistent with already published results[78].

NIPA shift in cells treated with IR is not so apparent as it was by ultraviolet radiation (Fig. 3.1 C). Phosphorylation kinetics of the protein is slower but much more intense. First phosphorylation can be observed after 30 min, at the same time being most pronounced, followed by gradual decrease of phosphorylation over time. The strongest phopho-signal was induced foremost after higher IR intensities (8 Gy, 10Gy – Fig. 3.1 D) suggesting a lower dependency for NIPA phosphorylation on IR dosis, contrasting with results obtained after UVC treatment.

These data confirm that NIPA is phosphorylated after DNA damage source, and that UVC drives a more distinct and complete response when compared to IR, which is consistent with results published before[160].

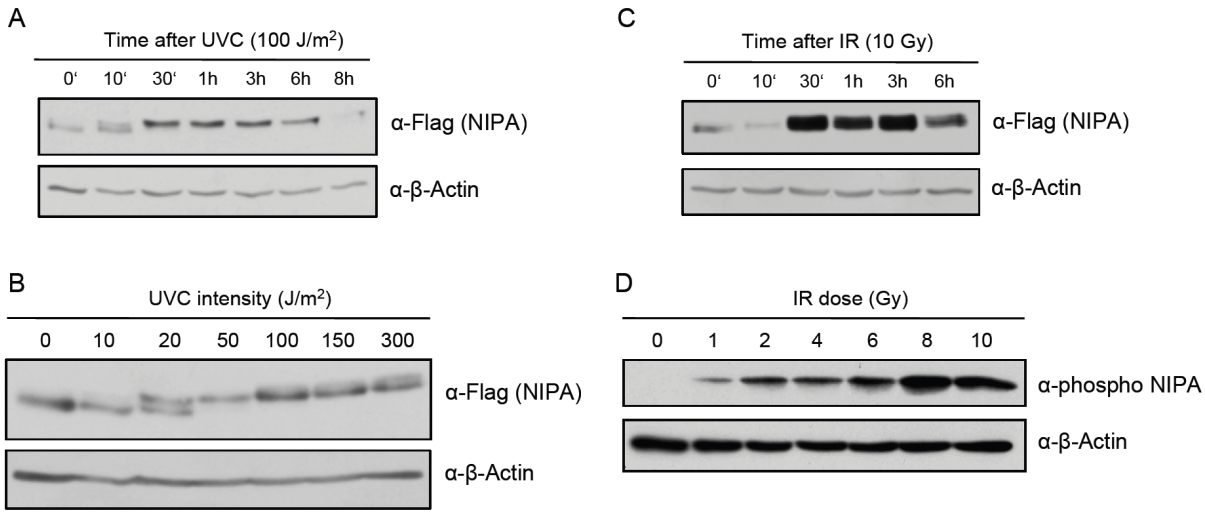

Fig. 3.1: NIPA is phosphorylated in a time and dose dependent manner after DNA damage. NIH/3T3 fibroblasts stable transfected with FLAG-NIPA were irradiated with 100 J/m^2 UVC (A) or treated with 10 Gy IR (C) and harvested after indicated time points. (B) NIH/3T3 fibroblasts stable transfected with FLAG-NIPA were irradiated with indicated dose of UVC or IR (D) and harvested after 1h.

3.1.2 NIPA phosphorylation status may be dependent on the source of DNA damage

NIPA is phosphorylated after IR (or radiomimetic drug bleomycin – BLM) treatment however not to the same, high extent as it was observed after UV irradiation (3.1 and data not shown). Kinetics of the phosphorylation was also not equal what could suggest a different pattern depending on the type of DNA damage. To address this question NIPA

was overexpressed in HEK 293T cells as NIPA-tandem-Strep-single-FLAG-tagged (NIPA-SF-TAP) construct. After 48 h cells were treated with BLM (25 μg/ml) or UV irradiated with 150 J/m^2 and harvested after 1 h. Tandem affinity purification was performed as already described (2.2.5.2) and samples were sent for the phosphosite identification by the proteomic approach.

Figure 3.2 represents the amino acid sequence of NIPA with highlighted phosphorylations on the depicted residues. Squares aligned at the top of an amino acid refer to as phosphorylation.

Fig. 3.2: NIPA phosphorylation pattern relies on the type of the damage. NIPA overexpressed in 293T cells was purified and sent for proteomic phosphosite analysis. Squares depicted on the amino acid sequence represent phosphorylation: white – untreated control; red – UV treated; green – bleomycin treated. POLO BOX was highlighted as a recognition site for PLK1 kinase.

White squares indicate phospho sites in the wild type protein, taken as a control without any treatment. Red square is a characteristic of the phosphorylation site after UV irradiation, whereas green squares denote changes in phosphorylation status of NIPA after bleomycin treatment. Remarkably, only status of serines and threonines has been changed with no phosphorylation detected at tyrosines (Fig. 3.2). Ser24, Ser62, Ser321, Ser338, Ser344 and Ser407 are phosphorylated in the control as well as with both

induction stimuli. Furthermore, treatment with BLM or UV induced phosphorylation features with only partially overlapping phosphorylation patterns. This corresponds to Ser58, Ser370 and Ser395. The last one is particularly interesting since it was reported as a phosphorylation site of CyclinB1/CDK1 complex at the G_2/M transition[84]. It is noteworthy that phospho status of Ser354 and Ser359 has not been changed neither after BLM nor UV treatment and these sites are phosphorylated by ERK2 during G_2/M phase of the cell cycle[85].

As shown in Fig. 3.2 NIPA treated with UV has only one unique phosphorylation at Thr373, while BLM treatment induced six of them (at Ser53, Ser56, Ser86, Ser329, Thr333 and Ser471). One of these phosphorylation sites (Ser53) is located at the PLK1 recognition motif (so called "POLO BOX") suggesting an involvement of PLK1 in bleomycin-induced phosphorylation of NIPA.

These data suggest differential regulation of DNA damage induced phosphorylation of NIPA in relation to the treatment. Depending on the damage stimuli (DSBs, SSBs), a variable response in phosphorylation pattern should be considered.

3.1.3 Phosphorylation of NIPA after DNA damage does not directly influence the interaction with SCF complex

Phosphorylation of NIPA at the G2 phase of the cell cycle leads to dissociation of NIPA-SKP1 binding and, as a result, to inactivation of the SCF^{NIPA} complexes[83]. To investigate if phosphorylation of NIPA after different DNA damaging stimuli has an impact on the interaction with SCF complex what could abrogate SCF^{NIPA} activity, coimmunoprecipitation assays using FLAG-tagged NIPA protein were performed (Fig. 3.3). NIH/3T3 cells stable transfected with pBabe FLAG-NIPA were treated either with 150 J/m^2 UV or with 25 μg/ml BLM and harvested after indicated time points. NIH/3T3 parental cells were used as a negative control. NIPA was immunoprecipitated with FLAG-beads and blotted for SCF subunits SKP1 and CUL1. Inputs, presented in Fig. 3.3 A and B both in lower panels, show equal amounts of proteins in loading control. As shown in Fig. 3.3 A, NIPA is phosphorylated in a higher extent by the UV treatment in comparison to bleomycin treated cells (Fig. 3.3 B). This is consistent with the previous findings (Fig. 3.1). However in both experiments phosphorylated form of NIPA is still binding to SKP1 subunit of the SCF complex. Also interaction with CUL1 (Fig. 3.3 A), a scaffold protein, which constitutes the core component of the SCF complex, is not

affected. First reduction of the binding can be observed at 6 h after treatment, hower at the same time NIPA expression level is also decreasing.

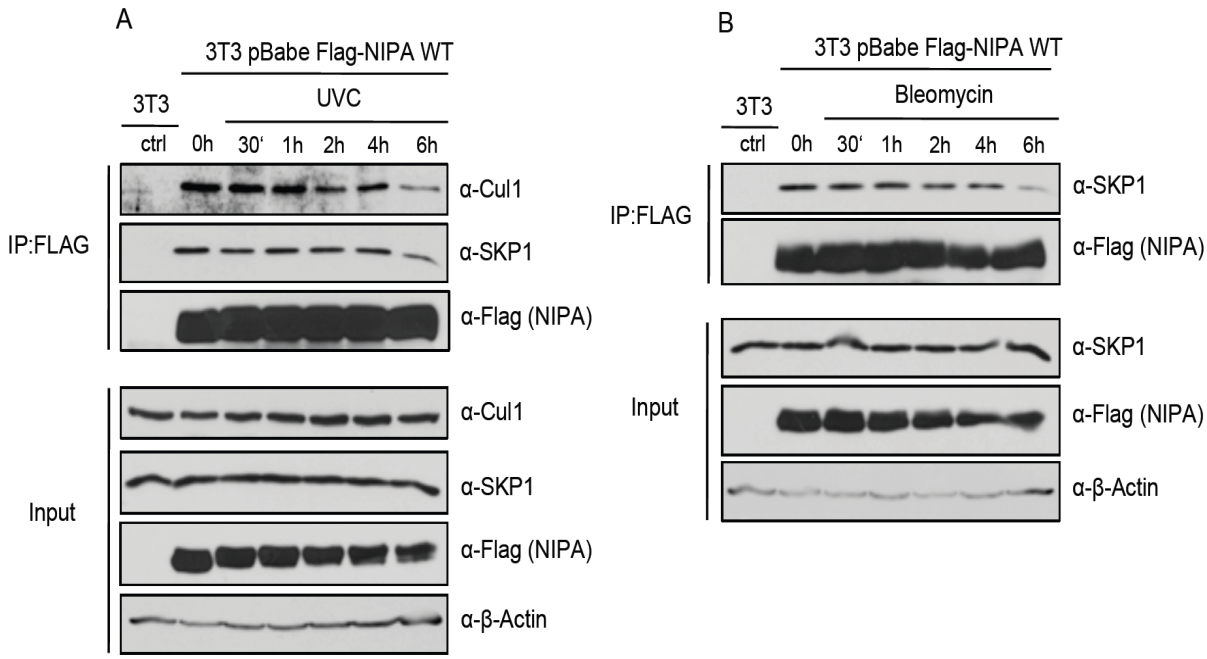

Fig. 3.3: Phosphorylation of NIPA after DNA damage does not directly influence the interaction with SCF complex. (A) NIH/3T3 cells with stable expression of FLAG-NIPA were treated with 150 J/m^2 UVC or 25 μg/ml BLM (B) and harvested after indicated time points. Lysates were incubated with FLAG-beads and the bound protein complexes separated by gel electrophoresis. Input shows the amount of protein in the lysates before immunoprecipitation with FLAG-beads (lower panels in A and B)

Although the DNA damage driven phosphorylation of NIPA was suggested to abrogate binding to the SKP1[78], these data indicate that DNA damage induced phosphorylation of NIPA does not directly influence the interaction with SCF complex like in the case of the normal cell cycle. However it still remains elusive if this art of phosphorylation could abrogate ubiquitination activity of the SCF^{NIPA} complexes.

3.2 The role of NIPA in DNA damage response

3.2.1 NIPA deficient cells display sustained phosphorylation of histone H2A

Stress signals from either physiological processes or exogenous stimuli, such as ionizing radiation or DNA-damaging agents, initiate a DNA damage response manifested with morphological, biochemical and molecular changes. A number of methods have been developed to examine these alterations. When cells are exposed to DNA damage, double-strand breaks are generated. One of the most sensitive marker, correlative with each DSB, is phosphorylation of the histone H2A at Ser139 (γH2A.X) rapidly emerging after the exposure to ionizing radiation or DNA-damaging chemotherapeutics[161]. It can be used to study DNA damage repair in the cell culture model.

To determine the impact of NIPA deficiency on the phosphorylation status of the histone H2A after DNA damage, mouse embryonic fibroblasts lacking NIPA versus wild type were treated with various DNA damaging agents and γH2A.X level was followed after 1.5 h on Western blot (Fig. 3.4).

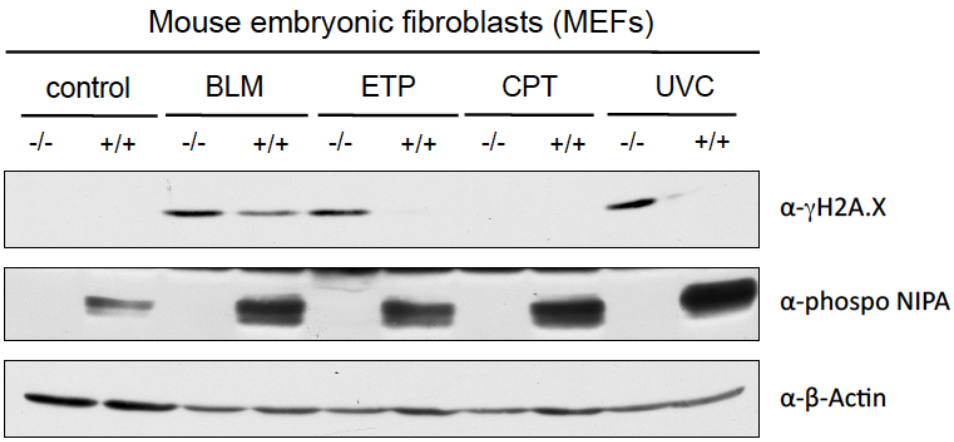

Fig. 3.4: The status of histone H2A phosphorylation (γH2A.X) after the treatment with various DNA-damaging chemotherapeutics. Mouse embryonic fibroblasts (MEFs) with homozygous NIPA depletion (-/-) or wild type (+/+) were treated with: bleomycin (BLM); etoposide (ETP); campthothecin (CPT) and ultraviolet radiation (UVC). Cell lysates were prepared 1.5 h after treatment and subjected to Western bloting.

Significant phosphorylation of histone H2A was observed in response to etoposide or UVC in NIPA$^{-/-}$ cells in contrast to the wild type (Fig. 3.4) after indicated time point. Also BLM treatment induced H2A phosphorylation to the higher extent in NIPA deficient cells, when compared to the wild type. Histone H2A phosphorylation in both wild type

and NIPA$^{-/-}$ cells was not detected after the treatment with campthothecin. This howevercannot be referred to the mode of action of CPT, which is a specific inhibitor of topoisomerase I. CPT causes single-strand breaks, which can undergo conversion to the

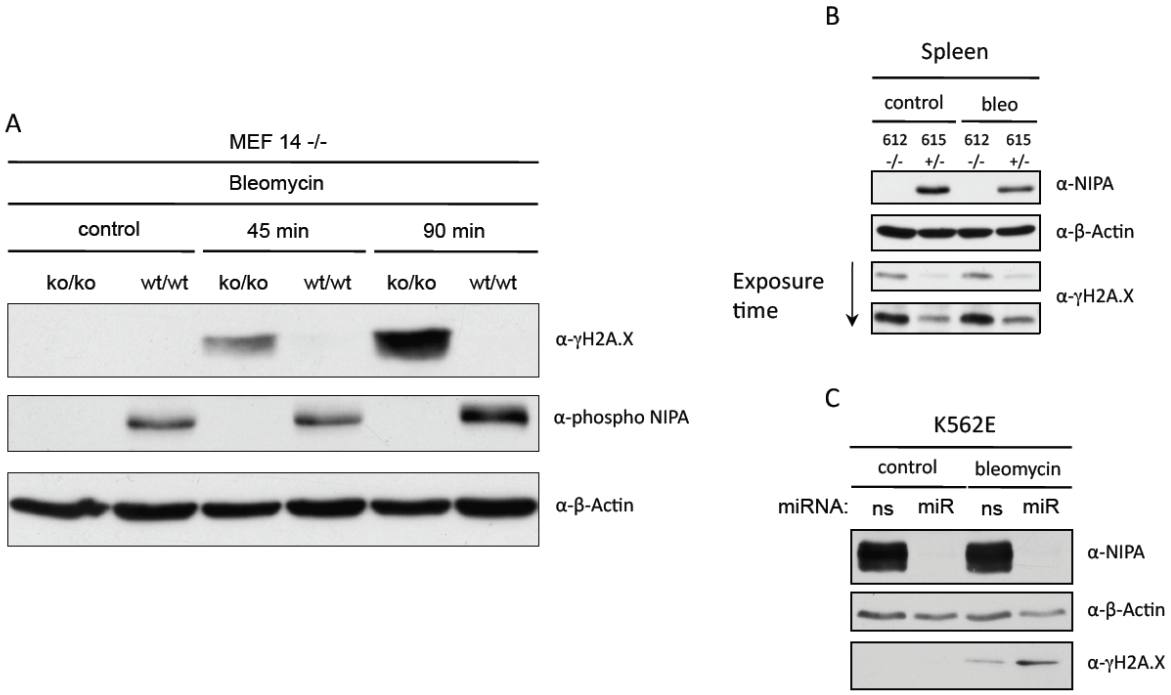

Fig. 3.5: Histone H2A phosphorylation after bleomycin treatment. Cells lacking NIPA display high levels of phosphorylated histone H2A (A) Fibroblasts from the wild type or NIPA -/- mice were treated with bleomycin, harvested at time points 45 min and 90 min, and assayed for H2A phosphorylation by Western blotting. (B) Whole cell compartment isolated from homozygous (NIPA -/-) or heterozygous (NIPA +/-) mice spleen was mock-treated or treated with bleomycin (25 μg/ml) for 1 h. Lysates were subjected to immunoblotting with indicated antibodies. (C) K562 cells expressing ecotropic receptor (K562E) were retroviral transfected with non-silencing miRNA (ns) or NIPA miRNA (miR), treated with BLM (25 μg/ml) for 1 h and the lysates were subjected to imunoblotting.

double-strand breaks by advancing replication forks[162]. In contrast, UVC although considered to generate stalk replication forks and not DSBs, still induces high phosphorylation of histone H2A in treated cells (Fig. 3.4). Additionally UVC treatment is difficult in handling especially with cells growing in the suspension or obtained from the mouse. For that reason bleomycin as an easy to use radiomimetic was used for further studies (Fig. 3.5). As shown in Fig. 3.5 A, H2A phosphorylation in NIPA$^{-/-}$ cells is high and increases over time. In striking contrast, only minimal or none γH2A.X phosphorylation was observed in BLM treated WT cells, what most probably correlates with an ongoing repair of DSBs. Similar phenomenon was found in extracts from cells isolated from NIPA$^{-/-}$ or NIPA$^{+/-}$ mouse spleen, showing elevated levels of γH2AX already without drug addition (Fig. 3.5 B) in NIPA deficient cells. After the treatment with BLM

phosphorylation was even higher when compared to the cells where one of the NIPA alleles was still present. To exclude the cell specific effects on the histone H2A phosphorylation, an additional experiment with K562 cells, retroviral transfected with NIPA miRNA *versus* control (Fig. 3.5 C), was performed. Again in the cells where NIPA was depleted, a higher expression of γH2A.X was detected when compared to control.

DNA damage triggers a signaling pathway, which results in the recruitment of DNA repair proteins to the sites of genomic lesion. This includes accumulation of DNA damage sensors, like γH2A.X, as well as other signaling-repair complexes into the IR induced foci (IRIF)[163].

To examine foci formation of γH2A.X in response to DNA damage, DSBs were introduced in HeLa cells, transiently transfected with NIPA or control siRNA, using IR irradiation (Fig. 3.6).

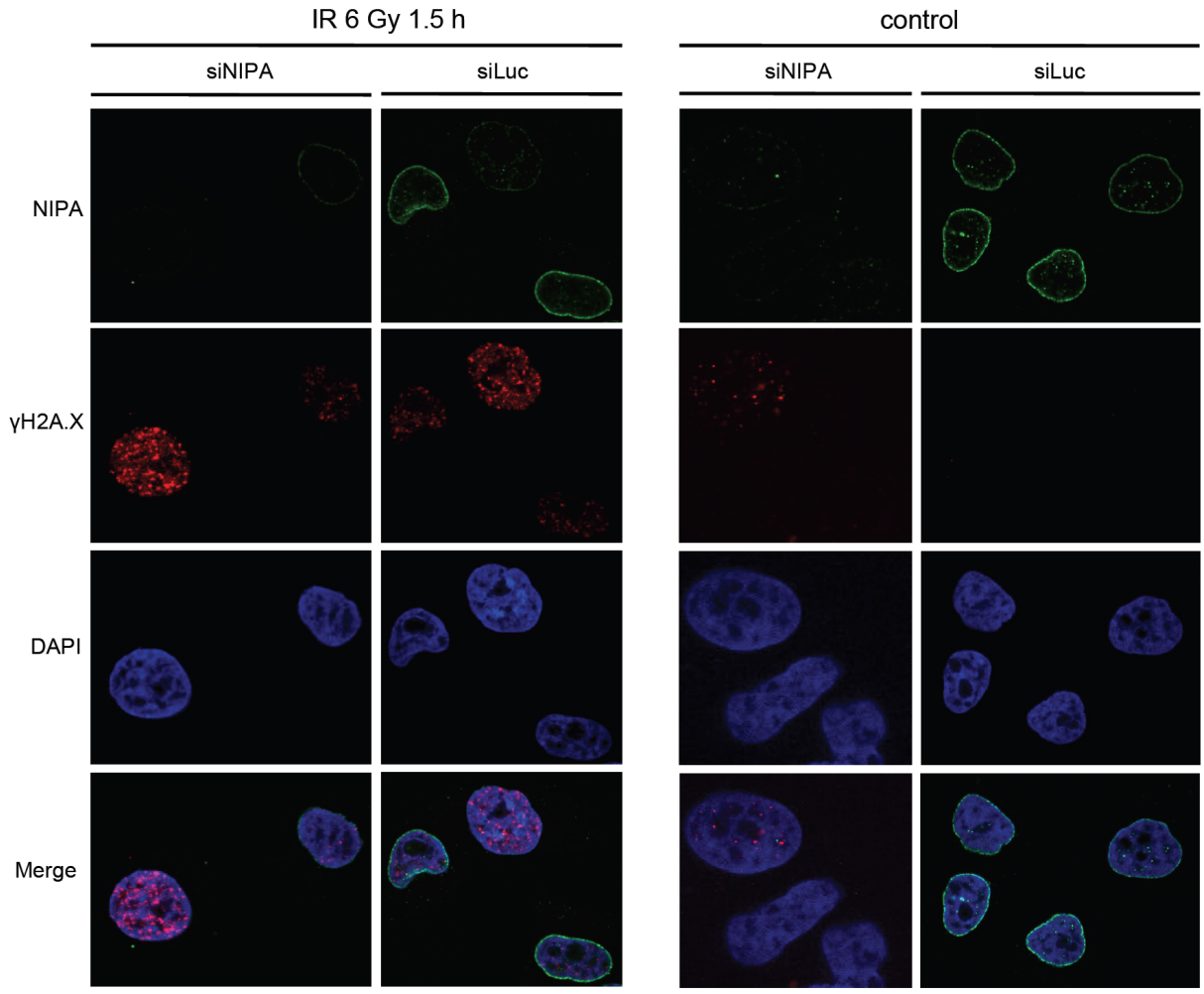

Fig. 3.6: NIPA depletion results in sustained foci formation of γH2A.X at IRIF. Figure shows indirect immunofluorescence performed in HeLa cells, transiently transfected with either NIPA siRNA or Luciferase siRNA (siLuc) as a control. Cells were irradiated with 6 Gy or mock treated (right panel) and after 1.5 h fixed in formaldehyde followed by staining with indicated antibodies. DAPI was used to stain nuclei.

As shown in the right panel of Fig. 3.6, without stimulation siLuc transfected cells didn't exhibit any focus formation of γH2A.X. Similar result was observed in NIPA siRNA with only minimal γH2A.X localization without treatment, what is consistent with the data obtained from mouse spleen (Fig. 3.5 B), where the phosphorylation of histone H2A was observed already before the application of damaging agent. However after irradiation with 6 Gy NIPA depleted cells displayed profound accumulation of γH2A.X foci in contrast to siLuc transfected cells (Fig. 3.6). Also the cells, where NIPA downregulation was not efficient, show less γH2A.X focus formation, what can be regarded as a confirming internal control. Altogether these data suggest either an involvement of NIPA in γH2A.X focus formation at IRIF or the role in dispersal of γH2A.X foci subsequent to the ongoing repair of DSBs.

3.2.2 Lack of NIPA results in impaired DNA damage repair

Given that NIPA deficiency is responsible for the prolonged histone H2A phosphorylation, it is conceivable that NIPA may be required for the maintenance of

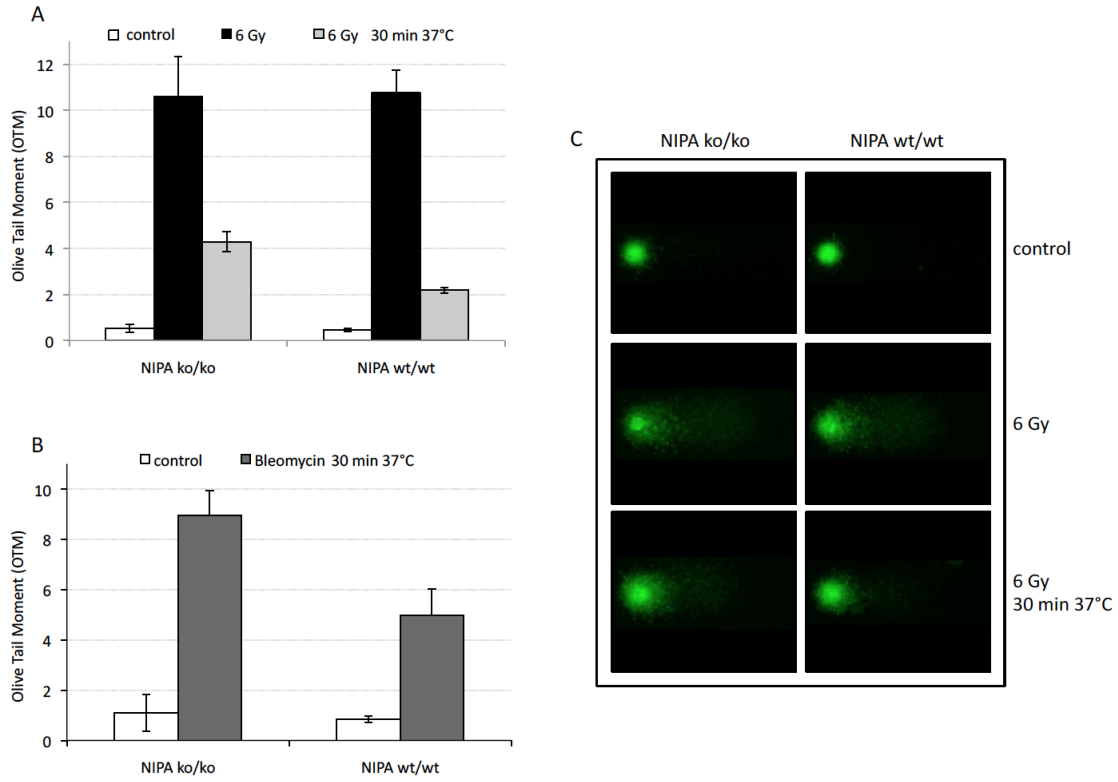

Fig. 3.7: DNA damage repair is compromised in the absence of NIPA. Lymphocytes from peripheral blood of NIPA-/- or NIPA +/+ mice were isolated by centrifugation with percol and subjected to the comet assay. (A) Samples were divided in 0 Gy fraction (control), 6 Gy fraction and 6 Gy after 30 min at 37°C to mimic repair conditions. Lymphocytes were treated analogical with bleomycin (B). An exemplary image of IR treated cells after electrophoresis was shown in (C).

genomic stability. However it still remained elusive if such a phenotype relies on higher sensitivity towards DNA damage or rather repair of the damage has been compromised.
To answer this question, a common and well-established method of measuring exogenously introduced DNA damage – comet assay – has been used. In this method damaged DNA is fragmented and migrates in the electrical field forming a "comet", what can be measured and quantified. Figure 3.7 A and B shows such a quantification after treatment with ionizing radiation or bleomycin treatment, respectively. Lymphocytes from NIPA$^{-/-}$ and NIPA$^{+/+}$ mice were isolated, treated with indicated agents and subjected to electrophoresis. To mimic repair conditions, 30 min incubation at 37°C was performed. As shown in Fig. 3.7 A treatment of the cells with 6 Gy radiation triggered similar response measured by olive tail moment (OTM) independently of NIPA status. The same can be observed on the exemplary image of this assay (Fig. 3.7 C). OTM reflects the distance between center of the comet head and center of the tail constituting the unit of DNA damage. The outcome changes completely, when cells were allowed to repair the damage. If the cell was lacking NIPA, repair abilities were severely compromised when compared to the wild type in both DNA damage regimes (Fig. 3.7 A and B). A longer comet tail in these cells serves as an illustration (Fig. 3.7 C).
These data strongly suggest that NIPA is an important factor in the DNA damage response and its deficiency leads to insufficient repair of the damaged lesions compromising the integrity of genomic stability.

3.2.3 NIPA deficiency has a negative impact on cell survival

Previous results demonstrate that NIPA could play an important role during DNA damage response[78,160]. Because defects in the DDR pathway frequently lead to the genomic instability, colony formation assay was performed to examine the role of NIPA in cell proliferation *in vitro*. To test the influence of various DNA damaging stimuli on NIPA depletion for colony formation abilities, clonogenic assay was carried out using IR and UVC radiation (Fig. 3.8 and Fig. 3.9). Equal numbers (600 per well for IR and 1000/well for UVC) of mock-depleted (non silencing miRNA - ns miR) or NIPA-depleted (NIPA miRNA - NIPA miR) U2OSE cells were seeded in a 6-well plate and immediately after attachment to the dishes irradiated with indicated doses of ionizing or ultraviolet radiation. Cells where then cultured for 10 days, and the colonies were stained with crystal violet.

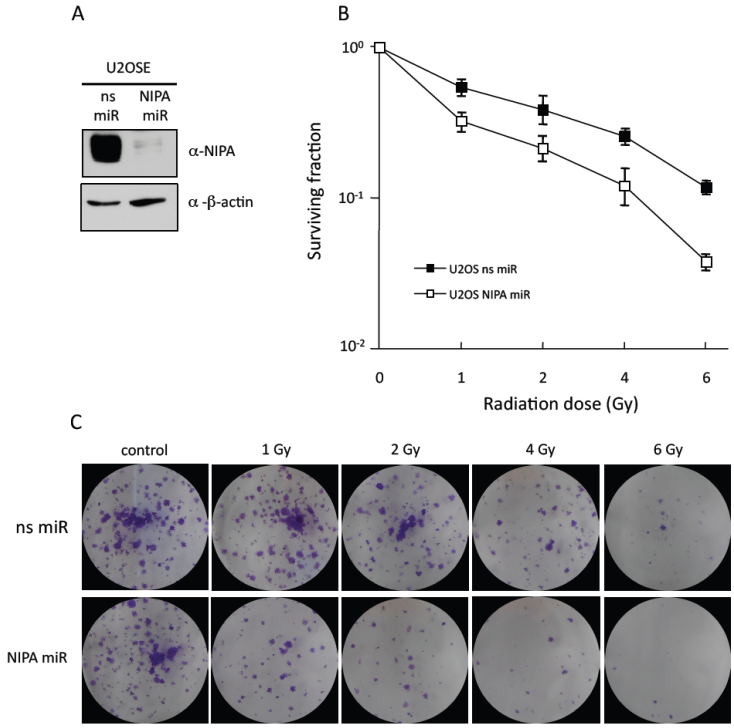

Fig. 3.8: NIPA down-regulation leads to the reduced survival of U2OS cells after gamma irradiation. U2OSE cells transfected with control non-silencing miRNA (ns miR) or NIPA miRNA (NIPA miR) were treated with various doses of IR, and the survival rate of these cells was determined by the colony formation assay. Results are presented as mean values ±SD, n=3. (A) Western blot with down-regulation efficiency. (B) Quantification of surviving fraction. (C) Representative image of surviving cells after indicated dose of ionizing radiation.

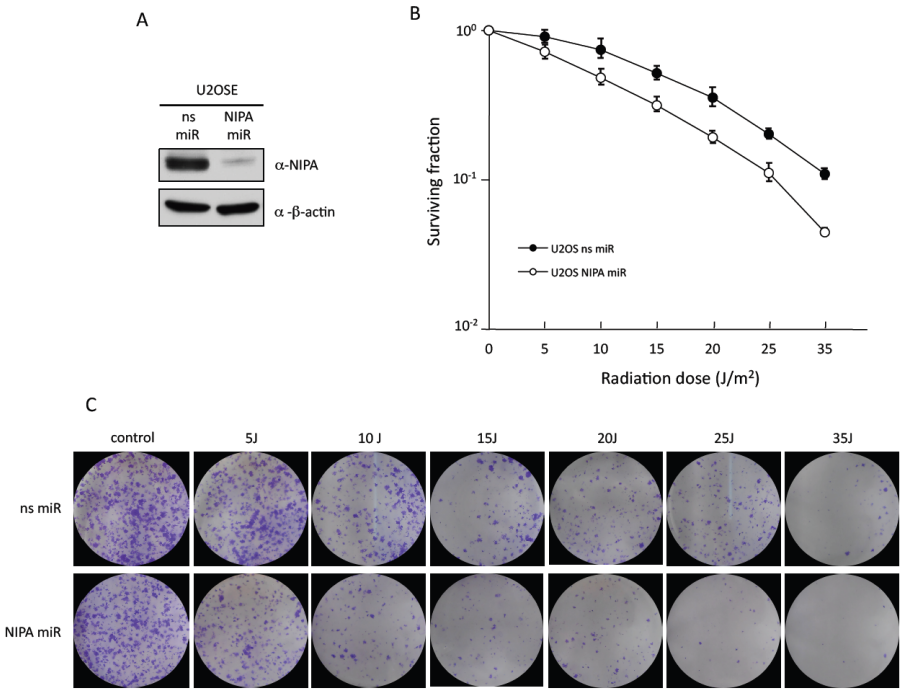

Fig. 3.9: NIPA down-regulation leads to the reduced survival of U2OS cells after UVC irradiation. U2OSE cells transfected with control non-silencing miRNA (ns miR) or NIPA miRNA (NIPA miR) were treated with various doses of UVC, and the survival rate of these cells was determined by the colony formation assay. Results are presented as mean values ±SD, n=3. (A) Western blot with down-regulation efficiency. (B) Quantification of surviving fraction. (C) Representative image of surviving cells after indicated dose of UV radiation.

Efficiency of NIPA downregulation was determined by the Western blot (Fig. 3.8 A and 3.9 A). Cells in untreated controls formed similar number of colonies what was taken into account by estimating the surviving fraction as plating efficiency, to exclude mistakes by counting the cells for the experiments. As shown in Fig. 3.8 B, NIPA deficiency leads to about 40% impairment in the survival at the lower IR doses when compared to the control. At higher irradiation dose (> 4 Gy) this discrepancy is increasing with only median colony formation of 8 in cells lacking NIPA and 25 colonies in control (Fig. 3.8 C). In case of UVC irradiated cells (Fig. 3.9 B), differences in survival between NIPA knock-down and wild type were not as much profound at the lower intensities, but severe at a high dose of UVC (Fig. 3.9 C). The data suggest that depletion of NIPA reduces clonogenic potential of U2OS osteosarcoma cells and is consistent with results published by Grogro[160]. Therefore it can be speculated that deregulation or repression of NIPA might be a key event in tumorigenesis for some types of cancers.

3.2.4 Downregulation of NIPA leads to enhanced apoptotic phenotype after DNA damage

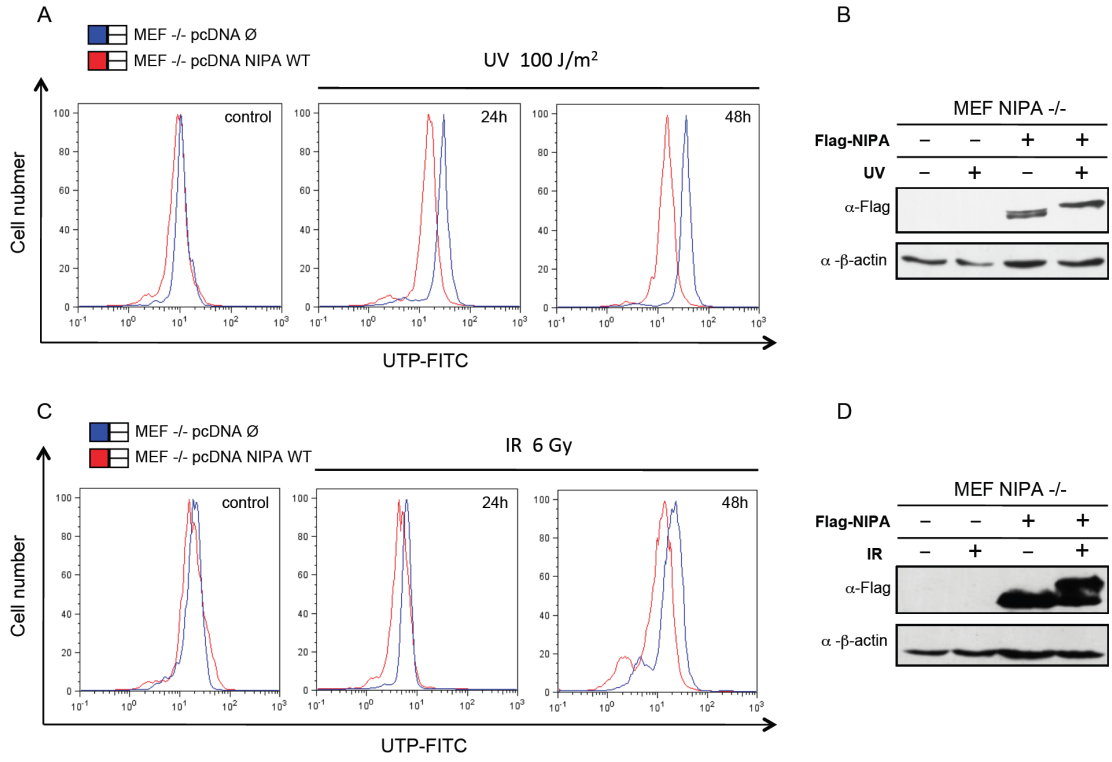

Fig. 3.10: Enhanced apoptotic phenotype in cells with NIPA deficiency. Mouse embryonic fibroblasts derived from NIPA -/- mouse were transfected with pcDNA empty vector for control or FLAG-NIPA to reconstitute NIPA expression. After the treatment cells were stained with APO-DIRECT™ Kit for TUNEL assay as described (2.2.4.7) and analyzed by flow cytometry. FACS analysis of UV (100 J/m²) treated (A) and IR (6 Gy) treated (C) cells after 24 and 48 h, stained with TUNEL assay. NIPA status and phosphorylation after UV (B) and IR (D) was presented in Western blot.

Reduced clonogenic ability of NIPA knockdown cells challenged with DNA damage raised a question of which mechanism has been involved in compromised survival of these cells. It is important to determine if defects in DDR resulted in programmed cell death – apoptosis. To investigate apoptosis, common method for detection of DNA fragments in situ using the terminal deoxyribonucleotidyl transferase (TdT)-mediated biotin-16-dUTP nick-end labeling (TUNEL assay) was used (Fig. 3.10).

Figure 3.10 A and C, show flow cytometry plots from FITC channel, where the shift of the histogram towards higher values is directly proportional to the signal intensity of the dUTP labeled DNA fragments. As demonstrated (Fig. 3.10 A), NIPA deficiency leads to enhanced apoptosis after UV in MEF cells transfected with an empty vector. Reconstitution of NIPA (Fig. 3.10 B) was efficient enough to protect the cells from apoptosis. UVC treatment has induced phosphorylation of NIPA as previously described (Fig.3.10 B). Treating the cells with ionizing radiation instead, didn't induce apoptosis to such an extent as with UVC (Fig. 3.10 C). As well in this case, NIPA was sufficiently reconstituted and phosphorylated (Fig. 3.10 D).

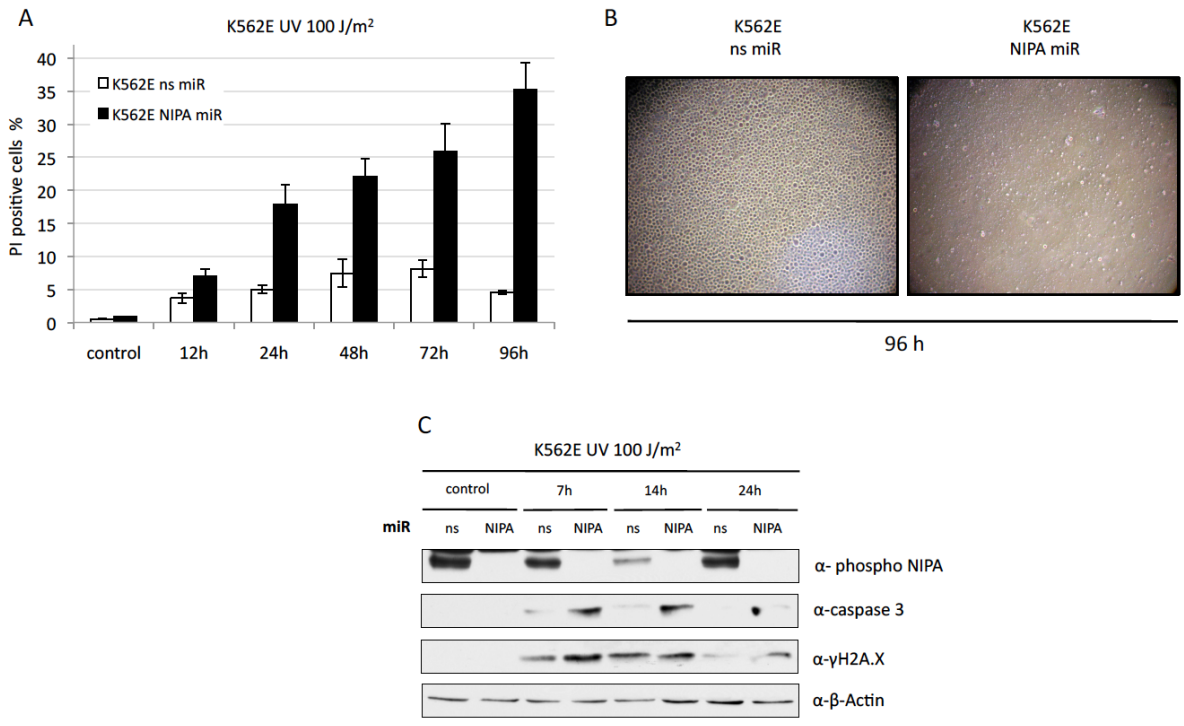

Fig. 3.11: NIPA knock-down induces a strong apoptotic phenotype in K562E cells after UVC treatment. K562E cells transfected with non-silencing (ns miR) or NIPA miRNA (NIPA miR) were treated with 100 J/m² UV. After indicated time points cells were stained with PI and analyzed by FACS. (A) A quantification of the PI positive $SubG_1$ cell compartment from independent experiments, n=3. (B) Effect of UV irradiation on the cell morphology from A (72h time point). Cells were harvested at indicated time points after treatment and lysates subjected to Western bloting using denoted antibodies (C).

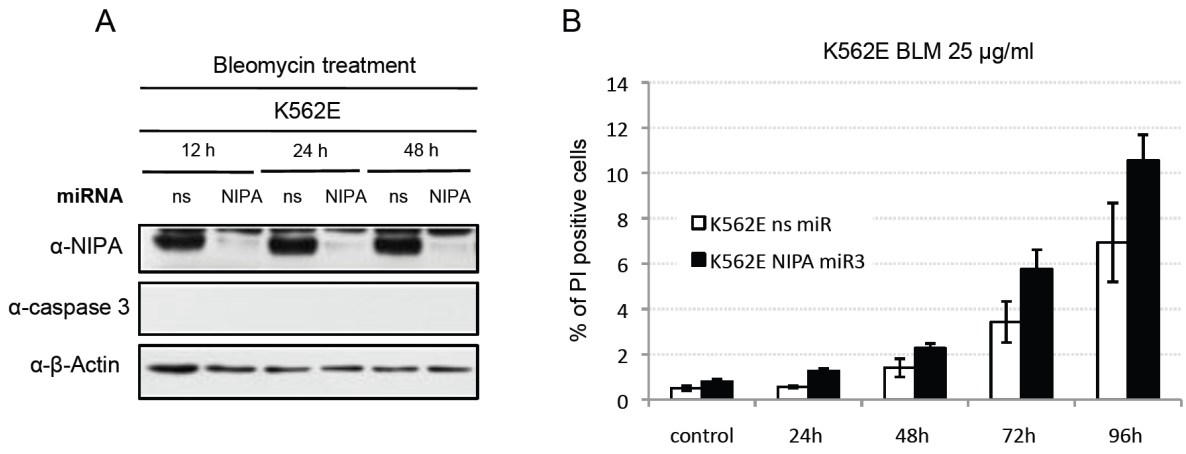

Fig. 3.12: Milder apoptotic phenotype in NIPA depleted K562E cells after BLM treatment.
K562E cells transfected with non-silencing (ns miR) or NIPA miRNA (NIPA miR) were treated with 25 µg/ml bleomycin and harvested after indicated time points for Western blotting (A) or PI staining (B). $SubG_1$ cells were quantified from three independent experiments.

Although it is not possible to directly compare intensities of different source of radiation, it may be that 6 Gy is not enough to induce a similar damage as it was with 100 J/m^2 of UVC. In either of the treatment regimes the shift of TUNEL positive cells is not severe, what could suggest a collateral mechanism in addition to apoptosis. A cell specific effect also cannot be excluded since the contrary data were published in MEF cells[78]. Similar results were observed in K562E cells, where NIPA was depleted using miRNA (Fig. 3.11 and 3.12). Treating these cells with UVC in absence of NIPA provoked a severe cell death already after 24 h (Fig. 3.11 A) in contrast to the BLM treatment (Fig. 3.12 B). At longer time points (96 h) after UV, near all the NIPA miRNA transfected cells were death or featured altered morphology, when compared to control cells (Fig. 3.11 B). Also bleomycin treatment induced high rate of PI positivity after 96 h (Fig. 3.12 B) however not comparable to UVC. These data correspond to results published by Grogro, where NIPA knock out MEFs exhibited higher fraction of $SubG_1$ in comparison to the wild type cells[160]. In addition, overexpression of cleaved caspase 3 in NIPA miRNA cells was significantly higher than in control and correlates with elevated phosphorylation of histone H2A (Fig. 3.11 C). Interestingly, BLM treatment was not sufficient to induce cleavage of caspase 3 (Fig. 3.12 A), what could explain a lower $SubG_1$ fraction in these cells (Fig. 3.12 B).

Aforementioned results suggest an induction of DNA damage dependent apoptotic pathway in NIPA deficient cells. Most probably this phenotype is dependent on the source of the damage resulting in a different kinetics of the cell death program and is a cell type specific event. An additional mechanism, like senescence, cannot be excluded.

3.2.5 NIPA is required for the recruitment of repair factors to the DNA damage foci

DNA damage signaling cascade is a complex and coordinated event that requires the actions of various proteins whose functions can be categorized as DNA damage sensors, transducers, mediators and effectors[164]. Double strand breaks (DSBs) are the most deleterious of all lesions causing genetic instability that may lead to the malignant transformation or cell death. Cells respond to DSBs with an ordered recruitment of signaling and repair proteins to the sites of DNA breaks. Therefore it is important to investigate the status of crucial proteins involved in sensing and repair of DNA damage in the context of NIPA. For this reason, measurements of residual DNA repair foci assembled by several proteins including phosphorylated histone H2A (γH2A.X), recombinase Rad51, mediator of DNA damage checkpoint protein 1 (MDC1) and tumour suppressor p53 binding protein 1 (53BP1), which all co-localize with radiation-induced DNA double-strand breaks, has been performed[165].

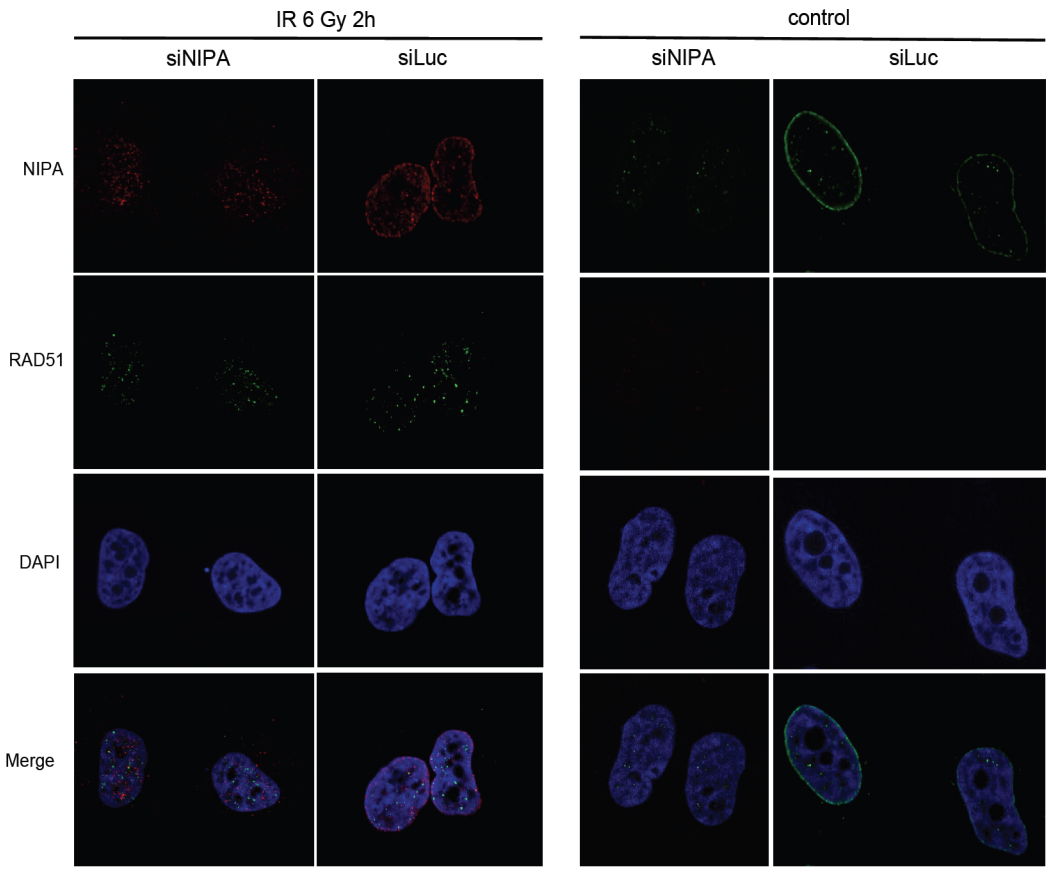

Fig. 3.13: Recruitment of Rad51 to the sites of DNA damage does not rely on NIPA. HeLa cells were transfected with NIPA siRNA (siNIPA) or Luciferase siRNA (siLuc) directly on the microscope cover glasses for 48 h and irradiated with 6 Gy. After 2 h cells were fixed with formaldehyde and stained with indicated antibodies for immunofluorescence analysis. DAPI was used to stain nuclei.

As already shown (Fig. 3.6) NIPA deficiency leads to profound foci formation of histone γH2A.X, well established as the early detectable marker for DSBs[161]. Since these foci are essential in facilitating the assembly of key repair factors at the damage sites, analysis of RAD51 focus formation, a critical protein that functions in homologous recombination repair and which knockout is embryonic lethal, has been performed (Fig. 3.13)[128]. For this reason, HeLa cells were transiently transfected with NIPA and control siRNAs for 48 h and irradiated with 6 Gy two hours prior to fixation in formaldehyde. In unchallenged cells any foci formation has been detected (Fig. 3.13 right panel) neither in the control cells nor in the NIPA deficient ones. After ionizing radiation RAD51 formed foci at the sites of DNA damage, however independently of NIPA status (Fig. 3.13 left panel). These data suggest that NIPA has no influence on the RAD51 recruitment following DNA damage.

Next, relocalization to the nuclear foci of yet another important protein involved in the DNA damage signaling pathway – MDC1 – was studied (Fig. 3.14).

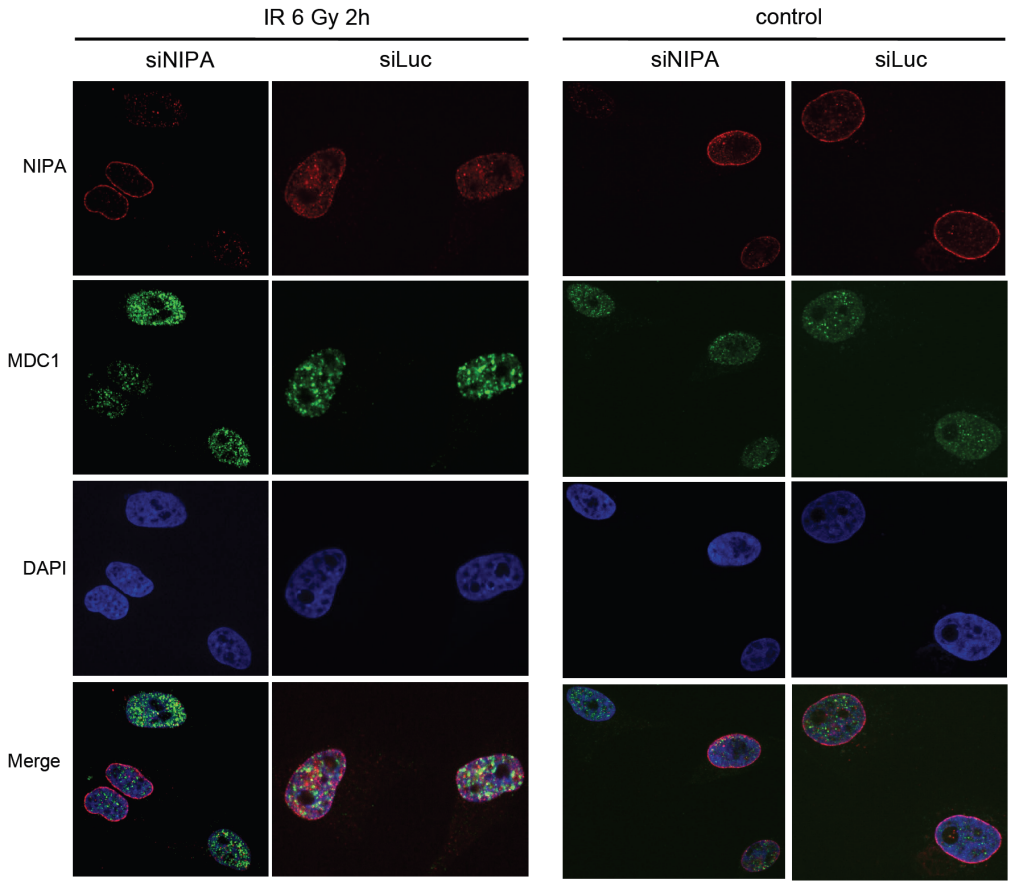

Fig. 3.14: MDC1 exhibit sustained focus formation in NIPA depleted cells following DNA damage. HeLa cells were transfected with NIPA siRNA (siNIPA) or Luciferase siRNA (siLuc) directly on the microscope cover glasses for 48 h and irradiated with 6 Gy. After 2 h cells were fixed with formaldehyde and stained with indicated antibodies for immunofluorescence analysis. DAPI was used to stain nuclei.

MDC1 regulates many aspects of DDR, such as the intra-S phase checkpoint, the G2/M checkpoint as well as foci formation of the MRN complex, 53BP1, and BRCA1[166-168]. As a mediator protein, MDC1 promotes histone H2A phosphorylation and is acting as a bridge for the interaction between ATM and γH2A.X[169]. After IR, MDC1 gets hyperphosphorylated and localizes to the damage induced foci. Therefore it is important to investigate MDC1 expression in context of NIPA lost in immunofluorescence studies.

As already described, HeLa cells transiently transfected with NIPA siRNA or control siRNA were treated with 6 Gy IR and stained with indicated antibodies (Fig. 3.14). While untreated cells showed diffuse nuclear staining of MDC1 (Fig. 3.14 right panel) in both NIPA siRNA and control cells, exposure of cells to IR within 2 h resulted in localization of MDC1 to the prominent nuclear foci (Fig. 3.14 left panel), consistent with previous reports[166]. However, in cells where NIPA expression was downregulated by small interfering RNA (siRNA), MDC1 focus formation was significantly elevated when compared to the internal control, where not all of the cells exhibit equal level of NIPA downregulation (Fig. 3.14 left panel). Increased MDC1-IRIF formation in NIPA deficient cells correlates with γH2A.X levels in these cells (Fig. 3.6). Interestingly previous work reports focus formation of MDC1 to be dose-dependent, with the average number of MDC1 foci per cell increasing with IR dosage[166]. Thus authors used extremely high IR doses (range between 10 – 20 Gy) to induce MDC1 hyperphosphorylation in comparison to dosage used in this study (6 Gy). This may suggest a hypersensitivity of NIPA depleted cells towards ionizing radiation in relation to MDC1 focusing at IRIF. On the other hand it also indicates that NIPA could act downstream of MDC1.

MDC1 is phosphorylated by ATM after it binds to γH2A.X and stabilizes MRN complex[98]. This phosphorylation allows for the recruitment of the E3 ubiquitin ligase complex - RNF8/UBC13, which through the modification of histones leads to remodeling of the chromatin and subsequent exposure of methylated histone H4[170]. This event is crucial for the recruitment of p53 binding protein 1 (53BP1), an important protein implicated in regulation of the G_2/M phase checkpoint as well as repair of DNA DSBs via non-homologous end-joining (NHEJ)[171-173].

To further investigate NIPA behavior in the DNA damage response, immunofluorescence studies involving 53BP1 were carried out (Fig. 3.15 and 3.16). NIPA was downregulated in HeLa cells by small interfering RNA and subjected to immunofluorescence analysis. In control cells, under normal conditions, 53BP1 exhibits pan-nuclear localization (Fig. 3.15 right panel, second lane) consistent with previous reports[174].

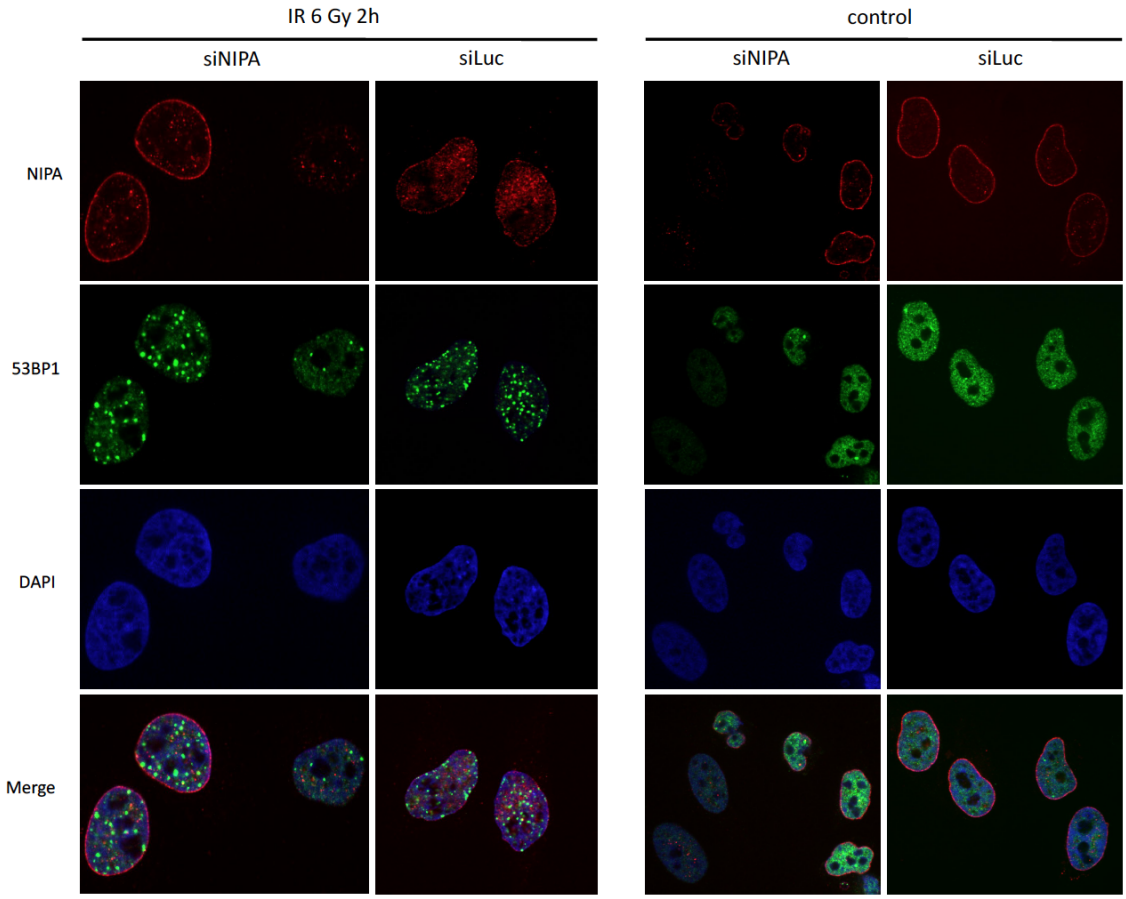

Fig. 3.15: 53BP1 fails to relocalize to the DNA damage induced foci in absence of NIPA. HeLa cells were transfected with NIPA siRNA (siNIPA) or Luciferase siRNA (siLuc) directly on the microscope cover glasses for 48 h and irradiated with 6 Gy. After 2 h cells were fixed with formaldehyde and stained with indicated antibodies for immunofluorescence analysis. DAPI was used to stain nuclei.

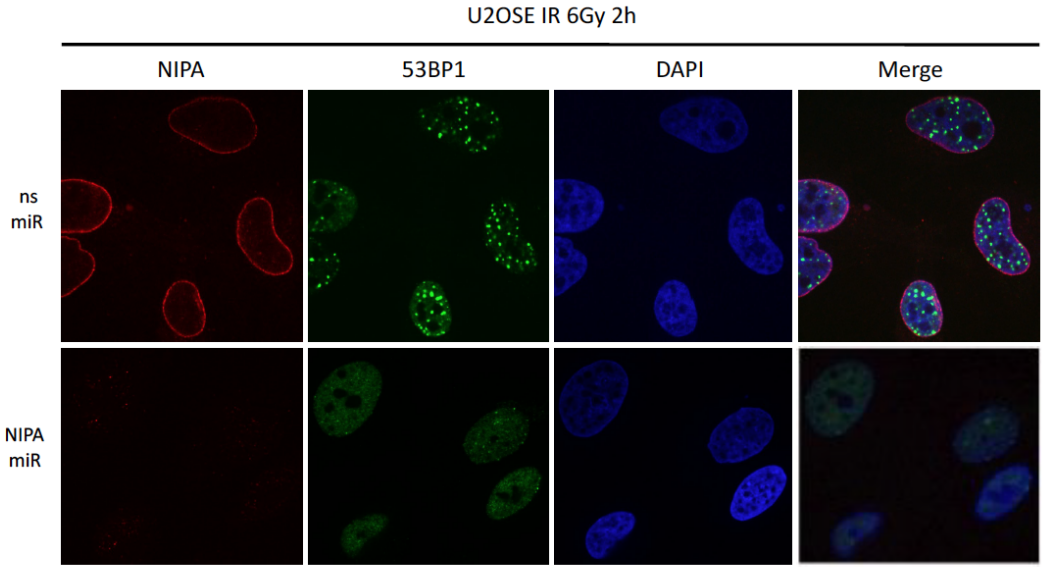

Fig. 3.16: 53BP1 fails to relocalize to the DNA damage induced foci in absence of NIPA. U2OSE cells expressing stable knockdown of NIPA (NIPA miR) or control (ns miR) were directly irradiated with 6 Gy on the microscope cover glasses and after 2 h cells were fixed with formaldehyde and stained with indicated antibodies for immunofluorescence analysis. DAPI was used to stain nuclei.

It is striking that after NIPA depletion 53BP1 expression is diminished or limited only to the nuclear background staining (Fig. 3.15 right panel, first lane). Additionally, upon exposure of cells to genotoxic stress, 53BP1 was rapidly redistributed to the distinct nuclear foci at the sites of DNA strand breaks only in control cells (Fig. 3.15 left panel, second lane) but localization was severely reduced in cells lacking NIPA (Fig. 3.15 left panel, first lane). To confirm this observation U2OSE cells with stable expression of NIPA knockdown were used and treated as already described. Significantly, it was found that 53BP1 localization to IRIF was intact only in cells where NIPA was unperturbed (Fig. 3.16 upper panel), whereas cells lacking NIPA failed to localize 53BP1 to damage induced foci (Fig. 3.16 lower panel).

These data suggest that NIPA may be important for the nuclear import of 53BP1 and its recruitment to the DNA damage sites, but probably acts downstream of MDC1 and independent of RAD51.

3.2.6 NIPA is not recruited to the sites of DNA damage

Accumulating evidence from previous experiments suggests that NIPA could be a potential member of the DNA damage repair family. It is well established that ATM/ATR-dependent phosphorylation of diverse sensors and mediators of DNA damage signaling creates an initial signal for subsequent accumulation of various repair proteins to DNA lesions. Also sensors itself are recruited to form damage induced foci at the sites of DNA breaks. Therefore it is essential to study if NIPA is recruited to the sites of DNA damage, to be able to answer the question if NIPA belongs to the group of sensors, mediators or effectors of the DNA damage repair mechanism. From the immunofluorescence studies any signs of recruitment of NIPA to the damage induce foci could be observed (Fig. 3.13 – 3.16). Thus microirradiation experiments were performed using 405 nm diode laser to definitely exclude this possibility. Microirradiation with a 405 nm laser generates a mixture of different types of DNA damage that are substrates for distinct DNA repair pathways involving XRCC1 and γH2A.X. XRCC1 (X-ray cross complementing factor 1) was reported to play a role of the loading platform, which coordinates repair at the sites of a single strand DNA damage[175]. As already described, γH2A.X detects mainly double strand breaks. Hence XRCC1 and γH2A.X were taken as a positive control. HeLa or NIH/3T3 cells stably expressing FLAG-

NIPA were locally irradiated with preselected lines of ~1 μm in diameter within the nucleus for 1 s (Fig. 3.17).

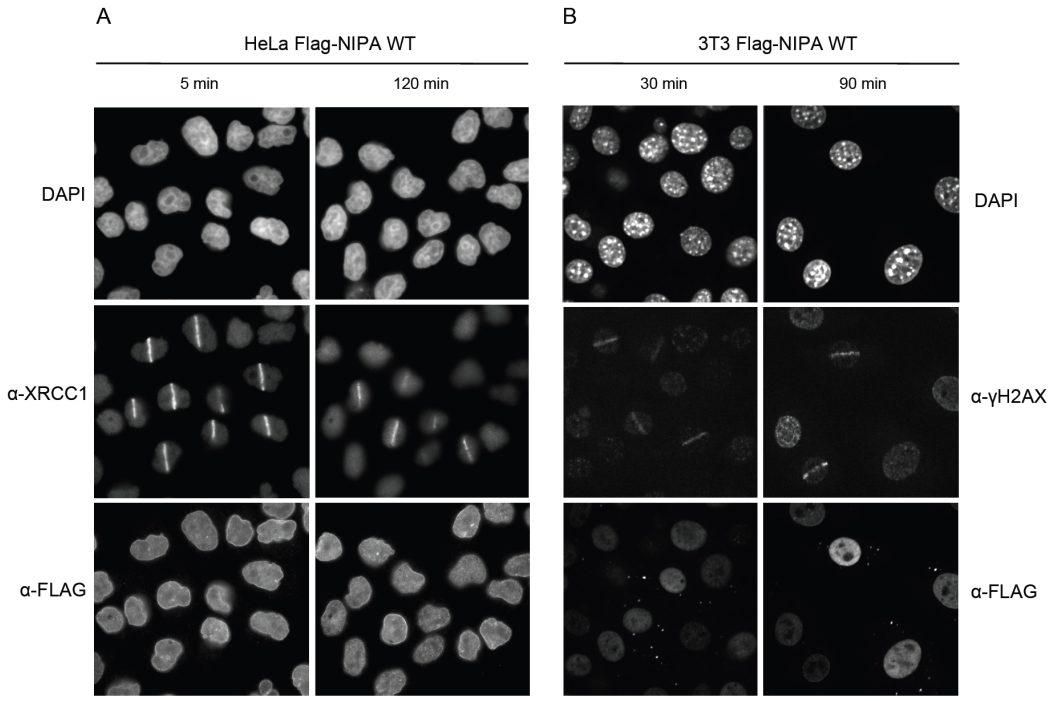

Fig. 3.17: NIPA is not recruited to the sites of DNA damage. HeLa (A) or NIH/3T3 (B) cells stably expressing FLAG-NIPA were microirradiated with 405 nm diode laser. Cells were fixed after indicated time points and stained with appropriate antibodies.

Microirradiated sites stained positive for XRCC1 (Fig. 3.17 A) as well as phophorlyated histone variant γH2A.X (Fig. 3.17 B), given that the irradiation of the cells was efficient. However neither in HeLa nor in 3T3/NIH cells any recruitment of NIPA to the sites of DNA damage could be detected (Fig. 3.17 A and B). These data reinforce previous observations and exclude the possibility of NIPA being a sensor of DNA damage. Thus NIPA is not recruited to the DNA breaks.

3.2.7 NIPA is attached to the nuclear membrane

Whereas in the previous experiments recruitment of NIPA to the DNA damage foci has been excluded, the protein dynamics still remained elusive. Precise information about NIPA mobility could be advantageous in determining the rol of NIPA in the DNA damage response. To address this question, fluorescence recovery after photobleaching (FRAP) and fluorescence loss in photobleaching (FLIP) has been performed (Fig. 3.18). FRAP involve bleaching of fluorescently tagged proteins in a region of interest (ROI) inside the cell with a high intensity laser pulse. When protein is transiently bound to the structures

in the photobleached region, the fluorescence recovers owing to exchange between fluorescently labeled diffusing molecules in the cytoplasm or membrane with the bound

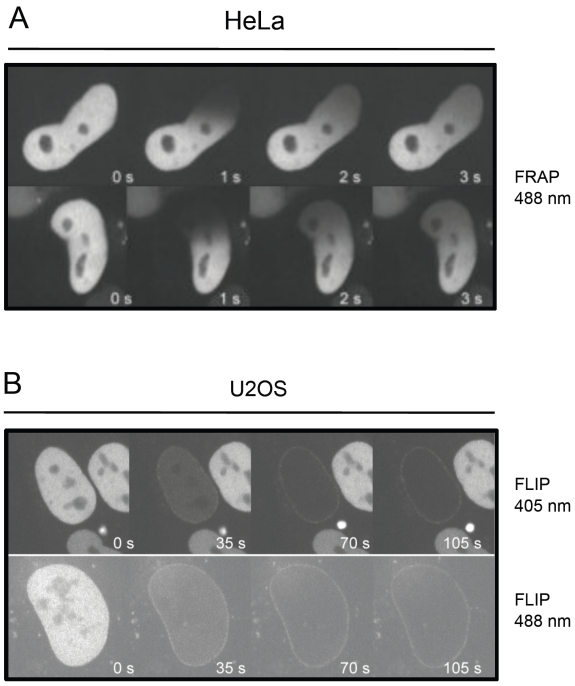

Fig. 3.18: NIPA localizes to the nuclear membrane. (A) HeLa cells were transiently transfected with GFP-NIPA fusion protein and FRAP experiment with 488 nm laser has been performed. (B) For FLIP experiment, U2OS cells transiently transfected with GFP-NIPA fusion protein were pulse irradiated with 405 and 488 nm laser. Images were taken using immunofluorescence microscope.

photobleached molecules in the bleached region[176]. As shown in Fig. 3.18 A, mobility of GFP-NIPA protein in the nuclear, diffuse fraction is very high with a recovery reached already after 3 seconds. This data suggest a fast kinetics of the diffuse fraction in the nu-

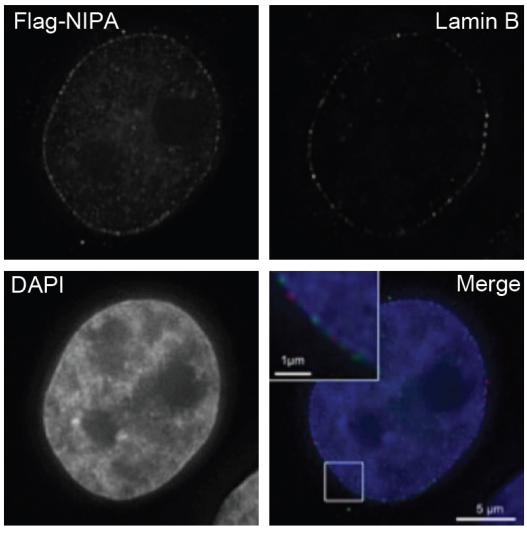

Fig. 3.19: NIPA localizes to the nuclear envelope. Images of NIPA from 3D-SIM showing nuclear envelope localization. Lamin B was stained as a positive control. HeLa cells stable expressing FLAG-NIPA were seeded on high precision microscope cover glasses (Roth) and fixed with formaldehyde prior to staining with indicated antibodies.

cleus. However very interesting observation was made after FLIP. In FLIP experiment, a region is repeatedly bleached by an intense laser pulse. A decrease of fluorescence of dye-tagged molecules outside the bleached region allows for assessing continuity between intracellular compartments and for measuring the kinetics of recruitment to the bleached region from various cellular areas[177]. When U2OS cells expressing GFP-NIPA were continuously illuminated at the ROI narroved to the nuclear middle zone, a fraction of the GFP-tagged protein was predominantly localized to the nuclear envelope (Fig. 3.18 B). After 10 s when the whole diffuse fraction was bleached out, NIPA was still present at the nuclear membrane. These data suggest a very strong attachment of NIPA to the nuclear periphery.

To further confirm that the localization pattern detected for the GFP-tagged protein did not reflect an artifact, an additional super-resolution 3D-structured illumination microscopy (3D-SIM) of cells expressing FLAG-tagged NIPA protein was carried out with antibody against the tag epitope (Fig. 3.19). Lamin B, a well established nuclear envelope protein[178], was used as a control to visualize nuclear membrane. Again, FLAG-tagged NIPA revealed a nuclear envelope staining, similar but not overlapping with Lamin B receptor (Fig. 3.19). On the basis of this analysis it can be concluded that NIPA is attached to the nuclear membrane.

When the membrane localization became known, the question arised whether distribution of NIPA at the nuclear envelope is cell cycle dependent.

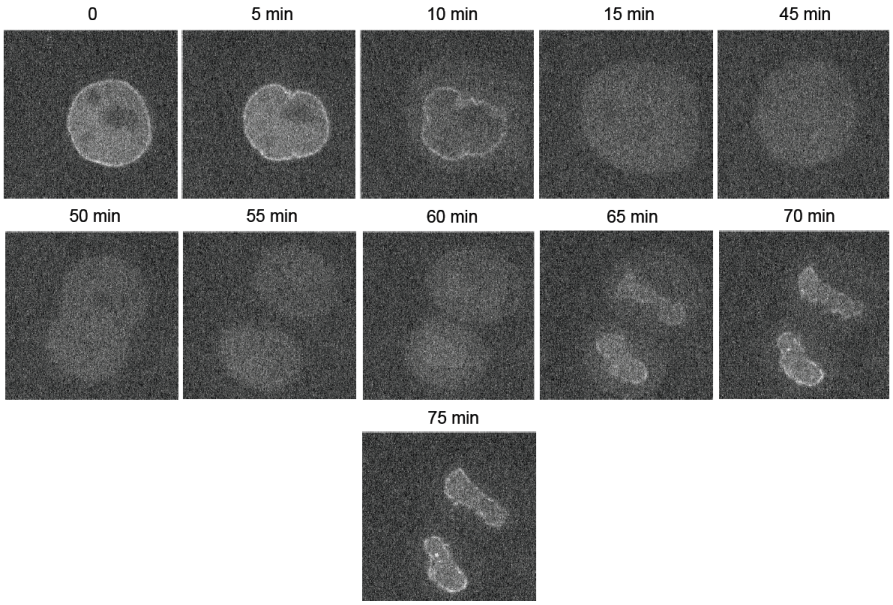

Fig. 3.20: NIPA is tightly bound to the nuclear envelope and becomes soluble after the nuclear envelope breakdown. Live imaging of the GFP-NIPA transfected HeLa cell undergoing mitotic division. Images were taken after indicated time points.

Live imaging of the cell expressing GFP-NIPA was performed and followed until a full cell division has been accomplished (Fig. 3.20). It is well established, that the nuclear envelope is disassembled during mitosis in higher eukaryotes and that integral membrane proteins of the nuclear envelope, such as lamin receptors and integral membrane nuclear pore proteins, are dispersed throughout the endoplasmic reticulum[179]. NIPA showed a strong membrane colocalization until the cell reached mitosis where envelope localization disappeared after the nuclear envelope breakdown (NEB) at time point 10 min. (Fig. 3.20). This is the time when cell entered prometaphase and NIPA become soluble in the cytoplasm. Membrane staining reappears at time point 60 min. simultaneously with the nuclear envelope assembly (Fig. 3.20). These data support an assumption that NIPA might be not only nuclear protein, though particularly a nuclear membrane protein.

3.2.8 NIPA is localized to the nuclear pore complex (NPC)

To get more insight into precise localization of NIPA at the nuclear envelope, super-resolution imaging of FLAG-tagged NIPA together with nuclear pore complex component

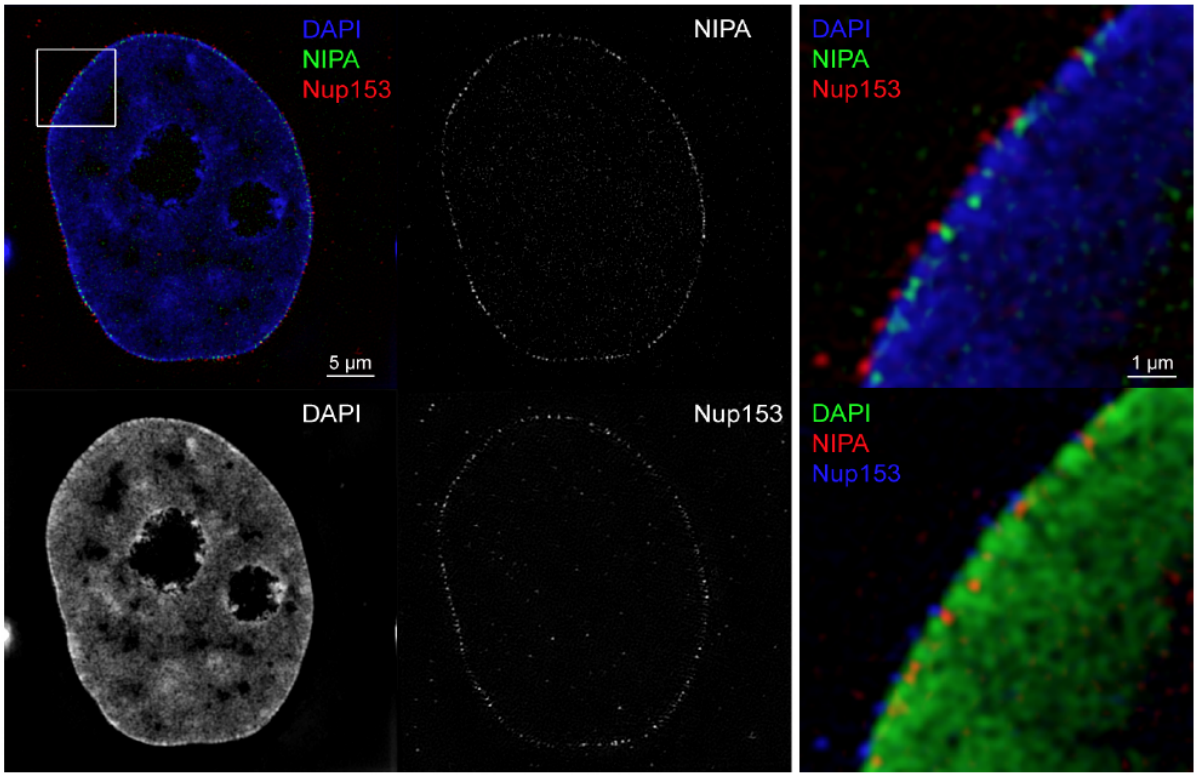

Fig. 3.21: NIPA localizes to the nuclear pore complex (NPC). 3D-SIM super-resolution imaging showing FLAG-NIPA associated to the nuclear pore complex. Nucleoporin 153 (Nup153) was co-stained as a positive control for the NPC.

Nup153 (nucleoporin 153 kDa) was performed (Fig. 3.21). As shown before, a characteristic nuclear membrane localization of NIPA could be observed (Fig. 3.21 left panel). Surprisingly, in the higher resolution image (Fig. 3.21 right panel) NIPA is localized directly at the nuclear pore complex overlapping with Nup153. Staining pattern may suggest that NIPA is localized to the inner nuclear membrane based on its appearance well below Nup153 (Fig. 3.21). These data strongly indicate that NIPA is localized at the nuclear pore complex, possibly to the nuclear basket.

3.2.9 Identification of NIPA interaction partners

Nuclear pore complex is a unique gateway that facilitates transport of thousands of macromolecules between the nucleus and the cytoplasm thereby allows for the spatial segregation of replication and transcription in the nucleus and translation in the cytoplasm. The NPC represents one of the largest and most complex proteinaceous assemblies in the eukaryotic cell[135]. To ultimately decipher the underlying structure relevance of NIPA at the NPC, it is indispensable to shed more light on the direct interaction of NIPA with its potential binding partners in native condition as well as after DNA damage.

Identified protein	Accesion nr	Molecular Weight	NIPA WT	NIPA Bleo	NIPA UV
Isoform 1 of Nuclear-interacting partner of ALK|C3HC zinc finger-like	IPI00301421	55 kDa	497	431	477
Nucleoprotein TPR|TPR/MLP1/MLP2-like protein	IPI00742682	267 kDa	130	207	316
Serine/threonine-protein kinase PLK1|Protein _kinase_ domain;POLO box duplicated region	IPI00021248	68 kDa	14	25	60
Propionyl-CoA carboxylase beta chain, mitochondrial|Carboxyl transferase domain	IPI00007247	58 kDa	7	11	36
Isoform 1 of Ataxin-2-like protein|LsmAD domain; Ataxin-2 C-terminal region	IPI00456359	113 kDa	8	17	33
Propionyl-Coenzyme A carboxylase, alpha polypeptide isoform a precursor	IPI00744115	80 kDa	3	10	30
Isoform 1 of Nck-associated protein 1|Membrane-associated apoptosis protein	IPI00031982	129 kDa	11	7	24
Nucleolin| (FYDLN_acid);RNA recognition motif	IPI00604620	77 kDa	3	9	19
Isoform 1 of Heterogeneous nuclear ribonucleoprotein M|RNA recognition motif	IPI00171903	78 kDa	0	5	18
Isoform 1 of S-phase kinase-associated protein 1, SKP1	IPI00301364	19 kDa	15	14	14
Isoform 1 of Heterogeneous nuclear ribonucleoprotein K	IPI00216049	51 kDa	0	7	13
Isoform 1 of Serine/threonine-protein phosphatase PGAM5, mitochondrial| Phosphoglycerate mutase family	IPI00788907	32 kDa	0	2	13
ATP-dependent DNA helicase 2 subunit 2|Ku70/Ku80 beta-barrel domain; Ku70/Ku80 C-terminal arm;Ku70/Ku80 N-terminal alpha/beta domain;Ku C terminal domain	IPI00220834	83 kDa	5	7	10
Isoform 2 of Nucleophosmin|Nucleoplasmin NPM	IPI00220740	29 kDa	0	4	9

Table 1. List of NIPA interaction partners identified in mass spectrometry analysis.

Therefore NIPA-tandem-Strep-single-FLAG-tagged (NIPA-SF-TAP) construct was used to overexpress NIPA in HEK 293T cells and after tandem affinity purification, NIPA interactors were identified by proteomic approach. Selected proteins, with a highest score identified in this screen, were listed in Table 1. Additionally to the native conditions, cells expressing NIPA were treated with UV and BLM to identify NIPA interactors in DNA damage background. Table 1 consists of 6 columns: identified protein, it accession number and molecular weight as well as interaction partners in untreated control (NIPA WT), bleomycin treated (NIPA Bleo) and UV treated (NIPA UV) cells. Numbers in columns correspond to assigned spectra for each protein and are measure for the protein amount.

As expected, NIPA opens the list of identified proteins with the highest amount of assigned spectra, comparable in all treatment conditions. Also SKP1 identified in this screen was not surprising, since it constitutes SCF^{NIPA} complex. Interaction with SKP1 was equal independent of the treatment, in contrast to almost each other identified protein, where BLM or UV treatment triggered elevated association with NIPA. This data additionally suggest that the interaction of NIPA with SKP1 is not affected after UV or BLM treatment. A very interesting hint found in the screen turned to be nucleolin, a major nucleolar protein in growing eukaryotic cells. It was found associated with intranucleolar chromatin and pre-ribosomal particles and very recently in DNA DSB induced damage response through MDC1-dependent pathway[180]. Nucleolin binds NIPA very weakly in unperturbed cells but the binding rises tree-fold after BLM treatment and dramatically after UV.

Another interesting nucleolar protein listed is nucleophosmin (NPM1), extensively studied in the last two decades in the pathobiology of NPM-ALK (nucleophosmin-anaplastic lymphoma kinase) oncogenic fusion protein found in ALK-positive anaplastic large cell lymphoma[181]. NPM1 was reported in p53/p14ARF/MDM2 pathway to be responsible for retaining ARF in the nucleolus, what prevents ARF from interacting with MDM2 and promoting p53 activation[182]. It was also implicated in DNA damage response pathway by RNF8 dependent recruitment to sites of DNA damage after phosphorylation and as a candidate substrate for the E3 activity of BRCA1[183,184]. Previously NIPA was identified as a nuclear interaction partner of ALK what makes NPM-NIPA axis particularly interesting for further studies. NIPA does not bind NPM in untreated cells (Table 1), but the binding was detected after DNA damage treatment, with a stronger relation to UV.

The next relevant hint, a mitochondrial phosphoglyceratemutase (PGAM5), was identified as necrosome associated protein and characterized as proapoptotic neo-IBM class mitochondrial substrate of inhibitors of apoptosis proteins (IAPs)[185,186]. IAPs are the guardian ubiquitin ligases that regulate proapoptotic proteins. NIPA was characterized before to poses a prototypic BIR domain (Baculovirus Inhibitor of apoptosis Repeat; IAP)[80] what could suggest a potential role for PGAM5 as a substrate of NIPA. Binding of PGAM5 could not been observed in untreated cells, however was induced after the treatment, especially with UV. Moreover PGAM5 was found in a complex with PLK1 in NIPA proteomic screen (Table 1). PLK1 is a key positive regulator of mitosis, meiosis and cytokinesis but is also involved in DNA damage checkpoint response, spindle formation and mitotic exit[187]. Very recently PLK1 was reported to maintain homologous recombination by regulating the phosphorylation, together with CK2, of Rad51 during DNA double strand break repair[188]. NIPA was identified to contain a canonical PLK1 target sequence (Fig. 3.4) what makes it a potential substrate for this kinase. Table 1 shows that NIPA is binding to PLK1 in the native state and that the binding doubles after BLM treatment, raising almost five fold upon UV irradiation. These data suggest a prospect interplay between NIPA and PLK1.

Precision of non-homologous end joining repair depends on the Ku heterodimer (Ku70, Ku80), which binds and holds together broken DNA termini, allowing nucleases to trim excess ends and polymerases to fill the gaps. It recruits DNA-PKcs, by bridging two DNA ands and stimulating ligation[115]. Ku70/Ku80 was also identified in the screening for NIPA interactors, with a higher affinity after induction of DNA damage. Thus NIPA could be involved in NHEJ pathway, since it has been reported that Ku removal from DNA requires an active mechanism – ubiquitination – to allow for repair regulation and post-repair recovery[189].

Finally the strongest binding, by the highest amount of identified protein, was observed with translocated promoter region (TPR). TPR is a structural protein (267-kDa) and a conserved component at the nuclear side of the NPC. It has been suggested as the main architectural element of the nuclear basket[190]. It has also been implicated in mRNA export control, nuclear protein export, silent telomeric chromatin organization and DNA damage repair[191,192]. NIPA interacts with TPR with a very strong affinity in untreated cells (Table 1). Nevertheless interaction exaggerates after UV and, to lower extent, BLM treatment. These data together with previous reports suggest TPR to be the best candidate for further studies.

3.2.10 NIPA interacts with TPR at the NPC

Mass spectrometry data suggest an interaction of NIPA with nucleoporin TPR and along with immunofluorescence demonstrate that this localization may be restricted to the nuclear pore complex. To confirm the interaction between NIPA and TPR, immunoprecipitation assays have been performed in HEK293T cells (Fig. 3.22).

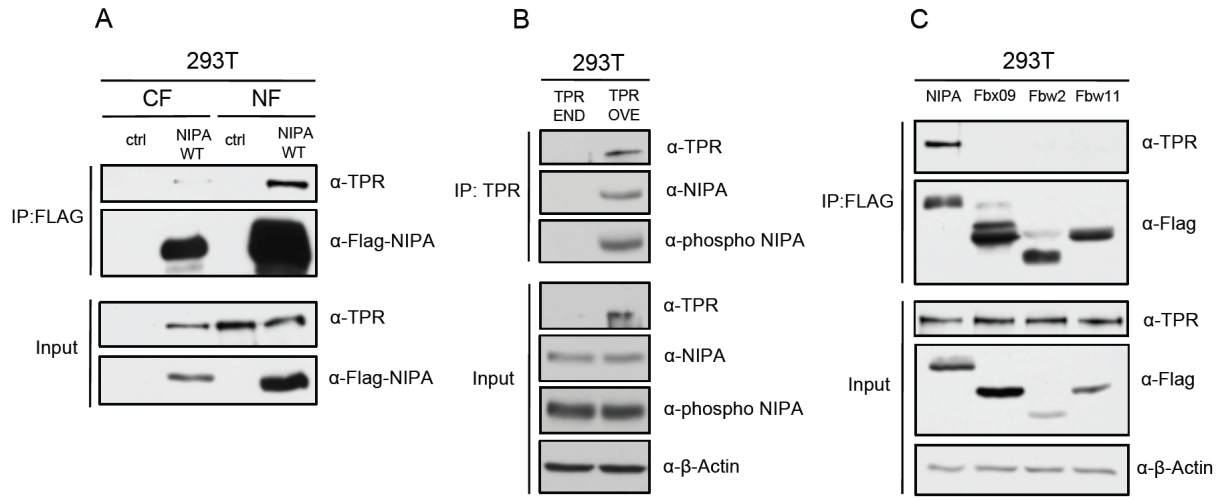

Fig. 3.22: NIPA interacts with TPR. (A) NIPA was expressed in HEK293T cells and cell fractionation was performed to obtain nuclear fraction (NF) and cytoplasmic fraction (CF). Immunoprecipitation (IP) was performed with anti-FLAG resin (Sigma) and coimmunoprecipitated TPR was detected in Western blot. (B) TPR was overexpressed (OVE) in HEK293T cells and together with endogenous (END) protein as a control, was immunoprecipitated (IP) with antibody against TPR. NIPA coimmunoprecipitation was detected in Western blot using NIPA andtibody and antibody against phosphorylated form of NIPA. (C) HEK293T cells were transfected with the indicated FLAG-tagged F-box protein constructs. Exogenous proteins were immunoprecipitated (IP) with anti-FLAG resin, and immunocomplexes were probed with antibodies against indicated proteins.

FLAG-tagged NIPA was overexpressed in HEK293T cells and after 48 h cells were fractionated using dounce homogenizer to obtain nuclear and cytoplasmic fraction (Fig. 3.22 A). Both fractions were then lysed and immunoprecipitation (IP) was performed using FLAG resin followed by probing of immunocomplexes with FLAG and TPR antibodies. As shown in Fig. 3.22 A, fractionation was not completely pure, resulting in some contamination of cytoplasmic fraction with a nuclear compartment. However coimmunoprecipitation led to detection of the clear signal with TPR antibody in FLAG-NIPA overexpressed cells but not in the control cells. Furthermore, immunoprecipitation with overexpressed TPR in HEK293T cells was performed (Fig. 3.22 B) and NIPA could be successfully coimmunoprecipitated using NIPA antibody and phospho-NIPA antibody. Binding was evident only in extracts with overexpressed TPR protein while amounts of endogenous protein were probably not sufficient to detect interaction.

To confirm the specific binding between NIPA and TPR, immunoprecipitation with three additional F-box proteins: FBXO9, FBW2 and FBW11 was carried out (Fig. 3.22 C). FLAG-tagged versions of these proteins along with NIPA were transfected into HEK293T cells and then immunoprecipitated to evaluate their interaction with endogenous TPR. Fig. 3.22 C demonstrates that NIPA was the only F-box protein able to coimmunoprecipitate with TPR. All the other F-box proteins did not bind endogenous TPR.

Thus, in agreement with previous findings from mass spectrometry, immunoprecipitation results show that NIPA specifically binds to the endogenous TPR, thereby localizes to the NPC.

3.2.11 NIPA's zinc-finger motif is indispensible for the interaction with TPR at the NPC

NIPA was previously characterized as an F-box protein, containing NLS domain for the nuclear localization as well as a zinc-finger like domain in the N-terminus as a potential substrate interaction motif[83,84]. Also phosphorylation of Ser354 was revealed as a key event in regulation of NIPA upon mitotic entry[83,85]. Following identification of TPR as an interaction partner of NIPA it is crucial to map the binding region. Therefore, immunoprecipitation experiment was implemented to analyze impact of TPR binding to NIPA after mutation of its characteristic motifs described above. For this reason HEK293T cells were transfected with FLAG-tagged NIPA constructs: wild type (WT); zinc-finger mutant (Δ ZnF); nuclear localization signal mutant (Δ NLS); F-box mutant (Δ F-box) and Ser354 mutant (S354A) along with empty vector as a control (Fig. 3.23).

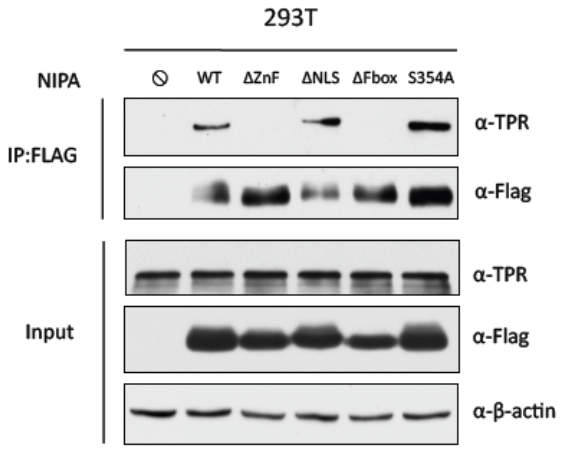

Fig. 3.23: Identification of the region responsible for binding to TPR. HEK293T cells were transfected with the indicated FLAG-tagged NIPA constructs. Exogenous proteins were immunuprecipitated (IP) from the cell extracts with anti-FLAG resin, and immunocomplexes were probed with antibodies to the indicated proteins.

IP was performed using FLAG beads and subjected to Western blot. Immunocomplexes were detected with indicated antibodies (Fig. 3.23). Consistently with previous results, wild type protein binds efficiently to TPR. The same observation was made after mutation of serine 354 to alanine. This mutant was still binding to TPR, suggesting that constitutively active NIPA is still binding TPR and is localized at the nuclear envelope. Also NLS mutation did not affect binding to TPR, what could be explained with experimental setup. Immunoprecipitation was performed on the whole cell lysates, making cytoplasmic localization of NLS mutant irrelevant, since the precipitation was still possible. Interestingly, NIPA zinc-finger mutation resulted in complete abrogation of binding to TPR, supporting hypothesis of the substrate interaction abilities of this domain (Fig. 3.23). Similar result was detected for F-box mutant, which was also unable to bind TPR. These data suggested abrogation of NIPA binding to TPR by either potential loss of binding domain (Δ ZnF) or by impairment in E3 ligase activity as a consequence of abolished binding to SKP1 (Δ F-box). To determine whether abrogation of TPR binding by zinc-finger or F-box mutant altered their localization to the nuclear envelope, live imaging using GFP-fusion proteins has been performed (Fig. 3.24 and 3.25). Overexpression of GFP-tagged proteins led to a pan-nuclear localization what, as expected, restrained the possibility to investigate nuclear membrane localization (Fig. 3.24 A and B left panels).

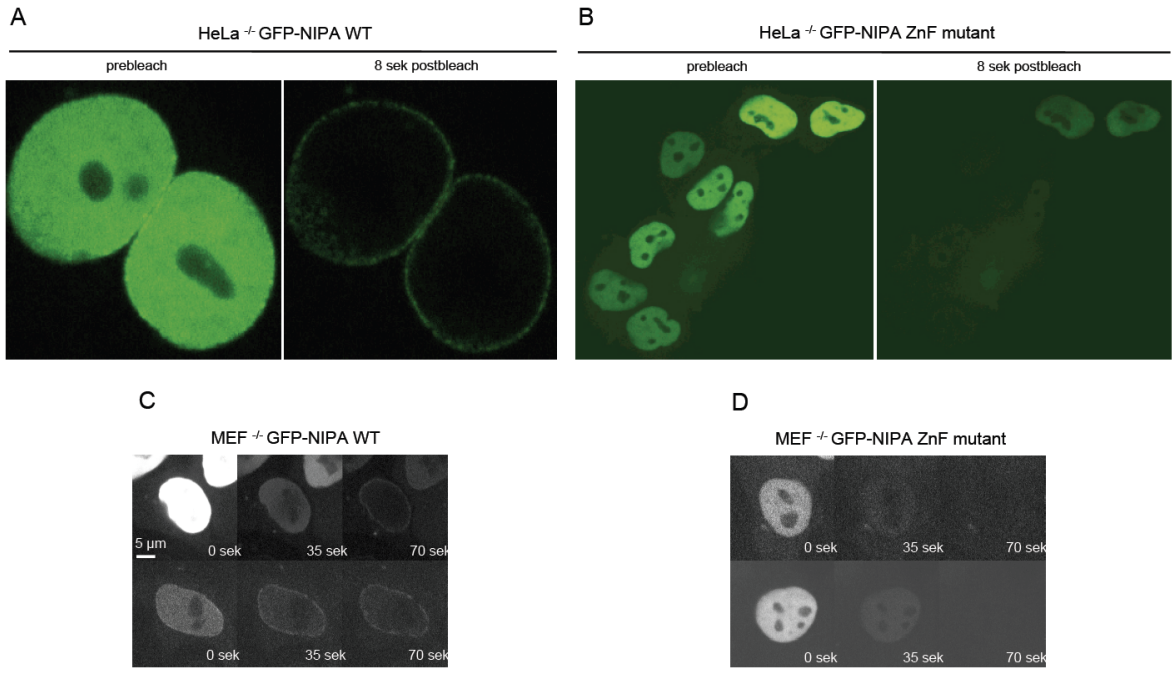

Fig. 3.24: NIPA zinc-finger mutant failed to localize to the nuclear membrane. FLIP experiment in HeLa cells overexpressed with NIPA wild type GFP-fusion protein (A and C) as well as with NIPA zinc-finger mutation GFP-fusion protein (B and D). Images represent different periods of photobleaching.

FLIP was employed to solve this issue. Cells were repeatedly photobleached in regions narrowed to the nuclear middle zones, and images were taken after different time points postbleach. NIPA wild type protein was localized at the nuclear membrane in short (Fig. 3.24 A) as well as longer periods after photobleaching (Fig. 3.24 C). In contrast to this finding, zinc finger mutant did not localize to the nuclear envelope and GFP expression was completely abolished after photobleaching (Fig. 3.24 C and D).

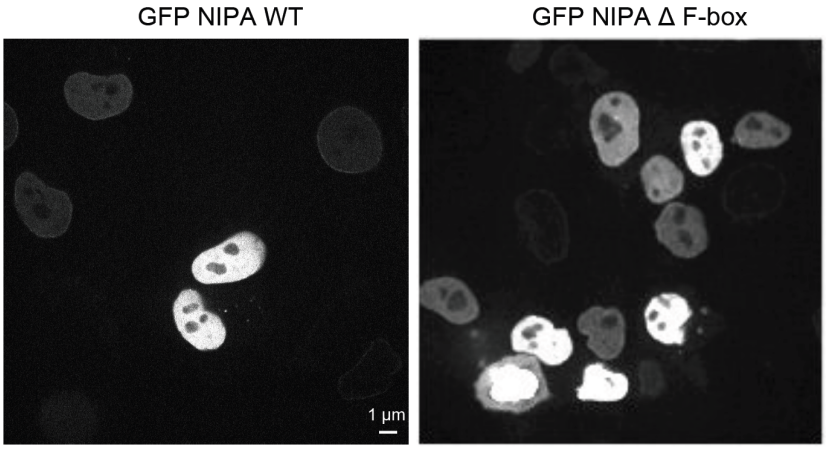

Fig. 3.25: NIPA F-box mutant still localizes to the nuclear membrane. Live imaging of HeLa cells transfected with NIPA wild type (GFP NIPA WT) and NIPA F-box mutant (GFP NIPA Δ F-box) GFP-fusion proteins.

The same phenotype was expected for F-box mutant according to the binding studies obtained from immunoprecipitation (Fig. 3.23). Surprisingly live imaging experiment, using GFP-fusion NIPA F-box mutant protein demonstrated sustained membrane localization, similar to the wild type protein (Fig. 3.25). This contradiction could be explained either by the close proximity of an F-box domain to the zinc-finger motif or by the lower expression of the F-box mutant in immunoprecipitation studies. It is also possible that due to the close proximity disruption of F-box had an influence on zinc-finger motif leading to insufficient binding in immunoprecipitation experiments. On the other hand, expression of FLAG-tagged F-box protein mutant in lysates (Fig. 3.23) was lower in comparison to expression of other proteins, possibly leading to defective coimmunoprecipitation of TPR. Altogether these data suggest that only zinc finger motif in NIPA is indispensible for TPR binding at the nuclear membrane.

To pinpoint the importance of NIPA's zinc-finger domain for the nuclear pore complex localization, super-resolution microscopy of wild type and zinc-finger mutant GFP-fusion proteins was employed (Fig. 3.26). In agreement with previous findings, wild type

protein was located at the NPC overlapping with co-staining of TPR. NIPA zinc-finger mutant instead resulted in mislocalization of the protein from the NPC (Fig. 3.26).

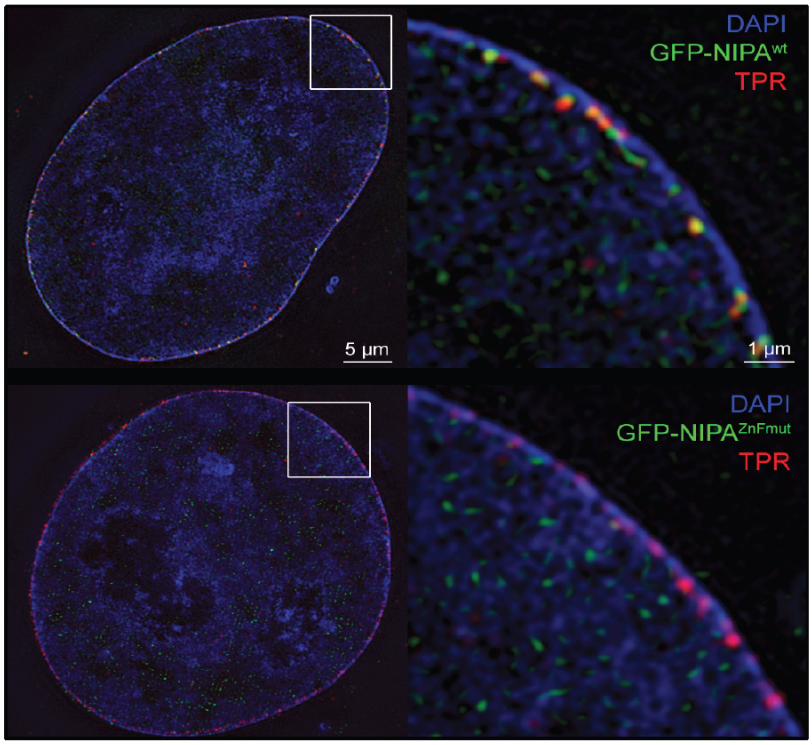

Fig. 3.26: NIPA zinc-finger mutant failed to localize to the NPC. 3D-SIM super-resolution imaging of GFP-NIPA wild type (WT) and GFP-NIPA zinc-finger mutant (ZnF mut) at the nuclear pore complex. TPR was stained in red to visualize interaction at the NPC.

These data strongly suggest that zinc-finger domain encoded in the N-terminus of NIPA is responsible for an interaction with nucleoporin TPR and that this binding localizes NIPA to the nuclear pore complex.

3.2.12 TPR is a scaffolding protein for NIPA

Docking site motifs regulate protein interactions between MAP kinases and substrates, activators, and scaffolding proteins[193]. MAPK family member ERK2, was implemented in cell survival, growth and differentiation, and very recently was shown to phosphorylate NIPA at the G_2/M transition[85]. In its inactive state ERK2 is anchored in the cytoplasm and upon activation is translocated to the nucleus where it is believed to function in phosphorylating nuclear targets such as transcription factors. Direct binding with nucleoporins (Nup153 and Nup214) has been suggested in the translocation mechanism[193,194]. Additionally, TPR was shown to be both a substrate and a scaffold for

activated ERK2[195]. Thus we hypothesize, that TPR could be a platform facilitating ERK2 interaction with NIPA, what allows for the ERK2 mediated NIPA phosphorylation also after DNA damage.

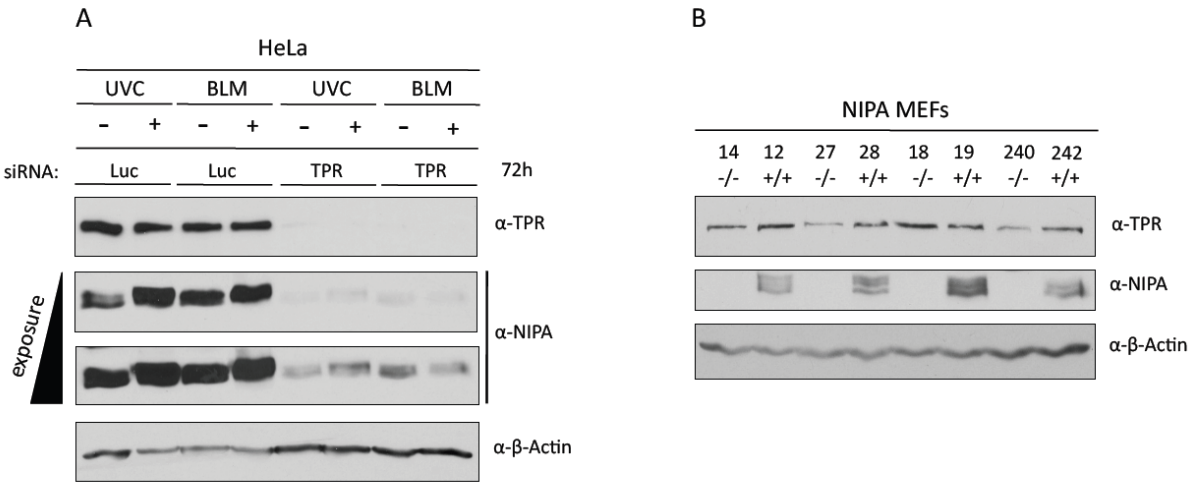

Fig. 3.27: TPR anchors NIPA to the NPC. (A) HeLa cells were transfected with TPR or Luciferase siRNA and after 72 h treated with bleomycin or UV irradiation. Protein extracts were probed with antibodies to the indicated proteins. (B) Mouse embryonic fibroblasts derived from homozygous NIPA knockout mice (-/-) or NIPA wild type mice (+/+) were analyzed by immunoblotting for TPR expression.

To test this hypothesis, TPR was downregulated in HeLa cells by using synthetic siRNAs and after 72 h cells were treated with bleomycin or UV irradiation to induce NIPA phosphorylation. Strikingly, TPR depletion led to almost complete downregulation of NIPA. At longer film exposition a slight NIPA signal has been observed, however treatment induced phosphporylation was reduced upon TPR silencing when compared to the control (Fig. 3.27 A). Thus, these results do not clearly reveal the role of TPR in ERK2 mediated NIPA phosphorylation upon DNA damage though strongly indicate anchoring abilities of TPR towards NIPA at the NPC.

Next, to exclude an opposite possibility, namely NIPA scaffolding TPR to the NPC, several mouse embryonic fibroblast cell lines derived from NIPA$^{-/-}$ mice were probed against TPR levels along with NIPA$^{+/+}$ cells as a control. As shown in Fig. 3.27 B, TPR was still present after NIPA knockout in all tested cell lines. However, in some cell lines (14$^{-/-}$; 27$^{-/-}$ and 240$^{-/-}$) expression level of TPR was reduced in comparison to NIPA wild type cells. This may indicate a role of NIPA in stabilization of TPR. Taken together, these results indicate that TPR is a scaffolding protein for NIPA and that this binding tethers NIPA to the NPC.

3.2.13 TPR may be ubiquitously regulated by NIPA

Given that NIPA specifically interacts with TPR and that the binding is mediated through a potential substrate-binding motif – zinc-finger, it is conceivable that NIPA may ubiquitously regulate TPR. It has been suggested that nucleoporins are ubiquitously expressed in all cell types and at all developmental stages[196].

In order to investigate if TPR is regulated by ubiquitination, HeLa cells were first treated with cycloheximide, which inhibits *de novo* protein synthesis. In addition, proteasome inhibitor, MG132, was used to control proteasomal degradation (Fig. 3.28 A).

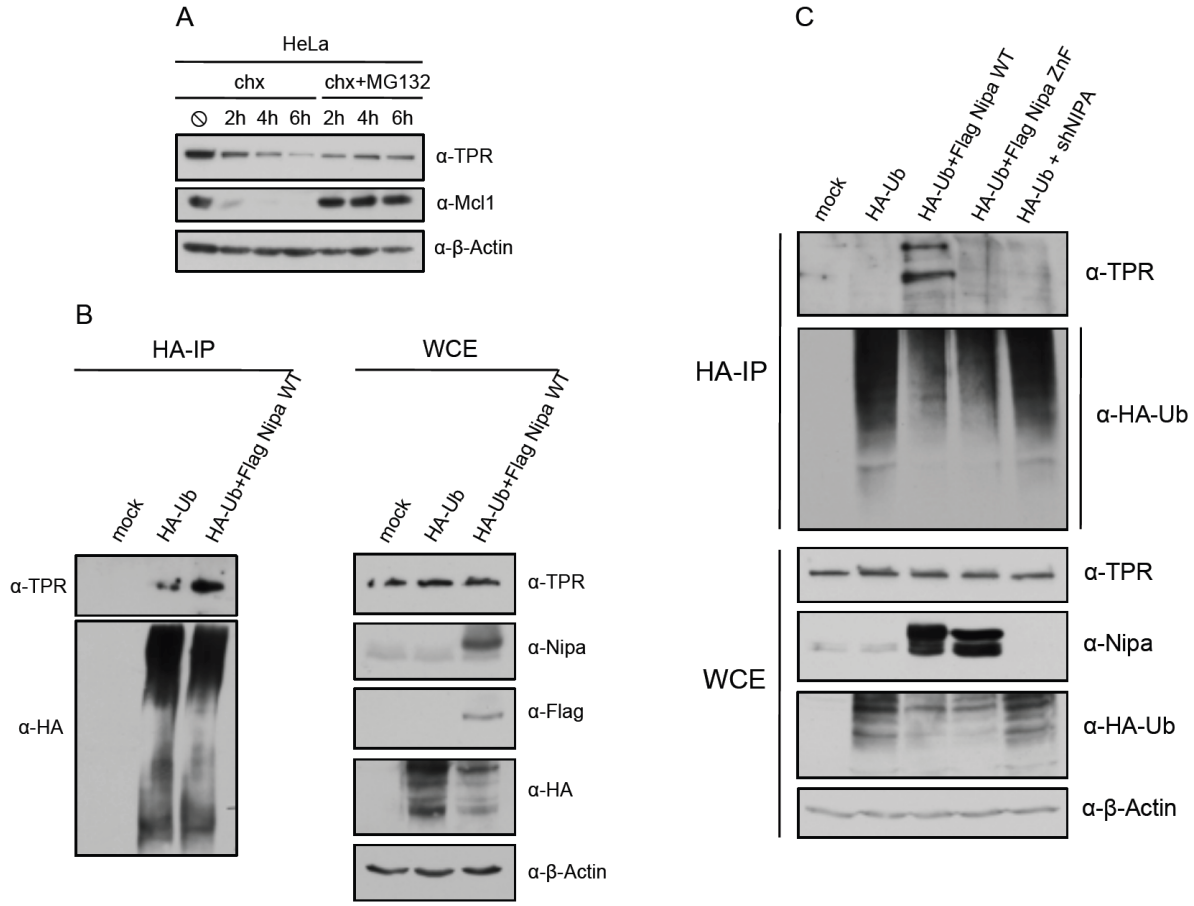

Fig. 3.28: NIPA may be regulating TPR by ubiquitination. (A) HeLa cells were treated with cycloheximide to block *de novo* protein synthesis. Proteasome inhibitor - MG132 was used to control protein degradation. Mcl1 served as an internal control for degradation. Cell extracts were probed with antibodies against indicated proteins. (B) In vivo ubiquitination assay in HEK293T cells transfected with HA-tagged ubiquitin along with FLAG-tagged NIPA was performed by immunoprecipitation with HA resin. Coimmunoprecipitation was visualized in Western blot with indicated antibodies. (C) *In vivo* ubiquitylation was performed like in (B) with an addition of zinc finger mutant overexpression as well as NIPA siRNA.

It is shown in Fig. 3.28 A that already after 2 h incubation with cycloheximide, TPR expression is reduced to about 50 %. With the longer time points tendency is clearly augmented. MCL1 expression, the anti-apoptotic BCL-2 family member known for very

fast degradation kinetics[197], was almost completely abrogated, corroborating cycloheximide activity. As expected, addition of proteasome inhibitor MG132, sustained TPR expression indicating the proteasomal degradation pattern.

To gain further insight into how NIPA could regulate TPR, it was studied whether NIPA is able to ubiquitylate TPR *in vivo*. Indeed, TPR was coimmunoprecipitated in ubiquitylation assay with HA-ubiquitin (Fig. 3.28 B). The interaction is stronger after FLAG-NIPA overexpression. Thus, the signal differs from the typical ubiquitylation pattern and could be explained by the TPR molecular mass. TPR is a large protein of 267 kDa therefore an addition of 8.5 kDa ubiquitin molecules may not result in characteristic ubiquitylation smearing.

Since the binding between TPR and NIPA is mediated through the zinc-finger motif, it was aimed to establish if disruption of this motif would lead to the abrogation of TPR ubiquitylation (Fig. 3.28 C). Endogenous NIPA did not induce TPR ubiquitylation (Fig. 3.28 C, second lane). FLAG-NIPA overexpression instead was sufficient to immunoprecipitate TPR from HEK293T cells extract (Fig. 3.28 C, third lane), while NIPA-ZnF mutant compromised this effect (Fig. 3.28 C, fourth lane). The inability of NIPA-ZnF to promote TPR ubiquitination was most probably due to defects in NIPA ability to bind its substrate after zinc-finger disruption. Additional control using NIPA siRNA showed no ubiquitination of TPR, what verifies our previous findings (Fig. 3.28 C last lane). These results indicate that SCF^{NIPA} ligase activity may be required for the ubiquitination of TPR. However further *in vitro* ubiquitination studies have to be performed to definitely support this notion.

3.2.14 NIPA and TPR deficiency results in impaired homologous recombination repair

Having established a direct interaction between NIPA and TPR, and according to evidence suggesting their role in DNA damage response, it is likely that both proteins act in a concert to facilitate DNA damage repair. DNA double strand breaks represent the highest genotoxic risk for the cell survival and are mainly repaired by homologous recombination (HR) or non-homologous end joining (NHEJ). Repair pathway choice may be controlled by the early acting proteins that influence both repair pathways[198]. Once the commitment is made, pathway-specific proteins drive the reaction toward HR or NHEJ products. Recent reports demonstrate that, at least in cancer cells, choice of the

repair pathway is moved towards HR[199,200]. Thus, it was examined whether NIPA or TPR have an influence on homologous recombination repair (Fig. 3.29).

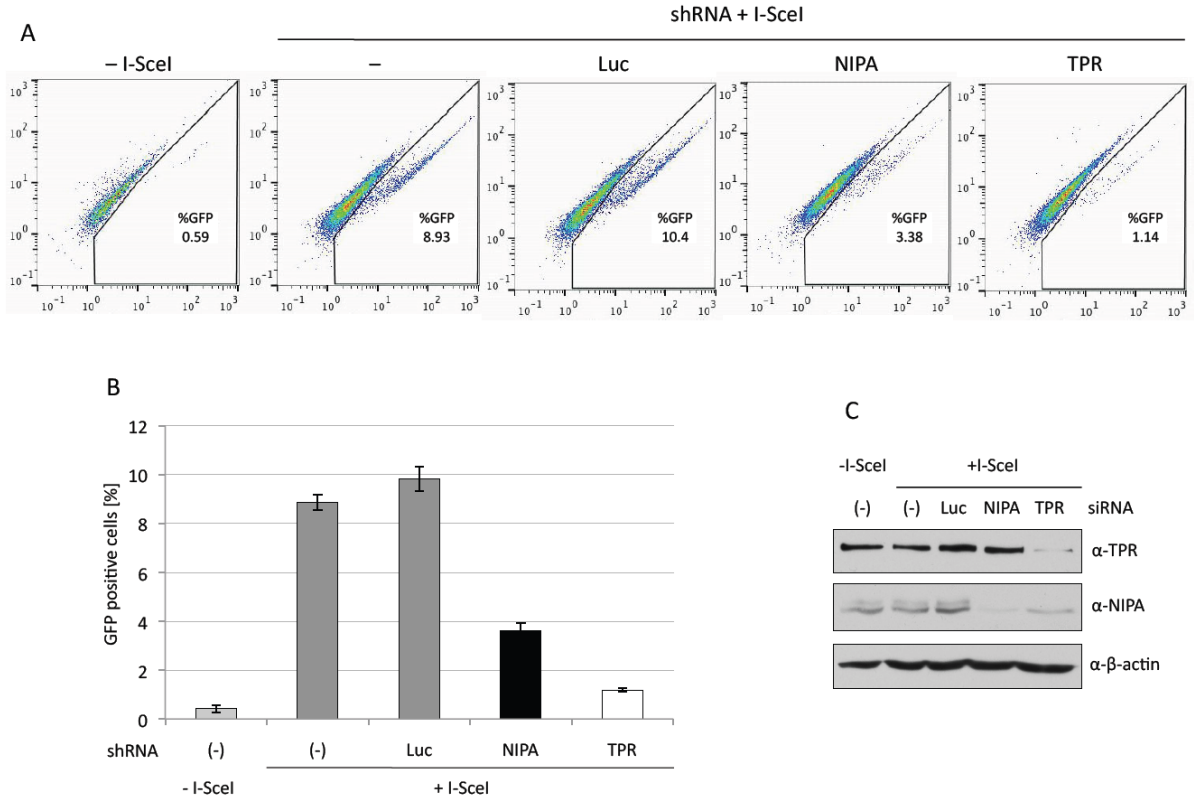

Fig. 3.29: NIPA and TPR depletion leads to impaired homologous recombination. U2OS cells with a single copy of the HR reporter substrate DR-GFP in a random locus were transiently transfected with indicated shRNAs along with I-SceI endonuclease (or without as a control). After 48 h, efficiency of HR was measured in flow cytometry. (A) Histograms showing % of GFP positive cells after transfection with shRNAs and with or without I-SceI. (B) Quantification of GFP positivity from (A). (C) The efficiency of siRNA was monitored in Western blot.

A well-established HR repair system to examine the role of NIPA and TPR has been used[154]. With this reporter, a DSB is introduced into the chromosome by expressing the I-SceI endonuclease, and, if HR occurs, GFP is expressed, which is quantifiable by flow cytometry. Dr. Shiaw-Yih Lin kindly provided U2OS cells with a single copy of the HR repair reporter substrate DR-GFP in a random locus. These cells were then transfected with siRNAs designed against luciferase, NIPA or TPR for 24 h, followed by I-SceI endonuclease transfection for 48 h to introduce single DSB. Control cells were not transfected with SceI to estimate the background of GFP positivity. Cells were then analyzed by flow cytometry to determinate the percentage of green fluorescent cells relative to the total cell number. Efficiency of siRNA transfection was monitored in Western blot (Fig. 3.29 C).

Figure 3.29 A demonstrates that in absence of the I-SceI expression, very few GFP positive cells were detected (0.59 %). Transient transfection of the I-SceI endonuclease revealed I-SceI inducible HR, producing GFP-positive cells quantified by flow cytometry (Fig. 3.29 A and B). Luiferase expression resulted in similar amount of GFP positive cells when compared to control. In NIPA-deficient cells, the percentage of I-SceI-induced GFP-positive cells was greatly reduced compared to control cells. In these cells, I-SceI induction led to an average of ~3.38% that were positive to GFP, which is 60% lower than the GFP-positive cells containing the Luc control siRNA (Fig. 3.29 A and B). Most striking result however, was observed in cells with TPR downregulation. GFP positivity induced by the I-SceI expression in these cells was dramatically compromised to an average of ~1.14%, what represents almost 90% reduction in HR efficiency when compared to control. The siRNA-mediated suppression of NIPA and TPR was specific to their respective target proteins, whereas siRNA directed against Luc had no effect on the levels of NIPA or TPR protein (Fig. 3.29 C). These results demonstrate that both NIPA and TPR deficiency leads to defects in a double strand break repair by the homologous recombination.

3.3 The role of NIPA in the regulation of cyclin B1

3.3.1 NIPA controls cyclin B1 nuclear localization

The G_2/M transition of the cell cycle is regulated by the activity of maturation promoting factor (MPF), which is a complex of CDK1 and B-type cyclin. The kinase activity of the MPF is regulated by the abundance of cyclin B, the association kinetics of cyclin B and CDK1, and by the phosphorylation state of CDK1[201]. Cyclin B1 from B-type cyclins was proposed to be the most important in mitotic regulation, since mice lacking cyclin B1 die during embryonic development[202]. Mitotic progression is dependent on active CDK1/cyclin B1 complex accumulation in the nucleus[203]. During interphase, cyclin B1 shuttles between the nucleus and the cytoplasm because constitutive nuclear import is counteracted by rapid nuclear export. Nuclear accumulation of cyclin B1 at the onset of mitosis requires phosphorylation of five serine residues within its cytoplasmic retention signal (CRS). Phosphorylation of CRS enhances cyclin B1 nuclear import by creating a nuclear import signal therefore being a critical step in the control of mitosis[204]. Cyclin B1 is ubiquitously marked for proteasomal degradation by the SCF^{NIPA} in interphase, constituting a further safeguard mechanism to protect the cell from premature cyclin B1 accumulation[83].

To study direct influence of NIPA on the nuclear cyclin B1 localization, cyclin B1 was cloned into RFP vector to obtain fluorescent-trackable protein (Fig. 3.30). A mutant form of cyclin B1 was prepared in which the CRS serine residues were altered to glutamic acids to mimic phosphorylation (mutant 5xE) (Fig. 3.30 A). This mutation generates artificial nuclear import signal therefore the mutant protein is constitutively localized in the nucleus (Fig. 3.30 B). After implementation of FLIP, fluorescence is bleached out from the nucleus and accumulation of cyclin B1 can be measured in time (Fig. 3.30 C).

The RFP-cyclin $B1^{5xE}$ construct was transfected into the mouse embryonic fibroblasts with wild type NIPA expression (MEF $\#12^{+/+}$) or to cells with NIPA knockout (MEF $\#14^{-/-}$) (Fig. 3.31). In both cell lines, mutant protein was efficiently accumulating in the nucleus with a higher tendency in $NIPA^{-/-}$ cells (Fig. 3.31 prebleach). Repeated photobleaching during FLIP diminished fluorescence of RFP-cyclin B1 from the nucleus, and after 30 min fluorescent signal has been observed neither in $\#12^{+/+}$ nor in $\#14^{-/-}$. However, after 60 min a bulk of cyclin B1 was already accumulated in NIPA deficient

cells, what was not the case in NIPA wild type cells (Fig. 3.31). Nuclear cyclin B1-RFP expression has reached plateau in 2 h after photobleaching in NIPA #14$^{-/-}$ cells.

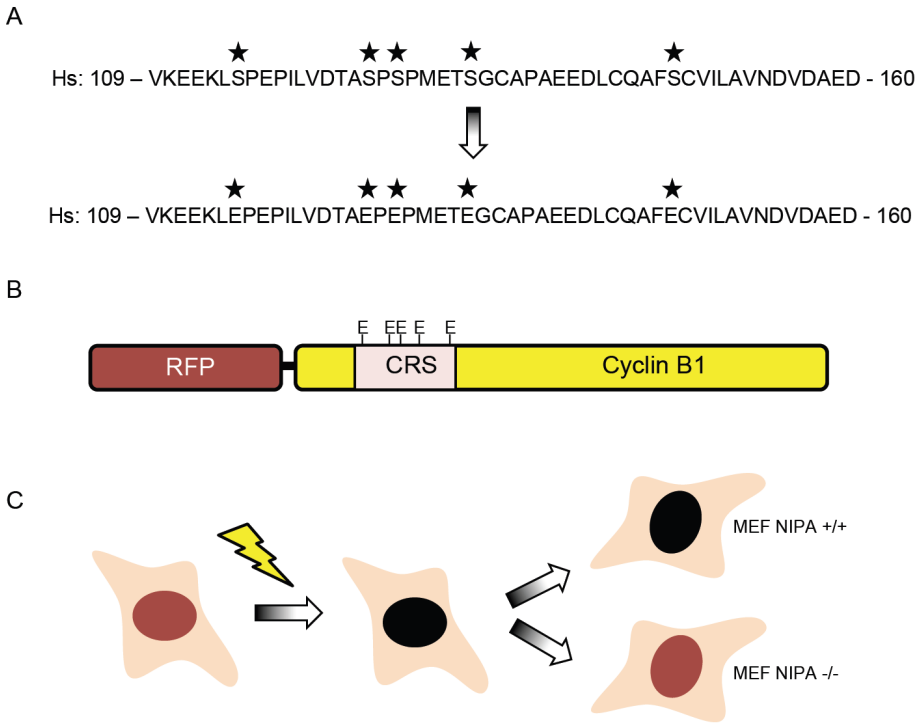

Fig. 3.30: Generation of the phosphomimic mutant of cyclin B1 (cyclin B1 5xE) constitutively expressed in the nucleus. (A) Five serines located in the CRS motif of cyclin B1 were mutated to glutamic acid by the site directed mutagenesis to generate a nuclear import signal. (B) Cyclin B1 5xE mutant was cloned into the RFP vector to allow for fluorescence tracking of the nuclear protein by live imaging. (C) Theoretical scenario of an experiment with cyclin B1 mutant. After transfection into the cells with different NIPA background (-/- or +/+), FLIP experiment is performed to bleach the fluorescence from the nucleus (yellow thunderbolt). Time-lapse imaging could be then performed to measure the kinetics of nuclear accumulation.

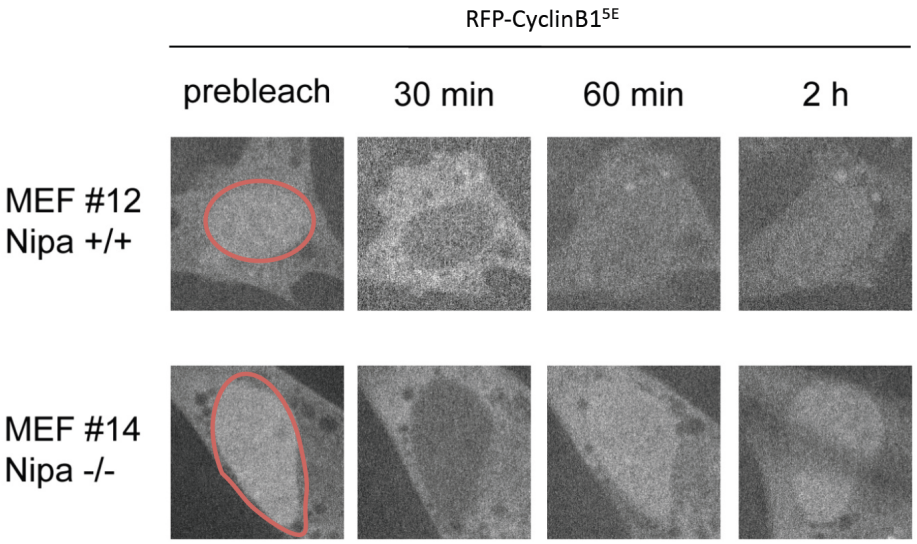

Fig. 3.31: NIPA deficiency leads to accelerated accumulation of the nuclear cyclin B1. Mouse embryonic fibroblasts NIPA #12 +/+ or NIPA #14-/- were transfected with RFP-cyclin B1 5xE construct and red fluorescence was followed in time after FLIP.

At the same time point, NIPA #12$^{+/+}$ cells were expressing decreased RFP-cyclin B1 levels when compared to the time before FLIP as well as in comparison with NIPA knockout cells (Fig. 3.31). Although observed in a very limited population of cells, these data demonstrate that RFP-cyclinB1^{5E} construct can be used as a model to study nuclear localization of cyclin B1 under the ubiquitin ligase control of NIPA.

3.3.2 Nuclear pore localization of NIPA may be important in controlling cyclin B1 nuclear accumulation

Given that generated RFP-cyclin B1^{5E} construct has been proven useful to study the role of NIPA in controlling cyclin B1 nuclear accumulation, it was next sought to examine the importance of NIPA localization at the nuclear pore in the context of cyclin B1 regulation.

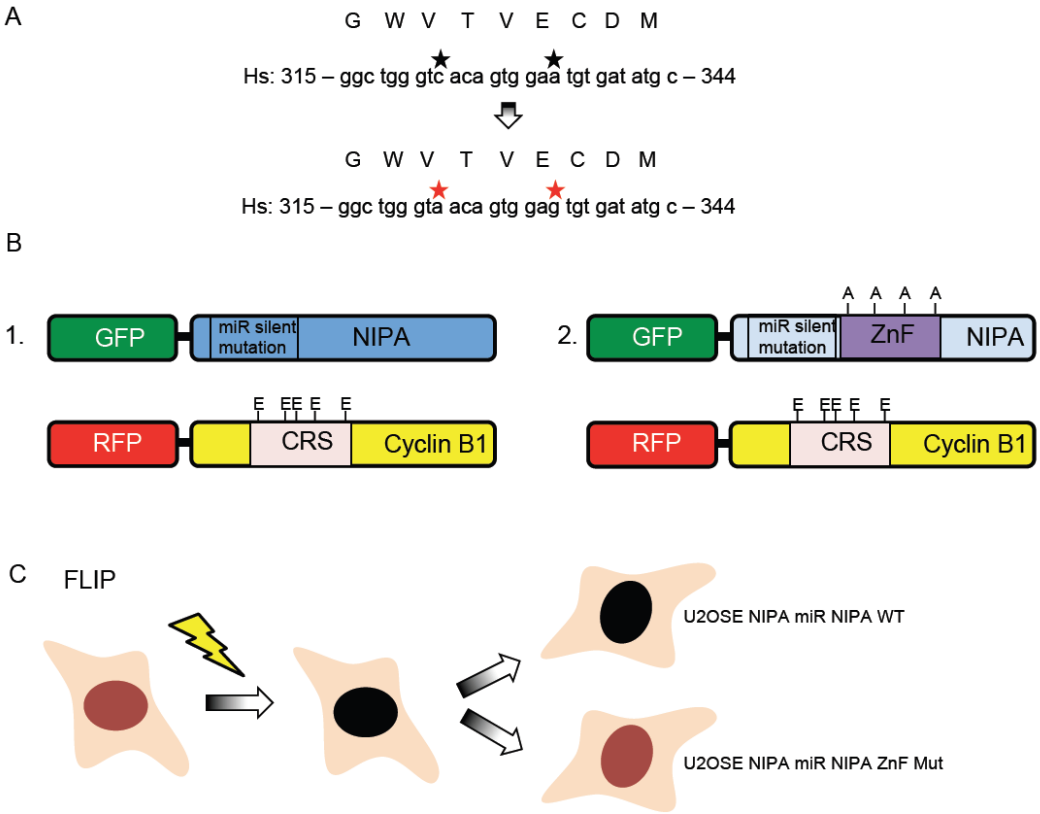

Fig. 3.32: Generation of the cyclin B1 expression model in U2OSE cells expressing stable NIPA knockdown. (A) To generate stable knockdown of NIPA in U2OSE cell line micro RNA (miR) was designed to recognize given nucleotide sequence (2.2.3.2.2). In this sequence, silent mutation was introduced (black to red star) to gain possibility to overexpress GFP-tagged NIPA in miRNA silenced U2OSE cells without any alteration of amino acid sequence. (B) A set of two construct pairs to examine the influence of NIPA nuclear localization on the cyclin B1 expression. 1. GFP-tagged NIPA with silent mutation in miRNA recognition sequence together with RFP-cyclin B1 5E. 2. GFP-tagged NIPA zinc finger mutant with silent mutation in miRNA recognition sequence together with RFP-cyclin B1 5E. (C) Theoretical scenario of an experiment using pairs of constructs (B) in U2OSE NIPA miRNA knockdown cells.

Localization of the ubiquitin ligase to the inner nuclear envelope where it can transfer ubiquitin to the proteins specifically when they cross the nuclear barrier, would suggest an intriguing mechanism for cyclin B1 degradation, by formation of a cyclin trap directly "at the gate" targeting cyclin B1 for ubiquitination just upon entry to the nucleus.

Due to the problems in overexpression of designed constructs in MEF cells, cyclin B1 regulation was studied in another model using U2OSE cells expressing stable NIPA downregulation. In these cells NIPA is depleted by micro RNA (miR30) based approach, where miRNA designed by an algorithm is recognizing a specific region in NIPA (Fig. 3.32 A) leading to degradation of mRNA and additionally to inhibition of translation. In order to elucidate the role of NIPA envelope association in the regulation of cyclin B1, GFP-NIPA wild type protein and GFP-NIPA zinc-finger mutant were introduced into experimental setup. Silent mutations were generated in miR recognition sequences of GFP-proteins, to avoid their downregulation by miRNA expression in U2OSE cells. These mutations most probably did not affect protein conformation, since the amino acid sequence has not been changed (Fig. 3.32 A).

Such prepared GFP-NIPA constructs were transfected together with previously generated RFP-cyclin $B1^{5E}$ into the U2OSE NIPA miRNA cells (Fig. 3.32 B). 24h after transfection cells were synchronized in G_1/S phase by single thymidine block for 12 h. After block release, cells were allowed to recover for 2 h. Then, the FLIP experiment was

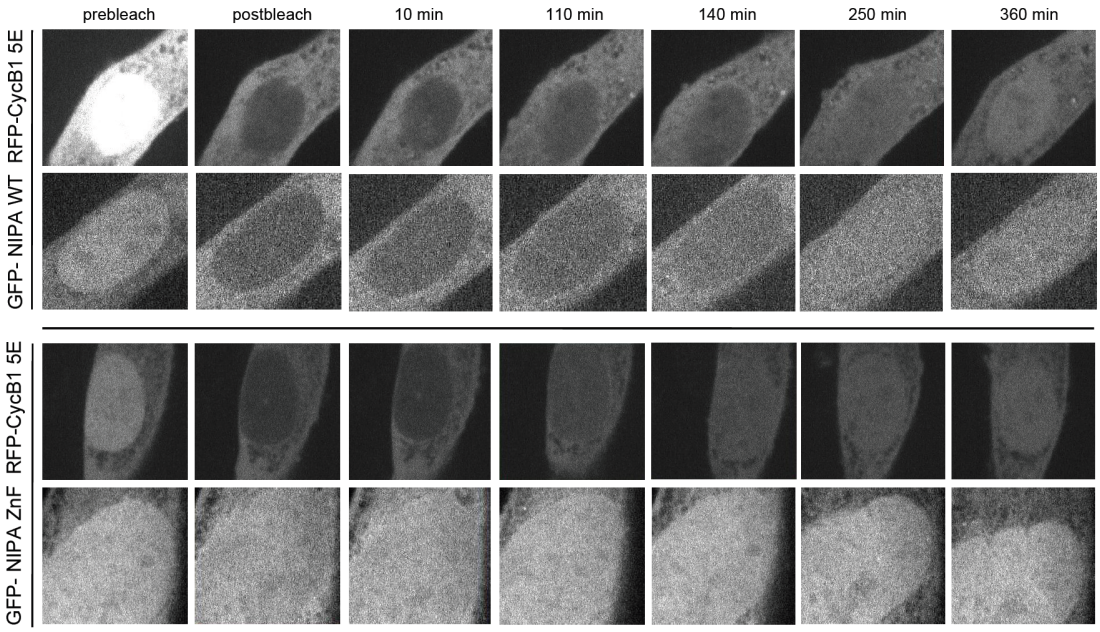

Fig. 3.33: Disruption of NIPA nuclear pore localization through zinc finger mutation, leads to accelerated accumulation of cyclin B1 in the nucleus. NIPA was reconstituted in U2OSE NIPA miRNA cells as GFP-NIPA WT or GFP-NIPA ZnF mutant and transfected together with RFP-cyclin B1-5E. Next FLIP experiment was performed to diminish nuclear fluorescence of cyclin B1.

performed and images were taken during live imaging microscopy after indicated time intervals (Fig. 3.33).

Only few cells were efficiently transfected with GFP-ZnF mutant in comparison to the wild type. This could be due to instability of NIPA after zinc-finger disruption, consistent with previous studies[78]. Also RFP-cyclin B1 expression was much higher in cells complemented with the GFP-NIPA^{ZnF} mutant than with the GFP-NIPA^{WT}. As shown in Figure 3.33, in cells expressing GFP-NIPA WT the balance in fluorescence of RFP-cyclin B1 between nucleus and cytoplasm is reached after 250 min whereas in GFP-ZnF complemented cells already after 110 min or even after 10 min in one cell (Fig. 3.33 lowest panel). Although comparable expression of both fusion proteins and similar transfection efficiency was not observed, excluding quantitative evaluation of the data, it could be suggested that NIPA localization at the NPC may play a distinct role in the regulation of cyclin B1 nuclear accumulation. These data hypothesize a novel role for the E3 ubiquitin ligase, directly controlling the traffick between cytoplasm and nucleus at the neuralgic transport channels – the nuclear pore complexes.

4 Discussion

4.1 NIPA is regulated after DNA damage

Post-translational modifications are the fundamental controlling mechanisms involved in the intracellular signaling pathways. Among them, one of the most important and potent events is protein phosphorylation and ubiquitination. The ubiquitin-proteasome system is increasingly gaining importance since it is involved in the control of numerous processes, including cell-cycle progression, transcriptional regulation, signal transduction, receptor down-regulation, apoptosis and DNA damage repair[61,205]. Targeting proteins for degradation was the best known function of ubiquitylation, until the recent studies of DNA damage response have significantly broadened the scope of ubiquitylation including non-proteolytic functions of ubiquitin[62].

NIPA was primarily identified as an F-box containing protein that defines a nuclear SCF-type ubiquitin ligase (SCF^{NIPA}), which targets nuclear cyclin B1 for ubiquitination and proteasomal degradation in intherphase thereby contributing to the timing of mitotic entry (Fig. 4.1)[83].

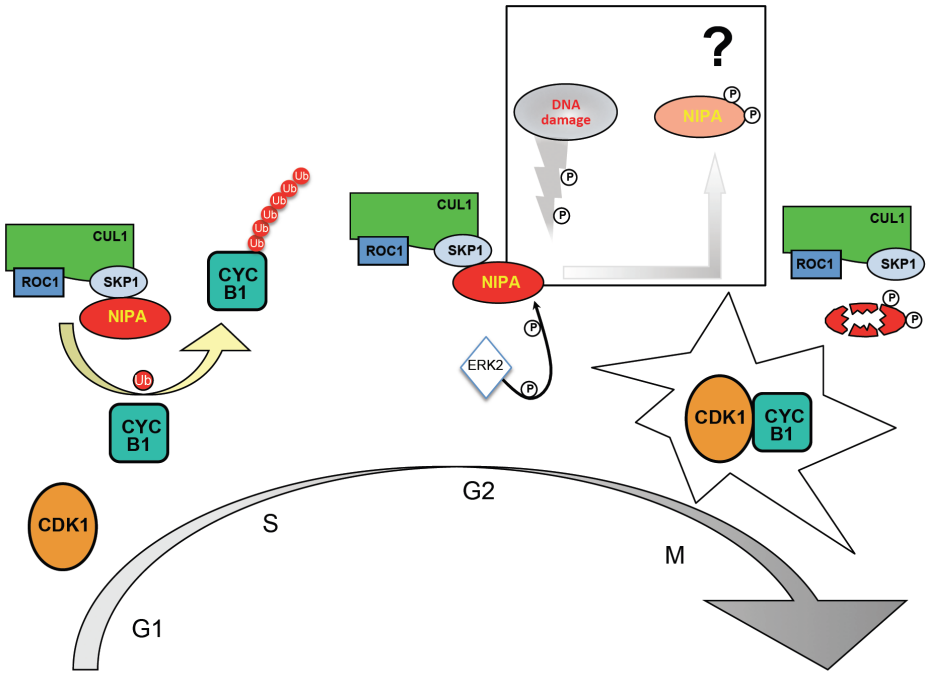

Fig. 4.1: Function of SCF^{NIPA} on the schematic illustration. The SCF^{NIPA} complex is targeting cyclin B1 for proteasomal degradation in interphase. At the G_2/M transition NIPA is phosphorylated by ERK2, what leads to dissociation from the SCF followed by its degradation. This allows for cyclin B1 accumulation in the nucleus, activation of MPF and subsequent mitosis. NIPA is also phosphorylated after DNA damage, which function still remains elusive (black frame square). CDK1-cyclin dependent kinase 1; CYCB1 – cyclin B1; CUL1-cullin 1; SKP1-S-phase kinase-associated protein 1; ERK2-extracellular signal-regulated kinase 2; ROC1-RING-box protein 1 (RBX1). (Adapted from van den Heuvel, 2005)[206].

In the normal cell cycle, phosphorylation at the G_2/M transition by ERK2 inactivates E3 ligase activity of NIPA allowing for the cyclin B1 accumulation and cell cycle progression towards mitosis[85]. Previous reports demonstrated that phosphorylation of NIPA can occur also independently of the cell cycle – after DNA damage induction[78,160]. Although many efforts have been made to disclose the function of this phosphorylation it still remains elusive. Here, NIPA phosphorylation was confirmed in cells after treatment with distinct DNA damaging agents, UV irradiation and IR (Fig. 3.1). Phosphorylation was strongly dependent on the radiation intensity and related to the type of damaging agent. It was clear that UV has driven complete NIPA phosphorylation, what however could not been observed in IR treated cells, consistent with previous studies[78,160]. Additionaly, proteomic approach revealed differential phosphorylation pattern for UV and for BLM, suggesting a diverse regulation pathway dependent on the type of DNA damage (Fig. 3.2).

Majority of proteins involved in DNA damage response are post-translationaly modified by phosphorylation. This type of protein modification plays a crucial role in many processes involved in DNA repair, like sensing the break, recruiting of mediator proteins or in the signal transduction to the numerous downstream effectors[207]. Thus uncovering the role of NIPA phosphorylation in response to DNA damage would shed more light on its function in DDR. In contrast to observations made during normal cell cycle, where phosphorylated form of NIPA could not bound to SKP1 anymore, damage driven phosphorylation did not affect this binding (Fig. 3.3). SCF complex subunit CUL1 and was efficiently coimmunoprecipitated up to 4 h after treatment. The source of the damage had no influence on the binding to SKP1 as well. These results suggest that the binding to SKP1 did not influence the E3 ligase activity of NIPA after exposition to genotoxic agents. Differential phosphorylation patterns obtained from the phosphpoproteomic analysis of NIPA after UV or bleomycin treatment (Fig. 3.2), revealed a lack of phosphorylation at Ser354 and Ser359, absolutely required for NIPA inactivation at the G_2/M transition in an unperturbed cell cycle[85]. These data suggest an active mode of action for NIPA after phosphorylation upon DNA damage. It is possible that after DNA damage driven phosphorylation, NIPA could change substrate specificity or participate in the signaling transduction of DDR by ubiquitylation, however such a hypothesis requires further studies, since these observations are not consistent with already published results[78].

4.2 NIPA is involved in the DNA damage response

4.2.1 Induction of apoptosis in response to DNA damaging agents in NIPA deficient background is a result of impaired DNA damage repair

NIPA knockout mice are viable and exhibit no severe phenotype[87]. Also cells derived from NIPA$^{-/-}$ mouse embryo or cells where NIPA was downregulated by small interfering RNA proliferate normally without critical consequences. However, as soon as NIPA$^{-/-}$ cells are exposed to agents causing damage in DNA, survival of these cells is severely compromised (Fig. 3.8 and 3.9). Sensitivity towards genotoxic stress seems to be dependent on the type of lesion. UV irradiation has induced dramatic apoptotic phenotype in K562E cells where NIPA was stable inactivated by the microRNA approach (Fig. 3.11). Interestingly, bleomycin treatment resulted in considerably milder effects (Fig. 3.12). DNA damage in NIPA deficient mouse embryonic fibroblasts was responsible for induction of apoptosis and measured with TUNEL assay. Re-expression of NIPA rescued these cells (Fig. 3.10). MEFs were also more sensitive to the UV treatment than to the ionizing radiation. In contrast, U2OSE cells expressing stable NIPA knockdown formed fewer colonies after IR exposure, showing compromised clonogenic potential towards the low doses of ionizing radiation. UV treatment induced similar phenotype but was less pronounced. Previous studies implicated NIPA in protection of Ba/F3 cells from apoptosis, induced by IL-3 withdrawal, with the correct nuclear localization being indispensable for this function[77]. Although the correlation of NIPA loss and the consequent apoptosis was clearly demonstrated[77,160], it still remains unknown if NIPA is directly involved in apoptotic-signaling pathway or if its loss leads to the disruption of other important signaling cascades, what, in turn, activates apoptosis.

It is crucial for the cell to repair DNA lesions as soon as possible in order to maintain genomic stability. If DNA damage repair fails, persistent, unrepaired DNA alterations often induce the signal for apoptotic elimination. Apoptotic phenotype in NIPA deficient cells after genotoxic stress could be a possible result of impaired DNA damage repair since lymphocytes derived from NIPA-/- mice present similar sensitivity to chemo- or radiotherapy when compared to NIPA wild type cells but exhibit distinct delay in the repair of DNA breaks (Fig. 3.7). Thhese observations strongly suggest that NIPA constitutes an important response threshold towards chromosomal insults, contributing to the genetic homeostasis.

4.2.2 NIPA localization at the nuclear pore is crucial for its cellular function

A cytological hallmark of DNA damage response is a formation of the nuclear foci of various proteins involved in sensing and recruiting of downstream proteins for DNA repair[208]. Experiments using microirradiation demonstrated, that NIPA is not recruited to the sites of DNA damage although recruitment of other well known sensing proteins for both ssDNA and dsDNA has been observed (Fig. 3.17). According to these data NIPA can be excluded as a sensor protein, what suggest a differential role not directly linked to the DNA damage foci.

Nevertheless, NIPA was localized to the nuclear envelope (Fig. 3.18 and Fig. 3.19). Recent studies in immunofluorescence clearly show almost exclusive localization at the nuclear membrane with only background staining in the nuclear interior (Fig. 3.13-3.16). Further experiments revealed direct association of NIPA with TPR protein at the nuclear pore complex (Fig. 3.21 and 3.22). This finding raises intriguing possibilities for the function of NIPA. Recently, several studies have shown that persistent, irreparable DSBs are relocalized to the nuclear periphery, pointing out a direct role for the NPC in DNA repair[209-211]. SUMOylation and ubiquitylation have been reported crucial in this process. Thus it could be speculated that not NIPA itself is localized at the damage site but unrepaired DNA breaks are brought in the close proximity to the nuclear pore for NIPA mediated repair.

Translocated promoter region (TPR) is a nucleoporin tethered to the nuclear basket by another nucleoporin, Nup153[140]. In addition to a role in NPC achitecture, TPR has been attributed to many functions including mRNA export control, nuclear protein export, spindle checkpoint control, TPR-Met oncogene activation, DNA damage and senescence[190,191,212-216]. TPR was shown to be scaffolding protein for NIPA (Fig. 3.27), whereas zinc finger domain, localized in the N-terminus of NIPA, was identified crucial for the binding and for localization at the NPC (Fig. 3.23 and 3.24). Thus NIPA can be classified as a novel nuclear pore associated protein. This association may have an interesting correlation with ERK2. Previous study demonstrated that TPR is both a substrate and a scaffold for activated ERKs[195]. They show that phosphoryaltion of TPR by ERK stabilizes interaction and that this interaction positions ERK2 for phosphorylation of other substrates. Additionally, EKR-TPR interaction regulates translocation of activated ERK2[195]. NIPA was also shown to be a substrate of ERK2

phosphorylation in the normal cell cycle, what led to inactivation of SCF^{NIPA} ligase at the G_2/M transition[85]. It can be speculated that TPR constitutes a sort of a platform for ERK2-mediated phosphorylation (Fig. 4.2). ERK2 phosphorylates proteins that interact with TPR and both ERK2-TPR and TPR-substrate association is necessary for this process. NIPA zinc-finger mutant could provide some additional evidence to support this hypothesis (Fig. 4.2 B). It was shown that mutation of zinc-finger domain disrupts the binding between NIPA and TPR (Fig. 3.23). Additionally, experiments with zinc-finger mutant demonstrated that after disruption of zinc-finger domain NIPA phosphorylation is abrogated (data not shown and C.v.Klitzing[78]). These observations suggest a

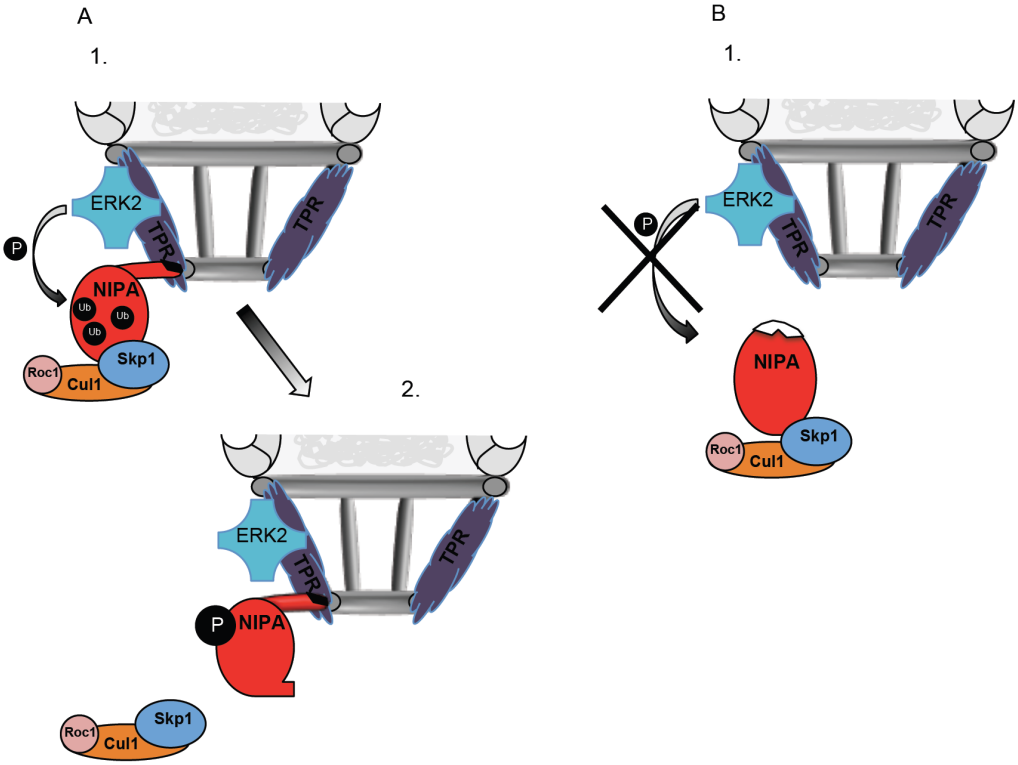

Fig. 4.2: Schematic illustration of TPR function in the ERK2 mediated phoshporylation of NIPA. (A) TPR constitutes a scaffold for both activated ERK2 and NIPA. At the G_2/M transition NIPA is phosphorylated by ERK2, what induces dissociation from the SCF complex and results in inactivation of SCF^{NIPA} ligase. (B) NIPA zinc-finger mutant, which cannot bind to TPR, escapes ERK2 mediated phoshporylation.

necessity of scaffold-mediated interaction between the kinase and the substrate for the efficient phosphorylation. Moreover, Vomastek et al. identified an additional, unknown TPR-interacting protein of ~60 kDa, which is phosphorylated by the TPR-bound active ERK2[195]. Interestingly such a molecular mass corresponds to NIPA.

It is still not clear if DNA damage driven phosphorylation of NIPA is impaired in cells lacking TPR, although some results indicate this notion. Here it was shown that TPR

downregulation using small interfering RNA is responsible for defects in NIPA phosphorylation after UV or BLM treatment characterized by a reduced shift of protein band in Western blot (Fig. 3.27). Thus, accumulating evidence reveals the strong relationship between NIPA localization at the nuclear pore and its cellular functions.

4.2.3 NIPA deficiency disorganizes DNA damage repair

Although NIPA deficiency results in no severe phenotype, NIPA$^{-/-}$ mice recapitulated many characteristics of H2AX$^{-/-}$, MDC1$^{-/-}$ and ATM$^{-/-}$ mice, including growth retardation, male infertility, chromosome instability and DNA repair defects[87,169,217,218]. Since γH2A.X accumulation together with its binding partner MDC1 is a widely accepted, critical step in the early DDR, it was interesting to follow ATM-γH2A.X-MDC1 axis in regard to the loss of NIPA. NIPA deficient cells were accumulating phosphorylated histone H2A.X after damaging their DNA with various genotoxic agents (Fig. 3.4), what could not been observed in the wild type cells. This phenotype was particularly prominent after induction of DSBs (Fig. 3.6) and was augmented over time (Fig. 3.5). Even in untreated cells, the higher levels of γH2A.X were observed, as it was shown in cells derived from NIPA$^{-/-}$ mouse spleen (Fig. 3.5). Thus, it has become more evident that NIPA is involved in DNA repair signaling.

Recruitment of MDC1, an important mediator in DDR, to the site of damage is an important step in the signal transduction, following accumulation of γH2A.X. It has been demonstrated that MDC1 stabilizes the MRN complex thereby promoting further accumulation of MRN and activated ATM[169]. In the absence of NIPA, sustained focus formation of MDC1 has been observed (Fig. 3.14), correlating with accumulation of phosphorylated histone H2A.X, since these proteins interact directly and colocalize at the damage foci[98]. This finding suggests a role for NIPA downstream of histone H2A.X and MDC1.

In addition, MDC1 is also involved in coordinating the assembly of other repair/checkpoint proteins to the surrounding chromatin[166]. This secondary response is coordinated by the ubiquitylation through RNF8, after MDC1 gets phosphorylated by ATM[101]. RNF8, by the lysine-63 poly-ubiquitination, triggers chromatin remodeling into a more relaxed conformation allowing for histone methylation, that signal activation and recruitment of a second component of the DNA repair cascade – 53BP1[170]. After NIPA depletion, basal levels of 53BP1 are reduced already in untreated cells (Fig. 3.15).

However, most intriguing observation was made after induction of DSBs with ionizing radiation. In absence of NIPA, 53BP1 foci formation was severely compromised (Fig. 3.16). The question arises whether NIPA can directly contribute to this surprising phenotype.

53BP1 is a DNA damage checkpoint protein that facilitates ATM-dependent phosphorylation events in response to IR[171]. It is translocated rapidly to the sites of DNA DSBs, and was implicated in regulating activation of the G_2/M phase checkpoint as well as in the repair of DNA breaks via NHEJ[172,173]. By knocking down genes involved in ubiquitin-proteasome system together with genes encoding zinc-finger proteins, novel factors required for 53BP1 foci formation were recently identified[219]. Interestingly, NIPA was also found in this screen with a very high score (Table 2), way above an average Z-score of some genes from the top-ten list[219]. Authors demonstrated that nucleoporin NUP153 could be responsible for the import of 53BP1 to the nucleus.

Gene name	Gene symbol	Highest Z-score
Ring finger protein 168	RNF168	- 2.11
Ring finger protein 8	RNF8	- 2.10
Mediator of DNA-damage checkpoint 1	MDC1	- 1.99
Nucleoporin 153 kDa	NUP153	- 1.93
Ubiquitin-like modifier activating enzyme 1	UBA1	- 1.92
Target of myb 1 (chicken)	TOM1	- 1.80
Anaphase promoting complex subunit 10	ANAPC10	- 1.79
Cyclin T2	CCNT2	- 1.55
Ataxin 7	ATXN7	- 1.54
Mitogen-activated protein kinase kinase kinase 3	MAP3K3	- 1.54
Nuclear interaction partner of ALK	ZC3HC1	-1.38

Table 2: Screen for suppressors of IR-induced 53BP1 focus formation. The list of 10 top-scoring genes plus NIPA – U2OS cell line. (Adapted from Moudry et al.)[219].

However, as it was shown before[140], NUP153 mediates binding of TPR to the periphery of the nuclear pore complex. Having shown that TPR is also tethering NIPA to the NPC (Fig. 3.27) the extension of the model presented by Moudry and colleagues could be speculated (Fig. 4.3).

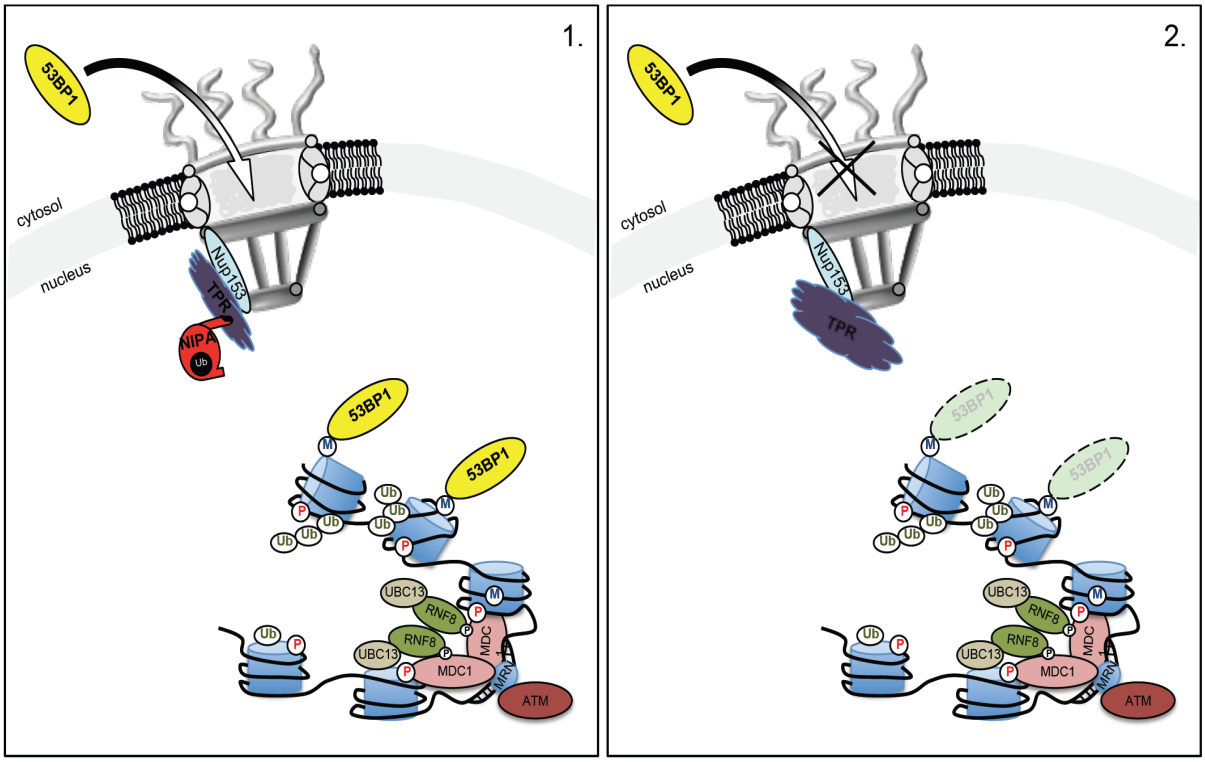

Fig. 4.3: Proposed model for NIPA function at the NPC facilitating the recruitment of 53BP1. 1. In the presence of NIPA, nuclear import of 53BP1 is unperturbed and after chromatin remodeling it can be localized to the DNA damage foci. 2. After NIPA depletion, TPR undergoes conformational change, what in turn makes NPC non persistent for 53BP1, preventing 53BP1 foci formation. P – phosphorylation; Ub – ubiquitylation; M – methylation. (Adapted from G.S. Stewart)[170].

NUP153 appears as a central scaffolding element tethering TPR-NIPA to the nuclear pore. If all components of this NUP153-TPR-NIPA "complex" are present, import of 53BP1 from the cytoplasm to the nucleus can precede unperturbed (Fig. 4.3 panel 1). However, the loss of only one link from this chain, in above model – NIPA, is sufficient to disrupt nuclear import of 53BP1, what in consequence disorganizes DNA damage repair by reduced localization of 53BP1 to the damage foci (Fig. 4.3 panel 2). It could be suggested that loss of NIPA leads to a conformational change in TPR, since it was shown that NIPA might regulate TPR *in vivo* by ubiquitylation (Fig. 3.28). Such a change possibly interrupts the proper function of the NPC and as a result is reducing permeability of the pore towards 53BP1. This hypothesis can be supported by recent report, where TPR was shown to constitute a scaffold, which excludes chromatin from an NPC-proximal zone to allow the access of large cargo complexes to the NPC translocation channel[220]. In absence of TPR the trafficking through NPC could be impeded by a meshwork of dense chromatin fibers. Thus it is conceivable that NIPA plays a regulatory role in this process.

Furthermore, TPR pore-associated intranuclear filaments were implicated in organization of chromatin-free tracks to guide the efficient translocation of macromolecules towards the nuclear interior[221]. Such a model hypothesize, that nuclear transport does not end after the cargo release from the nuclear basket, but instead the facilitated transport through the pore could continue on intranuclear tracks up to distinct nuclear sites[192]. It can be assumed, that after NIPA depletion, TPR loses an important regulatory factor what in turn results in disruption of efficient localization of 53BP1 at the damage-induced foci. TPR ubiquitylation additionally argues for regulatory function of NIPA, since the ubiquitin pattern does not reflect a typical lysine-48-linked degradation (Fig. 3.28), suggesting a possible signaling pathway, for instance, through a lysine-63-linked ubiquitylation.

An additional important role of the nuclear basket proteins, regarding DNA damage repair, was presented for NUP153[222]. Lamaitre and others showed that NUP153 is essential for proper activation of the DNA damage checkpoints and regulates the choice between NHEJ and HR. This function was attributed to the role of NUP153 in promoting 53BP1 nuclear localization[222]. Thus recent report solved the riddle how 53BP1 is able to promote one repair pathway over another[223]. Authors identified RIF1, ortholog of a yeast telomeric protein, as major factor acting downstream of 53BP1 to block the 5'-end resection. Homologous recombination requires extensive 5'-end resection to generate the 3' ssDNA tails for the formation of recombinase presynaptic filament. Hence, the DNA end-processing step is a crucial stage in determining which pathway is used to repair a DSB[224]. Thus in the model presented here, NIPA deficiency leads to an impaired 53BP1 localization and function, what in turn could abolish inhibition of RIF1 5'-end resection, forcing the cell onto HR repair pathway. However, without NIPA, HR cannot be properly executed leading to errors in DNA damage repair as shown in Figure 3.29. This hypothesizes that NIPA loss may affect more than one repair pathway in DDR (Table 1). Taken together, our results suggest that after induction of DSBs, depletion of NIPA may phenocopy the depletion of NUP153.

Although more work is needed to test whether above model holds true, it is compelling to consider the potential broad implications that such a mechanism of DNA-damage repair might have for the DDR.

4.3 NIPA – the NPC associated guardian of cyclin B1

New findings that revealed NIPA localization at the nuclear pore (Fig. 3.21), have opened a very interesting field for discussion, how localization of a protein can predestinate it function. This is especially relevant according to the best-characterized substrate of NIPA – cyclin B1. Using RFP-tagged cyclin B1 mutant, where five crucial serines in cytoplasmic retention signal (CRS) domain were mutated to mimic phosphorylation and force nuclear accumulation, it was demonstrated that in cells lacking NIPA cyclin B1 enrichment in the nucleus was elevated in comparison tthe wild type cells (Fig. 3.31). Overexpression of NIPA zinc-finger mutant, which cannot attach to the NPC, was not able to rescue this phenotype, suggesting that NIPA localization at the nuclear pore could be important for controlling cyclin B1 levels in the nucleus (Fig. 3.33). However, the model of cyclin B1 regulation presented in this work is supported only by preliminary results, since many hurdles occurred by overexpressing the nuclear cyclin B1 in cells in large amounts. In is obvious that a cell cannot tolerate a constitutive abundance of the nuclear cyclin B1, what makes the experiments with RFP-cyclin B1 difficult in terms of similar expression rates as well as reproducibility.

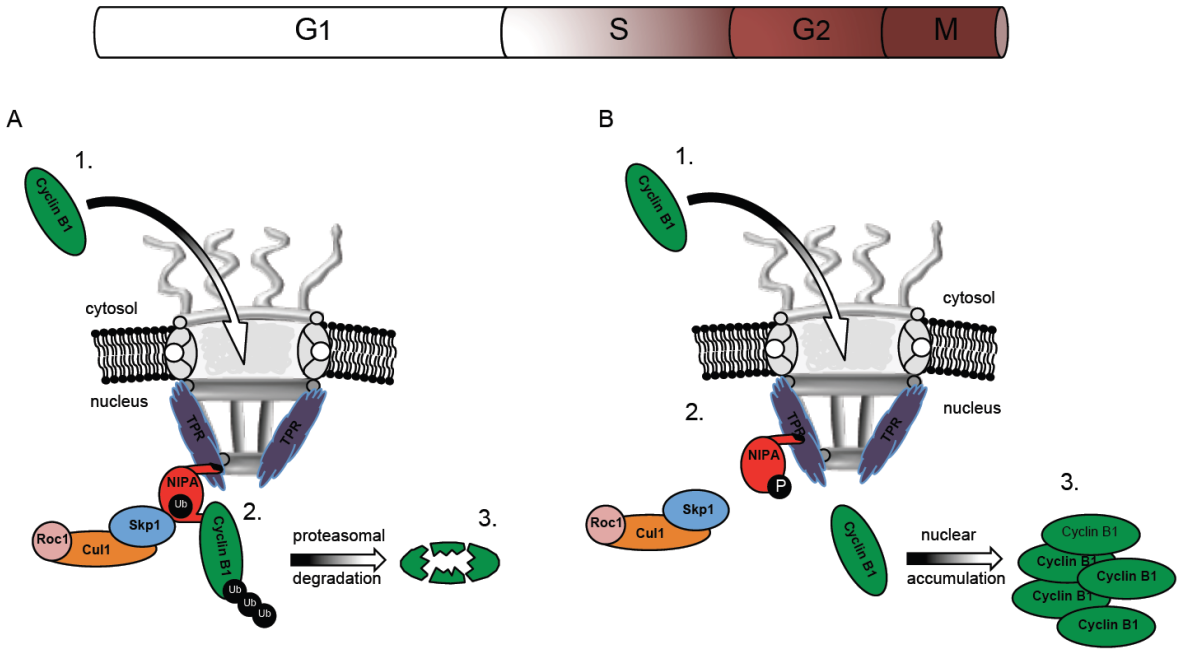

Figure 4.4: Theoretical model of SCF^{NIPA} activity in the regard to its nuclear localization. (A) Cyclin B1 enters the nucleus through the NPC (1), is directly phosphorylated (2) and headed for the proteasomal degradation (3). (B) In the G_2/M phase NIPA is phospohrylated (2), what leads to the dissociation of the SCF^{NIPA} complex and its subsequent inactivation. Cyclin B1 can accumulate in the nucleus (3) triggering the G_2 – M transition.

At least the localization of an ubiquitin ligase to the inner nuclear envelope, where it can transfer ubiquitin to the proteins specifically when they cross the nuclear barrier, would suggest an intriguing mechanism for cyclin B1 degradation by formation of a “cyclin trap” directly at the gate, targeting cyclin B1 for ubiquitination just upon entry to the nucleus in interphase (Fig. 4.4).

Noteworthy, several lines of evidence also suggest a link between nuclear localization of cyclin B1 and regulation of DNA damage-induced apoptosis[225,226]. Nuclear cyclin B1 was even implied in controlling mitotic entry after DNA damage[227].

Thus by controlling cyclin B1 level already upon the entrance to the nucleus, NIPA could execute a dual function, once taking charge of proper cell cycle progression, and second ensuring the accurate DNA damage repair. However, more work is needed to support this notion.

5 Summary

DNA damage response (DDR) is a highly sophisticated process composed of coordinated activation of cell cycle checkpoints and DNA repair, which has evolved to protect the cell from endogenous and environmental genomic threats. Failure in DDR, especially in repair of the most deleterious damage – double strand breaks (DSBs), lead to genomic instability, which is a characteristic hallmark of cancer development. Many processes of protein metabolism are involved in DDR, with accumulating evidence that weight in favour for the role of ubiquitin pathway in the DNA damage sensing and processing.

NIPA is a member of E3 ubiquitin ligase family, which targets nuclear cyclin B1 for degradation in interphase thereby contributes to the timing of mitotic entry. This study shows an additional role of NIPA in maintaining the proper DNA damage repair. NIPA was shown differentially regulated by phosphorylation regarding the source of DNA damage. It was confirmed that NIPA deficient cells are highly sensitive to exposure towards genotoxic agents (UV and IR). This sensitivity resulted in compromised survival of the cells and induction of apoptosis, due to impaired DNA damage repair. A severe DNA damage phenotype has been observed in cells with silenced NIPA expression after induction of DSBs. Sustained foci formation of γH2A.X and MDC1 at the sites of DNA breaks corroborated this notion. Although cells challenged to repair damaged DNA in absence of NIPA failed to appropriately execute homology-mediated repair, a direct role in repair process has not been observed, as NIPA was not recrutited to the sites of chromatin ruptures. Instead, a strong nuclear pore association has been identified. Loclaization at the NPC was mediated by an interaction with TPR throughout the zinc-finger domain located in the N-terminus of NIPA. Disruption of this domain leads to the dissociation of NIPA from the NPC and to destabilization of the protein. Hence studies on the function of NIPA suggested a close interaction of proteins at the nuclear pore to maintain meticulous nuclear loclization of crucial repair factors. This model stem from observations where NIPA depletion recapitulated depletion phenotype of NUP153, leading to mislocalization of the DNA reapair mediator - 53BP1. NIPA was proposed to guard genome integrity by regulating nuclear pore trafficking of important signaling proteins, thereby its loss results in disorganization of the DNA damge repair.

Additionally this study reveals the importance of NIPA association at the NPC for its cell cycle dependent phosphorylation by ERK2 kinase, as well as suggests an intriguing

molecular mechanism for the controlling of cyclin B1 abundance in the nucleus by the E3 ubiquitin ligase localized to the nuclear basket.

Since interplay between cell cycle regulation and DNA damage response is a potential target for anticancer therapies, this study provides an additional insight in understanding of these processes what could be advantageous in development of novel chemotherapeutics in fight against human malignancies.

6 Zusammenfassung

Die DNA-Schadensantwort, kurz DDR (DNA damage response), entwickelte sich um das Genom vor endogenen oder umweltbedingten DNA-Schäden zu schützen. Dieser hochentwickelter Prozess besteht aus der koordinierten Aktivierung von Zellzykluskontrollpunkten und der DNA-Reparatur. Fehlerhafte DDR führt zu genetischer Instabilität, speziell wenn sie bei der Reparatur des schwerwiegensten DNA-Schaden, den DNA Doppelstrangbrüchen DSBs (double strand breaks), auftritt. Diese genetische Instabilität ist ein charakteristicher Meilenstein bei der Entwicklung von Krebs. Viele Prozesse des Proteinmetabolismus sind an der DDR beteiligt, jedoch kristallisiert sich eine essenzielle Bedeutung des Ubiquitin Signalwegs beim Aufspüren und der Prozessierung des DNA-Schadens heraus.

NIPA, ein Mitglied der E3 Ubiquitin Ligasen Proteinfamilie, induziert die Degradation von Cyclin B1 in der Interphase des Zellzyklus und ist daher bei der zeitlichen Koordinierung des Mitosebeginns beteiligt. Die vorligende Studie zeigt eine weitere Funktion von NIPA bei der DNA-Schadensantwort auf. Es wurde bestätigt, dass NIPA, je nach Ursache des DNA-Schadens, einer differenziellen Phosphorylierung unterliegt und NIPA defiziente Zellen hochsensitiv gegenüber genotoxischen Agentien (UV und IR) sind. Die erhöhte Sensitivität manifestiert sich in einer geringeren Überlebensrate der Zellen sowie der Apoptoseinduktion, aufgrund von beschädigter DNA-Reparatur. Zellen mit reduzierter NIPA-Expression zeigen nach Induktion von DSBs einen schweren DNA-Schadens Phänotyp. Dies beinhaltet anhaltende γH2A.X und MDC1 Foci Formierung an den Stellen der DSB. Obwohl NIPA defiziente Zellen an der ordentlichen Homologie-abhängigen DNA-Reparatur scheitern, konnte keine Rekrutierung von NIPA an die beschädigte DNA festgestellt werden. Stattdessen ist NIPA stark an die Kernpore NPC (nuclear pore complex) gebunden. Die Interaktion mit dem NPC wird durch TPR vermittelt und ist abhängig vom Zinkfingermotif am N-Terminus von NIPA. Wird dieses Motif zerstört, dissoziiert NIPA vom NPC und wird destabilisiert. Dieses Modell stammt von der Beobachtung das die Depletion von NIPA dem Phänotyp von NUP153 depletierten Zellen (Fehllokalisierung des DNA-Reparaturmediators 53BP1) ähnelt. Die Ergebnisse dieser Studie schlagen vor, dass NIPA die Integrität des Genoms beschützt indem es den Kerntransport von wichtigen Signalproteinen reguliert und der Verlust von NIPA daher die Organisation der DNA-Reparatur stört.

Darüberhinaus zeigt diese Arbeit, dass die NPC Lokalisation von NIPA für die Zellzyklus-abhängige Phosphorylierung durch die ERK2 Kinase essentiell ist. Zudem kann ein attractives molekulares Modell vorgeschlagen werden, bei dem die NPC Lokalisation der E3 Ubiquitinligase die nukleäre Lokalisation von Cyclin B1 kontrolliert. Das Zusammenspiel von Zellzyklus und DNA-Schadensantwort ist ein potentielles Ziel für die Krebstherapie. Die vorliegende Studie gibt weitere Einblicke in das Verständnis dieser Prozesse und könnte sich beim Design neuer Chemotherapeutika für die Behandlung schwerer Erkrankungen als nützlich erweisen.

References

1. Cooper, G. *The Cell: A molecular Approach*, (Sinauer Associates, Sunderland (MA), 2000).
2. Nurse, P. A long twentieth century of the cell cycle and beyond. *Cell* **100**, 71-78 (2000).
3. McIntosh, J.R. & Koonce, M.P. Mitosis. *Science* **246**, 622-628 (1989).
4. Pines, J. Four-dimensional control of the cell cycle. *Nat Cell Biol* **1**, E73-E79 (1999).
5. Malumbres, M. & Barbacid, M. Mammalian cyclin-dependent kinases. *Trends in biochemical sciences* **30**, 630-641 (2005).
6. Malumbres, M. & Barbacid, M. To cycle or not to cycle: a critical decision in cancer. *Nature reviews. Cancer* **1**, 222-231 (2001).
7. Weinberg, R.A. *The Biology of Cancer*, (Garland Science, Taylor & Francis Group, LLC, New York, 2007).
8. Deng, C., Zhang, P., Harper, J.W., Elledge, S.J. & Leder, P. Mice lacking p21CIP1/WAF1 undergo normal development, but are defective in G1 checkpoint control. *Cell* **82**, 675-684 (1995).
9. Matsuoka, S.*, et al.* p57KIP2, a structurally distinct member of the p21CIP1 Cdk inhibitor family, is a candidate tumor suppressor gene. *Genes & development* **9**, 650-662 (1995).
10. Polyak, K.*, et al.* Cloning of p27Kip1, a cyclin-dependent kinase inhibitor and a potential mediator of extracellular antimitogenic signals. *Cell* **78**, 59-66 (1994).
11. Johnson, D.G. & Walker, C.L. Cyclins and cell cycle checkpoints. *Annual review of pharmacology and toxicology* **39**, 295-312 (1999).
12. Morgan, D.O. Cyclin-dependent kinases: engines, clocks, and microprocessors. *Annual review of cell and developmental biology* **13**, 261-291 (1997).
13. Elledge, S.J. Cell cycle checkpoints: preventing an identity crisis. *Science* **274**, 1664-1672 (1996).
14. Hartwell, L.H. & Kastan, M.B. Cell cycle control and cancer. *Science* **266**, 1821-1828 (1994).
15. Vigo, E.*, et al.* CDC25A phosphatase is a target of E2F and is required for efficient E2F-induced S phase. *Molecular and cellular biology* **19**, 6379-6395 (1999).
16. Draetta, G. & Eckstein, J. Cdc25 protein phosphatases in cell proliferation. *Biochimica et biophysica acta* **1332**, M53-63 (1997).
17. Mailand, N.*, et al.* Rapid destruction of human Cdc25A in response to DNA damage. *Science* **288**, 1425-1429 (2000).
18. Molinari, M., Mercurio, C., Dominguez, J., Goubin, F. & Draetta, G.F. Human Cdc25 A inactivation in response to S phase inhibition and its role in preventing premature mitosis. *EMBO reports* **1**, 71-79 (2000).
19. Costanzo, V.*, et al.* Reconstitution of an ATM-dependent checkpoint that inhibits chromosomal DNA replication following DNA damage. *Molecular cell* **6**, 649-659 (2000).
20. Bartek, J. & Lukas, J. Pathways governing G1/S transition and their response to DNA damage. *FEBS letters* **490**, 117-122 (2001).
21. Weinberg, R.A. The retinoblastoma gene and gene product. *Cancer surveys* **12**, 43-57 (1992).

22. Dyson, N. The regulation of E2F by pRB-family proteins. *Genes & development* **12**, 2245-2262 (1998).
23. Trimarchi, J.M. & Lees, J.A. Sibling rivalry in the E2F family. *Nature reviews. Molecular cell biology* **3**, 11-20 (2002).
24. Lomazzi, M., Moroni, M.C., Jensen, M.R., Frittoli, E. & Helin, K. Suppression of the p53- or pRB-mediated G1 checkpoint is required for E2F-induced S-phase entry. *Nature genetics* **31**, 190-194 (2002).
25. Cam, H. & Dynlacht, B.D. Emerging roles for E2F: beyond the G1/S transition and DNA replication. *Cancer cell* **3**, 311-316 (2003).
26. Vousden, K.H. & Prives, C. Blinded by the Light: The Growing Complexity of p53. *Cell* **137**, 413-431 (2009).
27. Levine, A.J. p53, the cellular gatekeeper for growth and division. *Cell* **88**, 323-331 (1997).
28. Ko, L.J. & Prives, C. p53: puzzle and paradigm. *Genes & development* **10**, 1054-1072 (1996).
29. Tanimura, S.*, et al.* MDM2 interacts with MDMX through their RING finger domains. *FEBS letters* **447**, 5-9 (1999).
30. Wade, M. & Wahl, G.M. Targeting Mdm2 and Mdmx in cancer therapy: better living through medicinal chemistry? *Molecular cancer research : MCR* **7**, 1-11 (2009).
31. Shieh, S.Y., Ikeda, M., Taya, Y. & Prives, C. DNA damage-induced phosphorylation of p53 alleviates inhibition by MDM2. *Cell* **91**, 325-334 (1997).
32. Meek, D.W. & Hupp, T.R. The regulation of MDM2 by multisite phosphorylation--opportunities for molecular-based intervention to target tumours? *Seminars in cancer biology* **20**, 19-28 (2010).
33. Wade, M., Li, Y.C. & Wahl, G.M. MDM2, MDMX and p53 in oncogenesis and cancer therapy. *Nature reviews. Cancer* **13**, 83-96 (2012).
34. Dumaz, N. & Meek, D.W. Serine15 phosphorylation stimulates p53 transactivation but does not directly influence interaction with HDM2. *The EMBO journal* **18**, 7002-7010 (1999).
35. Nevis, K.R., Cordeiro-Stone, M. & Cook, J.G. Origin licensing and p53 status regulate Cdk2 activity during G(1). *Cell Cycle* **8**, 1952-1963 (2009).
36. Stewart, Z.A. & Pietenpol, J.A. p53 Signaling and cell cycle checkpoints. *Chemical research in toxicology* **14**, 243-263 (2001).
37. Grallert, B. & Boye, E. The multiple facets of the intra-S checkpoint. *Cell Cycle* **7**, 2315-2320 (2008).
38. Hunt, T. Maturation promoting factor, cyclin and the control of M-phase. *Current opinion in cell biology* **1**, 268-274 (1989).
39. Russell, P. & Nurse, P. Negative regulation of mitosis by wee1+, a gene encoding a protein kinase homolog. *Cell* **49**, 559-567 (1987).
40. Mueller, P.R., Coleman, T.R., Kumagai, A. & Dunphy, W.G. Myt1: a membrane-associated inhibitory kinase that phosphorylates Cdc2 on both threonine-14 and tyrosine-15. *Science* **270**, 86-90 (1995).
41. Parker, L.L. & Piwnica-Worms, H. Inactivation of the p34cdc2-cyclin B complex by the human WEE1 tyrosine kinase. *Science* **257**, 1955-1957 (1992).
42. Kumagai, A. & Dunphy, W.G. The cdc25 protein controls tyrosine dephosphorylation of the cdc2 protein in a cell-free system. *Cell* **64**, 903-914 (1991).

43. Peng, C.Y.*, et al.* Mitotic and G2 checkpoint control: regulation of 14-3-3 protein binding by phosphorylation of Cdc25C on serine-216. *Science* **277**, 1501-1505 (1997).
44. Sanchez, Y.*, et al.* Conservation of the Chk1 checkpoint pathway in mammals: linkage of DNA damage to Cdk regulation through Cdc25. *Science* **277**, 1497-1501 (1997).
45. Matsuoka, S., Huang, M. & Elledge, S.J. Linkage of ATM to cell cycle regulation by the Chk2 protein kinase. *Science* **282**, 1893-1897 (1998).
46. Graves, P.R., Lovly, C.M., Uy, G.L. & Piwnica-Worms, H. Localization of human Cdc25C is regulated both by nuclear export and 14-3-3 protein binding. *Oncogene* **20**, 1839-1851 (2001).
47. Niculescu, A.B., 3rd*, et al.* Effects of p21(Cip1/Waf1) at both the G1/S and the G2/M cell cycle transitions: pRb is a critical determinant in blocking DNA replication and in preventing endoreduplication. *Molecular and cellular biology* **18**, 629-643 (1998).
48. Agarwal, M.L., Agarwal, A., Taylor, W.R. & Stark, G.R. p53 controls both the G2/M and the G1 cell cycle checkpoints and mediates reversible growth arrest in human fibroblasts. *Proceedings of the National Academy of Sciences of the United States of America* **92**, 8493-8497 (1995).
49. Taylor, W.R. & Stark, G.R. Regulation of the G2/M transition by p53. *Oncogene* **20**, 1803-1815 (2001).
50. Jin, S.*, et al.* The GADD45 inhibition of Cdc2 kinase correlates with GADD45-mediated growth suppression. *The Journal of biological chemistry* **275**, 16602-16608 (2000).
51. Hermeking, H.*, et al.* 14-3-3 sigma is a p53-regulated inhibitor of G2/M progression. *Molecular cell* **1**, 3-11 (1997).
52. Musacchio, A. & Ciliberto, A. The spindle-assembly checkpoint and the beauty of self-destruction. *Nature structural & molecular biology* **20**, 244 (2013).
53. Sudakin, V., Chan, G.K. & Yen, T.J. Checkpoint inhibition of the APC/C in HeLa cells is mediated by a complex of BUBR1, BUB3, CDC20, and MAD2. *J Cell Biol* **154**, 925-936 (2001).
54. Fry, A.M. & Yamano, H. APC/C-mediated degradation in early mitosis: how to avoid spindle assembly checkpoint inhibition. *Cell Cycle* **5**, 1487-1491 (2006).
55. Peters, J.M. The anaphase promoting complex/cyclosome: a machine designed to destroy. *Nature reviews. Molecular cell biology* **7**, 644-656 (2006).
56. D'Angiolella, V., Mari, C., Nocera, D., Rametti, L. & Grieco, D. The spindle checkpoint requires cyclin-dependent kinase activity. *Genes & development* **17**, 2520-2525 (2003).
57. Fang, G., Yu, H. & Kirschner, M.W. The checkpoint protein MAD2 and the mitotic regulator CDC20 form a ternary complex with the anaphase-promoting complex to control anaphase initiation. *Genes & development* **12**, 1871-1883 (1998).
58. Musacchio, A. & Salmon, E.D. The spindle-assembly checkpoint in space and time. *Nature reviews. Molecular cell biology* **8**, 379-393 (2007).
59. Sironi, L.*, et al.* Crystal structure of the tetrameric Mad1-Mad2 core complex: implications of a 'safety belt' binding mechanism for the spindle checkpoint. *The EMBO journal* **21**, 2496-2506 (2002).
60. King, R.W., Deshaies, R.J., Peters, J.M. & Kirschner, M.W. How proteolysis drives the cell cycle. *Science* **274**, 1652-1659 (1996).
61. Hershko, A. & Ciechanover, A. The ubiquitin system. *Annual review of biochemistry* **67**, 425-479 (1998).

62. Huang, T.T. & D'Andrea, A.D. Regulation of DNA repair by ubiquitylation. *Nature reviews. Molecular cell biology* **7**, 323-334 (2006).
63. Gao, M. & Karin, M. Regulating the regulators: control of protein ubiquitination and ubiquitin-like modifications by extracellular stimuli. *Molecular cell* **19**, 581-593 (2005).
64. Ciechanover, A., Gonen, H., Elias, S. & Mayer, A. Degradation of proteins by the ubiquitin-mediated proteolytic pathway. *The New biologist* **2**, 227-234 (1990).
65. Plechanovova, A., Jaffray, E.G., Tatham, M.H., Naismith, J.H. & Hay, R.T. Structure of a RING E3 ligase and ubiquitin-loaded E2 primed for catalysis. *Nature* **489**, 115-120 (2012).
66. Thrower, J.S., Hoffman, L., Rechsteiner, M. & Pickart, C.M. Recognition of the polyubiquitin proteolytic signal. *The EMBO journal* **19**, 94-102 (2000).
67. Chau, V.*, et al.* A multiubiquitin chain is confined to specific lysine in a targeted short-lived protein. *Science* **243**, 1576-1583 (1989).
68. Hochstrasser, M. Lingering mysteries of ubiquitin-chain assembly. *Cell* **124**, 27-34 (2006).
69. Ang, X.L. & Wade Harper, J. SCF-mediated protein degradation and cell cycle control. *Oncogene* **24**, 2860-2870 (2005).
70. Willems, A.R., Schwab, M. & Tyers, M. A hitchhiker's guide to the cullin ubiquitin ligases: SCF and its kin. *Biochimica et biophysica acta* **1695**, 133-170 (2004).
71. Deshaies, R.J. SCF and Cullin/Ring H2-based ubiquitin ligases. *Annual review of cell and developmental biology* **15**, 435-467 (1999).
72. Bai, C.*, et al.* SKP1 connects cell cycle regulators to the ubiquitin proteolysis machinery through a novel motif, the F-box. *Cell* **86**, 263-274 (1996).
73. Kipreos, E.T. & Pagano, M. The F-box protein family. *Genome biology* **1**, REVIEWS3002 (2000).
74. Ho, M.S., Tsai, P.I. & Chien, C.T. F-box proteins: the key to protein degradation. *Journal of biomedical science* **13**, 181-191 (2006).
75. Skowyra, D.*, et al.* Reconstitution of G1 cyclin ubiquitination with complexes containing SCFGrr1 and Rbx1. *Science* **284**, 662-665 (1999).
76. Cardozo, T. & Pagano, M. The SCF ubiquitin ligase: insights into a molecular machine. *Nature reviews. Molecular cell biology* **5**, 739-751 (2004).
77. Ouyang, T.*, et al.* Identification and characterization of a nuclear interacting partner of anaplastic lymphoma kinase (NIPA). *The Journal of biological chemistry* **278**, 30028-30036 (2003).
78. von Klitzing, C. (2009) Regulation des F-Box Proteins NIPA. *PhD thesis.*
79. Laity, J.H., Lee, B.M. & Wright, P.E. Zinc finger proteins: new insights into structural and functional diversity. *Current opinion in structural biology* **11**, 39-46 (2001).
80. Kokoszynska, K., Rychlewski, L. & Wyrwicz, L.S. The mitotic entry regulator NIPA is a prototypic BIR domain protein. *Cell Cycle* **7**, 2073-2075 (2008).
81. Miller, L.K. An exegesis of IAPs: salvation and surprises from BIR motifs. *Trends in cell biology* **9**, 323-328 (1999).
82. Zangemeister-Wittke, U. & Simon, H.U. An IAP in action: the multiple roles of survivin in differentiation, immunity and malignancy. *Cell Cycle* **3**, 1121-1123 (2004).
83. Bassermann, F.*, et al.* NIPA defines an SCF-type mammalian E3 ligase that regulates mitotic entry. *Cell* **122**, 45-57 (2005).

84. Bassermann, F.*, et al.* Multisite phosphorylation of nuclear interaction partner of ALK (NIPA) at G2/M involves cyclin B1/Cdk1. *The Journal of biological chemistry* **282**, 15965-15972 (2007).
85. Illert, A.L.*, et al.* Extracellular signal-regulated kinase 2 (ERK2) mediates phosphorylation and inactivation of nuclear interaction partner of anaplastic lymphoma kinase (NIPA) at G2/M. *The Journal of biological chemistry* **287**, 37997-38005 (2012).
86. Klitzing, C.*, et al.* APC/C(Cdh1)-mediated degradation of the F-box protein NIPA is regulated by its association with Skp1. *PloS one* **6**, e28998 (2011).
87. Illert, A.L.*, et al.* Targeted inactivation of nuclear interaction partner of ALK disrupts meiotic prophase. *Development* **139**, 2523-2534 (2012).
88. Vilenchik, M.M. & Knudson, A.G. Endogenous DNA double-strand breaks: production, fidelity of repair, and induction of cancer. *Proceedings of the National Academy of Sciences of the United States of America* **100**, 12871-12876 (2003).
89. Downs, J.A., Nussenzweig, M.C. & Nussenzweig, A. Chromatin dynamics and the preservation of genetic information. *Nature* **447**, 951-958 (2007).
90. Li, L. & Zou, L. Sensing, signaling, and responding to DNA damage: organization of the checkpoint pathways in mammalian cells. *Journal of cellular biochemistry* **94**, 298-306 (2005).
91. Dianov, G.L. & Hubscher, U. Mammalian Base Excision Repair: the Forgotten Archangel. *Nucleic acids research* (2013).
92. Altmeyer, M. & Lukas, J. To spread or not to spread-chromatin modifications in response to DNA damage. *Current opinion in genetics & development* (2013).
93. Thode, S., Schafer, A., Pfeiffer, P. & Vielmetter, W. A novel pathway of DNA end-to-end joining. *Cell* **60**, 921-928 (1990).
94. Karpenshif, Y. & Bernstein, K.A. From yeast to mammals: recent advances in genetic control of homologous recombination. *DNA repair* **11**, 781-788 (2012).
95. Canman, C.E.*, et al.* Activation of the ATM kinase by ionizing radiation and phosphorylation of p53. *Science* **281**, 1677-1679 (1998).
96. Bakkenist, C.J. & Kastan, M.B. DNA damage activates ATM through intermolecular autophosphorylation and dimer dissociation. *Nature* **421**, 499-506 (2003).
97. Rogakou, E.P., Pilch, D.R., Orr, A.H., Ivanova, V.S. & Bonner, W.M. DNA double-stranded breaks induce histone H2AX phosphorylation on serine 139. *The Journal of biological chemistry* **273**, 5858-5868 (1998).
98. Lukas, C.*, et al.* Mdc1 couples DNA double-strand break recognition by Nbs1 with its H2AX-dependent chromatin retention. *The EMBO journal* **23**, 2674-2683 (2004).
99. Lee, J.H. & Paull, T.T. Direct activation of the ATM protein kinase by the Mre11/Rad50/Nbs1 complex. *Science* **304**, 93-96 (2004).
100. Harper, J.W. & Elledge, S.J. The DNA damage response: ten years after. *Molecular cell* **28**, 739-745 (2007).
101. Huen, M.S.*, et al.* RNF8 transduces the DNA-damage signal via histone ubiquitylation and checkpoint protein assembly. *Cell* **131**, 901-914 (2007).
102. Wang, H.*, et al.* Histone H3 and H4 ubiquitylation by the CUL4-DDB-ROC1 ubiquitin ligase facilitates cellular response to DNA damage. *Molecular cell* **22**, 383-394 (2006).
103. Mochan, T.A., Venere, M., DiTullio, R.A., Jr. & Halazonetis, T.D. 53BP1, an activator of ATM in response to DNA damage. *DNA repair* **3**, 945-952 (2004).

104. Xu, B., Kim, S. & Kastan, M.B. Involvement of Brca1 in S-phase and G(2)-phase checkpoints after ionizing irradiation. *Molecular and cellular biology* **21**, 3445-3450 (2001).
105. Zou, L. & Elledge, S.J. Sensing DNA damage through ATRIP recognition of RPA-ssDNA complexes. *Science* **300**, 1542-1548 (2003).
106. Mordes, D.A., Glick, G.G., Zhao, R. & Cortez, D. TopBP1 activates ATR through ATRIP and a PIKK regulatory domain. *Genes & development* **22**, 1478-1489 (2008).
107. Garcia, V., Furuya, K. & Carr, A.M. Identification and functional analysis of TopBP1 and its homologs. *DNA repair* **4**, 1227-1239 (2005).
108. Yang, X.H. & Zou, L. Checkpoint and coordinated cellular responses to DNA damage. *Results and problems in cell differentiation* **42**, 65-92 (2006).
109. Lin, S.Y., Li, K., Stewart, G.S. & Elledge, S.J. Human Claspin works with BRCA1 to both positively and negatively regulate cell proliferation. *Proceedings of the National Academy of Sciences of the United States of America* **101**, 6484-6489 (2004).
110. Kastan, M.B. & Bartek, J. Cell-cycle checkpoints and cancer. *Nature* **432**, 316-323 (2004).
111. Rhind, N. Changing of the guard: how ATM hands off DNA double-strand break signaling to ATR. *Molecular cell* **33**, 672-674 (2009).
112. Jazayeri, A.*, et al.* ATM- and cell cycle-dependent regulation of ATR in response to DNA double-strand breaks. *Nat Cell Biol* **8**, 37-45 (2006).
113. Myers, J.S. & Cortez, D. Rapid activation of ATR by ionizing radiation requires ATM and Mre11. *The Journal of biological chemistry* **281**, 9346-9350 (2006).
114. Cuadrado, M.*, et al.* ATM regulates ATR chromatin loading in response to DNA double-strand breaks. *The Journal of experimental medicine* **203**, 297-303 (2006).
115. Walker, J.R., Corpina, R.A. & Goldberg, J. Structure of the Ku heterodimer bound to DNA and its implications for double-strand break repair. *Nature* **412**, 607-614 (2001).
116. Weterings, E., Verkaik, N.S., Bruggenwirth, H.T., Hoeijmakers, J.H. & van Gent, D.C. The role of DNA dependent protein kinase in synapsis of DNA ends. *Nucleic acids research* **31**, 7238-7246 (2003).
117. Moshous, D.*, et al.* Artemis, a novel DNA double-strand break repair/V(D)J recombination protein, is mutated in human severe combined immune deficiency. *Cell* **105**, 177-186 (2001).
118. Grawunder, U.*, et al.* Activity of DNA ligase IV stimulated by complex formation with XRCC4 protein in mammalian cells. *Nature* **388**, 492-495 (1997).
119. Gu, J., Lu, H., Tsai, A.G., Schwarz, K. & Lieber, M.R. Single-stranded DNA ligation and XLF-stimulated incompatible DNA end ligation by the XRCC4-DNA ligase IV complex: influence of terminal DNA sequence. *Nucleic acids research* **35**, 5755-5762 (2007).
120. Hartlerode, A.J. & Scully, R. Mechanisms of double-strand break repair in somatic mammalian cells. *The Biochemical journal* **423**, 157-168 (2009).
121. Williams, R.S.*, et al.* Nbs1 flexibly tethers Ctp1 and Mre11-Rad50 to coordinate DNA double-strand break processing and repair. *Cell* **139**, 87-99 (2009).
122. Sartori, A.A.*, et al.* Human CtIP promotes DNA end resection. *Nature* **450**, 509-514 (2007).
123. Shivji, M.K.*, et al.* The BRC repeats of human BRCA2 differentially regulate RAD51 binding on single- versus double-stranded DNA to stimulate strand exchange.

Proceedings of the National Academy of Sciences of the United States of America **106**, 13254-13259 (2009).
124. Brzovic, P.S., Rajagopal, P., Hoyt, D.W., King, M.C. & Klevit, R.E. Structure of a BRCA1-BARD1 heterodimeric RING-RING complex. *Nature structural biology* **8**, 833-837 (2001).
125. Zhang, F.*, et al.* PALB2 links BRCA1 and BRCA2 in the DNA-damage response. *Current biology : CB* **19**, 524-529 (2009).
126. Ohta, T., Sato, K. & Wu, W. The BRCA1 ubiquitin ligase and homologous recombination repair. *FEBS letters* **585**, 2836-2844 (2011).
127. Jensen, R.B., Ozes, A., Kim, T., Estep, A. & Kowalczykowski, S.C. BRCA2 is epistatic to the RAD51 paralogs in response to DNA damage. *DNA repair* (2013).
128. Kuznetsov, S.G., Haines, D.C., Martin, B.K. & Sharan, S.K. Loss of Rad51c leads to embryonic lethality and modulation of Trp53-dependent tumorigenesis in mice. *Cancer research* **69**, 863-872 (2009).
129. Bugreev, D.V., Mazina, O.M. & Mazin, A.V. Rad54 protein promotes branch migration of Holliday junctions. *Nature* **442**, 590-593 (2006).
130. Wu, L. & Hickson, I.D. The Bloom's syndrome helicase suppresses crossing over during homologous recombination. *Nature* **426**, 870-874 (2003).
131. Chen, X.B.*, et al.* Human Mus81-associated endonuclease cleaves Holliday junctions in vitro. *Molecular cell* **8**, 1117-1127 (2001).
132. Ip, S.C.*, et al.* Identification of Holliday junction resolvases from humans and yeast. *Nature* **456**, 357-361 (2008).
133. Svendsen, J.M.*, et al.* Mammalian BTBD12/SLX4 assembles a Holliday junction resolvase and is required for DNA repair. *Cell* **138**, 63-77 (2009).
134. Strambio-De-Castillia, C., Niepel, M. & Rout, M.P. The nuclear pore complex: bridging nuclear transport and gene regulation. *Nature reviews. Molecular cell biology* **11**, 490-501 (2010).
135. Hoelz, A., Debler, E.W. & Blobel, G. The structure of the nuclear pore complex. *Annual review of biochemistry* **80**, 613-643 (2011).
136. Raices, M. & D'Angelo, M.A. Nuclear pore complex composition: a new regulator of tissue-specific and developmental functions. *Nature reviews. Molecular cell biology* **13**, 687-699 (2012).
137. Rabut, G., Doye, V. & Ellenberg, J. Mapping the dynamic organization of the nuclear pore complex inside single living cells. *Nat Cell Biol* **6**, 1114-1121 (2004).
138. Walther, T.C.*, et al.* The nucleoporin Nup153 is required for nuclear pore basket formation, nuclear pore complex anchoring and import of a subset of nuclear proteins. *The EMBO journal* **20**, 5703-5714 (2001).
139. D'Angelo, M.A. & Hetzer, M.W. Structure, dynamics and function of nuclear pore complexes. *Trends in cell biology* **18**, 456-466 (2008).
140. Hase, M.E. & Cordes, V.C. Direct interaction with nup153 mediates binding of Tpr to the periphery of the nuclear pore complex. *Molecular biology of the cell* **14**, 1923-1940 (2003).
141. Dultz, E.*, et al.* Systematic kinetic analysis of mitotic dis- and reassembly of the nuclear pore in living cells. *J Cell Biol* **180**, 857-865 (2008).
142. Terry, L.J., Shows, E.B. & Wente, S.R. Crossing the nuclear envelope: hierarchical regulation of nucleocytoplasmic transport. *Science* **318**, 1412-1416 (2007).
143. Nakano, H.*, et al.* Unexpected role of nucleoporins in coordination of cell cycle progression. *Cell Cycle* **10**, 425-433 (2011).

144. Mullis, K.*, et al.* Specific enzymatic amplification of DNA in vitro: the polymerase chain reaction. *Cold Spring Harbor symposia on quantitative biology* **51 Pt 1**, 263-273 (1986).
145. Bradford, M.M. A rapid and sensitive method for the quantitation of microgram quantities of protein utilizing the principle of protein-dye binding. *Analytical biochemistry* **72**, 248-254 (1976).
146. Elbashir, S.M.*, et al.* Duplexes of 21-nucleotide RNAs mediate RNA interference in cultured mammalian cells. *Nature* **411**, 494-498 (2001).
147. Brummelkamp, T.R., Bernards, R. & Agami, R. A system for stable expression of short interfering RNAs in mammalian cells. *Science* **296**, 550-553 (2002).
148. Albers, C.*, et al.* An RNAi-based system for loss-of-function analysis identifies Raf1 as a crucial mediator of BCR-ABL-driven leukemogenesis. *Blood* **118**, 2200-2210 (2011).
149. Dickins, R.A.*, et al.* Probing tumor phenotypes using stable and regulated synthetic microRNA precursors. *Nature genetics* **37**, 1289-1295 (2005).
150. Franken, N.A., Rodermond, H.M., Stap, J., Haveman, J. & van Bree, C. Clonogenic assay of cells in vitro. *Nature protocols* **1**, 2315-2319 (2006).
151. Rosenberger, A.*, et al.* Validation of a fully automated COMET assay: 1.75 million single cells measured over a 5 year period. *DNA repair* **10**, 322-337 (2011).
152. Schindewolf, C.*, et al.* Comet assay as a tool to screen for mouse models with inherited radiation sensitivity. *Mammalian genome : official journal of the International Mammalian Genome Society* **11**, 552-554 (2000).
153. Pierce, A.J., Johnson, R.D., Thompson, L.H. & Jasin, M. XRCC3 promotes homology-directed repair of DNA damage in mammalian cells. *Genes & development* **13**, 2633-2638 (1999).
154. Peng, G.*, et al.* BRIT1/MCPH1 links chromatin remodelling to DNA damage response. *Nat Cell Biol* **11**, 865-872 (2009).
155. Schneider, K.*, et al.* Dissection of cell cycle-dependent dynamics of Dnmt1 by FRAP and diffusion-coupled modeling. *Nucleic acids research* (2013).
156. Lippincott-Schwartz, J. & Patterson, G.H. Development and use of fluorescent protein markers in living cells. *Science* **300**, 87-91 (2003).
157. Lippincott-Schwartz, J., Snapp, E. & Kenworthy, A. Studying protein dynamics in living cells. *Nature reviews. Molecular cell biology* **2**, 444-456 (2001).
158. Walter, J., Cremer, T., Miyagawa, K. & Tashiro, S. A new system for laser-UVA-microirradiation of living cells. *Journal of microscopy* **209**, 71-75 (2003).
159. Chevallet, M., Luche, S. & Rabilloud, T. Silver staining of proteins in polyacrylamide gels. *Nature protocols* **1**, 1852-1858 (2006).
160. Grogro, E. (2012) Die Rolle von NIPA im Zellzyklus nach DNS-Schädigung. *PhD thesis.*
161. Sharma, A., Singh, K. & Almasan, A. Histone H2AX phosphorylation: a marker for DNA damage. *Methods Mol Biol* **920**, 613-626 (2012).
162. Kuzminov, A. Single-strand interruptions in replicating chromosomes cause double-strand breaks. *Proceedings of the National Academy of Sciences of the United States of America* **98**, 8241-8246 (2001).
163. Rouse, J. & Jackson, S.P. Interfaces between the detection, signaling, and repair of DNA damage. *Science* **297**, 547-551 (2002).
164. Polo, S.E. & Jackson, S.P. Dynamics of DNA damage response proteins at DNA breaks: a focus on protein modifications. *Genes & development* **25**, 409-433 (2011).

165. Markova, E., Torudd, J. & Belyaev, I. Long time persistence of residual 53BP1/gamma-H2AX foci in human lymphocytes in relationship to apoptosis, chromatin condensation and biological dosimetry. *International journal of radiation biology* **87**, 736-745 (2011).
166. Goldberg, M.*, et al.* MDC1 is required for the intra-S-phase DNA damage checkpoint. *Nature* **421**, 952-956 (2003).
167. Stewart, G.S., Wang, B., Bignell, C.R., Taylor, A.M. & Elledge, S.J. MDC1 is a mediator of the mammalian DNA damage checkpoint. *Nature* **421**, 961-966 (2003).
168. Lou, Z., Minter-Dykhouse, K., Wu, X. & Chen, J. MDC1 is coupled to activated CHK2 in mammalian DNA damage response pathways. *Nature* **421**, 957-961 (2003).
169. Lou, Z.*, et al.* MDC1 maintains genomic stability by participating in the amplification of ATM-dependent DNA damage signals. *Molecular cell* **21**, 187-200 (2006).
170. Stewart, G.S. Solving the RIDDLE of 53BP1 recruitment to sites of damage. *Cell Cycle* **8**, 1532-1538 (2009).
171. DiTullio, R.A., Jr.*, et al.* 53BP1 functions in an ATM-dependent checkpoint pathway that is constitutively activated in human cancer. *Nat Cell Biol* **4**, 998-1002 (2002).
172. Wang, B., Matsuoka, S., Carpenter, P.B. & Elledge, S.J. 53BP1, a mediator of the DNA damage checkpoint. *Science* **298**, 1435-1438 (2002).
173. Difilippantonio, S.*, et al.* 53BP1 facilitates long-range DNA end-joining during V(D)J recombination. *Nature* **456**, 529-533 (2008).
174. Ward, I.M., Minn, K., Jorda, K.G. & Chen, J. Accumulation of checkpoint protein 53BP1 at DNA breaks involves its binding to phosphorylated histone H2AX. *The Journal of biological chemistry* **278**, 19579-19582 (2003).
175. Mortusewicz, O. & Leonhardt, H. XRCC1 and PCNA are loading platforms with distinct kinetic properties and different capacities to respond to multiple DNA lesions. *BMC molecular biology* **8**, 81 (2007).
176. Wu, J., Shekhar, N., Lele, P.P. & Lele, T.P. FRAP analysis: accounting for bleaching during image capture. *PloS one* **7**, e42854 (2012).
177. Wustner, D.*, et al.* Quantitative fluorescence loss in photobleaching for analysis of protein transport and aggregation. *BMC bioinformatics* **13**, 296 (2012).
178. Pyrpasopoulou, A., Meier, J., Maison, C., Simos, G. & Georgatos, S.D. The lamin B receptor (LBR) provides essential chromatin docking sites at the nuclear envelope. *The EMBO journal* **15**, 7108-7119 (1996).
179. Terasaki, M.*, et al.* A new model for nuclear envelope breakdown. *Molecular biology of the cell* **12**, 503-510 (2001).
180. Kobayashi, J.*, et al.* Nucleolin participates in DNA double-strand break-induced damage response through MDC1-dependent pathway. *PloS one* **7**, e49245 (2012).
181. Lai, R. & Ingham, R.J. The pathobiology of the oncogenic tyrosine kinase NPM-ALK: a brief update. *Therapeutic advances in hematology* **4**, 119-131 (2013).
182. Gjerset, R.A. DNA damage, p14ARF, nucleophosmin (NPM/B23), and cancer. *Journal of molecular histology* **37**, 239-251 (2006).
183. Koike, A.*, et al.* Recruitment of phosphorylated NPM1 to sites of DNA damage through RNF8-dependent ubiquitin conjugates. *Cancer research* **70**, 6746-6756 (2010).
184. Sato, K.*, et al.* Nucleophosmin/B23 is a candidate substrate for the BRCA1-BARD1 ubiquitin ligase. *The Journal of biological chemistry* **279**, 30919-30922 (2004).

185. Takeda, K.*, et al.* Mitochondrial phosphoglycerate mutase 5 uses alternate catalytic activity as a protein serine/threonine phosphatase to activate ASK1. *Proceedings of the National Academy of Sciences of the United States of America* **106**, 12301-12305 (2009).
186. Zhuang, M., Guan, S., Wang, H., Burlingame, A.L. & Wells, J.A. Substrates of IAP ubiquitin ligases identified with a designed orthogonal E3 ligase, the NEDDylator. *Molecular cell* **49**, 273-282 (2013).
187. Strebhardt, K. Multifaceted polo-like kinases: drug targets and antitargets for cancer therapy. *Nature reviews. Drug discovery* **9**, 643-660 (2010).
188. Yata, K.*, et al.* Plk1 and CK2 act in concert to regulate Rad51 during DNA double strand break repair. *Molecular cell* **45**, 371-383 (2012).
189. Postow, L. Destroying the ring: Freeing DNA from Ku with ubiquitin. *FEBS letters* **585**, 2876-2882 (2011).
190. Frosst, P., Guan, T., Subauste, C., Hahn, K. & Gerace, L. Tpr is localized within the nuclear basket of the pore complex and has a role in nuclear protein export. *J Cell Biol* **156**, 617-630 (2002).
191. David-Watine, B. Silencing nuclear pore protein Tpr elicits a senescent-like phenotype in cancer cells. *PloS one* **6**, e22423 (2011).
192. Kosova, B.*, et al.* Mlp2p, a component of nuclear pore attached intranuclear filaments, associates with nic96p. *The Journal of biological chemistry* **275**, 343-350 (2000).
193. Lee, T.*, et al.* Docking motif interactions in MAP kinases revealed by hydrogen exchange mass spectrometry. *Molecular cell* **14**, 43-55 (2004).
194. Matsubayashi, Y., Fukuda, M. & Nishida, E. Evidence for existence of a nuclear pore complex-mediated, cytosol-independent pathway of nuclear translocation of ERK MAP kinase in permeabilized cells. *The Journal of biological chemistry* **276**, 41755-41760 (2001).
195. Vomastek, T.*, et al.* Extracellular signal-regulated kinase 2 (ERK2) phosphorylation sites and docking domain on the nuclear pore complex protein Tpr cooperatively regulate ERK2-Tpr interaction. *Molecular and cellular biology* **28**, 6954-6966 (2008).
196. Asally, M.*, et al.* Nup358, a nucleoporin, functions as a key determinant of the nuclear pore complex structure remodeling during skeletal myogenesis. *The FEBS journal* **278**, 610-621 (2011).
197. Maurer, U., Charvet, C., Wagman, A.S., Dejardin, E. & Green, D.R. Glycogen synthase kinase-3 regulates mitochondrial outer membrane permeabilization and apoptosis by destabilization of MCL-1. *Molecular cell* **21**, 749-760 (2006).
198. Shrivastav, M., De Haro, L.P. & Nickoloff, J.A. Regulation of DNA double-strand break repair pathway choice. *Cell research* **18**, 134-147 (2008).
199. Mao, Z., Jiang, Y., Liu, X., Seluanov, A. & Gorbunova, V. DNA repair by homologous recombination, but not by nonhomologous end joining, is elevated in breast cancer cells. *Neoplasia* **11**, 683-691 (2009).
200. Xia, F.*, et al.* Deficiency of human BRCA2 leads to impaired homologous recombination but maintains normal nonhomologous end joining. *Proceedings of the National Academy of Sciences of the United States of America* **98**, 8644-8649 (2001).
201. Coleman, T.R. & Dunphy, W.G. Cdc2 regulatory factors. *Current opinion in cell biology* **6**, 877-882 (1994).

202. Brandeis, M.*, et al.* Cyclin B2-null mice develop normally and are fertile whereas cyclin B1-null mice die in utero. *Proceedings of the National Academy of Sciences of the United States of America* **95**, 4344-4349 (1998).
203. Gavet, O. & Pines, J. Activation of cyclin B1-Cdk1 synchronizes events in the nucleus and the cytoplasm at mitosis. *J Cell Biol* **189**, 247-259 (2010).
204. Hagting, A., Jackman, M., Simpson, K. & Pines, J. Translocation of cyclin B1 to the nucleus at prophase requires a phosphorylation-dependent nuclear import signal. *Current biology : CB* **9**, 680-689 (1999).
205. Kouranti, I. & Peyroche, A. Protein degradation in DNA damage response. *Seminars in cell & developmental biology* **23**, 538-545 (2012).
206. van den Heuvel, S. Cell-cycle regulation. in *WormBook* (ed. Community, T.C.e.R.) (2005).
207. Shiloh, Y. & Ziv, Y. The ATM protein kinase: regulating the cellular response to genotoxic stress, and more. *Nature reviews. Molecular cell biology* **14**, 197-210 (2013).
208. Martin, N.T., Nahas, S.A., Tunuguntla, R., Fike, F. & Gatti, R.A. Assessing 'radiosensitivity' with kinetic profiles of gamma-H2AX, 53BP1 and BRCA1 foci. *Radiotherapy and oncology : journal of the European Society for Therapeutic Radiology and Oncology* **101**, 35-38 (2011).
209. Nagai, S.*, et al.* Functional targeting of DNA damage to a nuclear pore-associated SUMO-dependent ubiquitin ligase. *Science* **322**, 597-602 (2008).
210. Oza, P., Jaspersen, S.L., Miele, A., Dekker, J. & Peterson, C.L. Mechanisms that regulate localization of a DNA double-strand break to the nuclear periphery. *Genes & development* **23**, 912-927 (2009).
211. Oza, P. & Peterson, C.L. Opening the DNA repair toolbox: localization of DNA double strand breaks to the nuclear periphery. *Cell Cycle* **9**, 43-49 (2010).
212. Krull, S., Thyberg, J., Bjorkroth, B., Rackwitz, H.R. & Cordes, V.C. Nucleoporins as components of the nuclear pore complex core structure and Tpr as the architectural element of the nuclear basket. *Molecular biology of the cell* **15**, 4261-4277 (2004).
213. Ben-Efraim, I., Frosst, P.D. & Gerace, L. Karyopherin binding interactions and nuclear import mechanism of nuclear pore complex protein Tpr. *BMC cell biology* **10**, 74 (2009).
214. Paddy, M.R. The Tpr protein: linking structure and function in the nuclear interior? *American journal of human genetics* **63**, 305-310 (1998).
215. Byrd, D.A.*, et al.* Tpr, a large coiled coil protein whose amino terminus is involved in activation of oncogenic kinases, is localized to the cytoplasmic surface of the nuclear pore complex. *J Cell Biol* **127**, 1515-1526 (1994).
216. Lee, S.H., Sterling, H., Burlingame, A. & McCormick, F. Tpr directly binds to Mad1 and Mad2 and is important for the Mad1-Mad2-mediated mitotic spindle checkpoint. *Genes & development* **22**, 2926-2931 (2008).
217. Celeste, A.*, et al.* Genomic instability in mice lacking histone H2AX. *Science* **296**, 922-927 (2002).
218. Barlow, C.*, et al.* Atm-deficient mice: a paradigm of ataxia telangiectasia. *Cell* **86**, 159-171 (1996).
219. Moudry, P.*, et al.* Nucleoporin NUP153 guards genome integrity by promoting nuclear import of 53BP1. *Cell death and differentiation* **19**, 798-807 (2012).
220. Krull, S.*, et al.* Protein Tpr is required for establishing nuclear pore-associated zones of heterochromatin exclusion. *The EMBO journal* **29**, 1659-1673 (2010).

221. Strambio-de-Castillia, C., Blobel, G. & Rout, M.P. Proteins connecting the nuclear pore complex with the nuclear interior. *J Cell Biol* **144**, 839-855 (1999).
222. Lemaitre, C*., et al.* The nucleoporin 153, a novel factor in double-strand break repair and DNA damage response. *Oncogene* **31**, 4803-4809 (2012).
223. Zimmermann, M., Lottersberger, F., Buonomo, S.B., Sfeir, A. & de Lange, T. 53BP1 regulates DSB repair using Rif1 to control 5' end resection. *Science* **339**, 700-704 (2013).
224. Niu, H., Raynard, S. & Sung, P. Multiplicity of DNA end resection machineries in chromosome break repair. *Genes & development* **23**, 1481-1486 (2009).
225. Porter, L.A., Cukier, I.H. & Lee, J.M. Nuclear localization of cyclin B1 regulates DNA damage-induced apoptosis. *Blood* **101**, 1928-1933 (2003).
226. Toyoshima, F., Moriguchi, T., Wada, A., Fukuda, M. & Nishida, E. Nuclear export of cyclin B1 and its possible role in the DNA damage-induced G2 checkpoint. *The EMBO journal* **17**, 2728-2735 (1998).
227. Jin, P., Hardy, S. & Morgan, D.O. Nuclear localization of cyclin B1 controls mitotic entry after DNA damage. *J Cell Biol* **141**, 875-885 (1998).

Acknowledgments

Many people were directly or indirectly involved in succesfull accomplishment of this work. Here I would like to express my highest appreciation for their contribution.

First of all I would like to thank Prof. Dr. Justus Duyster for giving me the chance to work on this project in his research group. His deep scientific knowledge and incredible sense of research has always guided our efforts in the right direction, turning this work into success. I wish to thank him for inspiring scientific discussions.

I wish to express my thanks to Prof. Dr. Michael Groll for his willingness to supervise this thesis at the Department of Chemistry and Biochemistry, Technical University of Munich.

I wish to thank Prof. Dr. Christian Peschel, Director of III Internal Medicine, for providing the facilities and infra structure that was needed to complete the project work.

I am very grateful to Dr. Anna Lena Illert for encouragement and professional reviewing of the manuscript. I greatly appreciate her skillful scientific support.

I would like to express a special thanks to our cooperation partners:

Prof. Dr. Heinrich Leonhardt from Faculty of Biology, Ludwig-maximilians University Munich for giving me the opportunity to learn high-end immunofluorescence techniques at his Department.
Most of all I would like to thank Katrin Schneider from the group of Prof. Leonhardt, for her invaluable help in performing bioimaging experiments. Without her commitment and professional skills this work would not reach it final form.

Dr. Maria Gomolka and Dr. Ute Rüssler from Budnesamt für Strahlensutz, Helmholtz Zentrum München for help in performing comet assay in their facility. I would like to thank Susanne Wiedemann for introducing into the technique and Frank Bunk for data collection and evaluation.

Prof. Bernhard Küster from Department of Proteomics and Bioanalytics, Technical University of Munich and foremost Dr. Simone Lemeer for performing proteomic analysis and data evaluation.

Special thank to Dr. Shiaw-Yih Lin from MD Anderson Cancer Center for providing me with U2OS DR-GFP reporter cell line.

I also would like to thank Vanesa for her help with ubiquitylation experiments and company during lunch breaks.

Special thanks go to Richard for his certified sense of humour and helpful discoussions.

I am grateful to Cathrin, Nico and Sabine for funny microinvaironment in the “small lab”.

I wish to take this opportunity to express special thanks to all my colleagues from AG Duyster lab: Richard, Cathrin, Tini, Chuang Yang, Sabine, Günther, Nico, Melanie, Astrid, Claudia, Sebastian, Rama, Michael, Natalie, Hari, Becky, Bin, Hannes, Jana, Corinna, Melanie, Anja, Tony, Sara, Christoph, Wibke, Nicole, Konstantin, Charlotte, Nadya, Maggi and Stefanie for a wonderful atmosphere at work. I wish to thank Frau Budak for her outstanding effort in keeping the lab running.

Serdecznie dziękuję wszystkim najbliższym mi osobom za wsparcie w dążeniu do celu i wiarę jaką we mnie pokładali. Bez Was nigdy nie osiągnąłbym tak wiele.

Ani dziękuję za radość życia.